学位論文

Plasma Transport and Energization in the Earth's Magnetosphere

地球磁気圏におけるプラズマの加速・輸送過程

2001年

堀　智昭

学位論文

Plasma Transport and Energization in the Earth's Magnetosphere

地球磁気圏におけるプラズマの加速・輸送過程

2001年

堀　智昭

Acknowledgements

First of all, I would like to express my sincere appreciation to my research supervisor Prof. Kiyoshi Maezawa for his continual guidance, stimulating and helpful suggestions throughout the present study. His helpful advice and invaluable discussions helped this study to be accomplished in the present form.

I am especially grateful to Prof. Koujun Yamashita, my supervisor at Nagoya University, for his encouragement and suggestions with tender care.

I am very thankful to all people who belong and/or belonged to I-laboratory (Now Up-laboratory) in Department of Physics, Nagoya University; M. Fujimoto, T. Fukui, H. Shirai, M. Nakamura, K. Asai, T. Hayashi, N. Kuriyama, K. Hara, H. Hasegawa, I. Baba, T. Nonaka, and T. Iwata, for their general encouragement. I especially acknowledge Takeshi Takashima for his hearty encouragement and also kind help in processing the GEOTAIL-HEP data.

The present study is totally based on data from the GEOTAIL mission carried out with help of many researchers. I am very grateful to all the members of the GEOTAIL science team for fruitful discussions.

Finally, I thank my wife, Satoko Hiraizumi, and my parents for their continual support for my daily life in Nagoya which enabled me to concentrate on the present work.

Abstract

The plasma sheet, which is confined around the equatorial region of the magnetosphere, is one of the most active site where the particle distribution consists of not only the thermal component (~several keV) but also the suprathermal component (~several tens to hundreds of keV) as a result of various acceleration and transport processes. These two components of magnetospheric plasma behave and affect plasma and field structures in the magnetosphere in different ways. The thermal component is a major component of plasma in the plasma sheet and plays a main role in global interaction with the ambient magnetic and electric fields, hence their spatial distribution and also global transport processes are closely related to large-scale field structures of the plasma sheet. On the other hand, the suprathermal component is a minor component and usually their abundance is negligibly small as compared to the thermal component. However they are generated abundantly during geomagnetically disturbed periods such as substorms and transported into the inner region of the magnetosphere. These energetic particles generate a large-scale current system around the Earth and thereby cause significant variations in the geomagnetic field near the Earth. Thus in order to understand dynamics of the magnetosphere comprehensively, it is essential to examine the contribution of both thermal and suprathermal plasmas to the formation of the magnetospheric plasma and field structures and also to the energization processes occurring in the plasma sheet. Therefore, in this dissertation, I investigate typical magnetospheric phenomena relating to the acceleration and transport processes for thermal and suprathermal components of plasmas, using the data obtained by the GEOTAIL spacecraft, and discuss the fundamental processes of plasma acceleration and subsequent transport in the magnetosphere.

First I made a statistical study on ion flows, pressure, and the magnetic field directly observed in the plasma sheet and derived their large-scale structures. It was shown that the average ion flow in the plasma sheet has a significant duskward component in the local midnight to dusk side regions, but is directed almost sunward on the dawn side. Since this asymmetry probably resulted from the contribution of the ion pressure gradient drift, we estimated the true distribution of the convection electric field by correcting the observed V×B field by the observed ion pressure gradient. The result is that, in addition to the duskward component of the electric field representing the sunward convection, the electric field has a significant sunward and anti-sunward

(Ex) component on the dawn and dusk sides of the tail, respectively. This means that the earthward convection has a tendency to bifurcate at the midnight meridian toward dawn and dusk in a relatively symmetric way. It is also found that the magnitude of Ex is significant even at downtail distances of $R > 15\ R_E$, showing that the bifurcation occurs at much greater distances than predicted by earlier models. The important result is that there are significant differences between the convection patterns of ions (deduced from ion velocity) and magnetic flux (deduced from the electric field) in the near-Earth plasma sheet. This difference suggests that the frozen-in condition does not hold for ions in the near-Earth plasma sheet and thus ions and magnetic fluxes are transported in different ways.

Next, I studied the acceleration and transport processes of energetic particles by investigating spatial and temporal characteristics of flux enhancements of energetic particles and also their correlation with substorm activities on the basis of GEOTAIL HEP-LD observation. I found that some of these flux enhancements exhibit either clear energy-dispersed or dispersionless features in temporal variations of particle fluxes. These characteristics give us import clues to estimate how far away the observation points are from the source of the energetic particles. Using these clues, I examined properties of enhanced energetic particles during substorms. I found that the dispersed events of energetic ions are distributed preferentially on the dusk side, while most of the dispersed electron events are found dawnward of the midnight meridian. On the other hand, the dispersionless events are found only on the night side and are mostly distributed within $R < 15\ R_E$ from the Earth. From these results, it is interpreted that energetic particles forming such flux enhancements are generated on the night side, and subsequently drift azimuthally, and then reach the observation points. A detailed analysis shows that ion dispersionless events are found more frequently than electron events. This fact implies that the acceleration mechanism is less effective for electrons. I also examined their correlation with substorm activities in detail. It was found that almost all of the dispersionless and dispersed events are associated with substorms. The dispersionless flux enhancements occurred within about +/- 2 minutes of the corresponding substorm expansion onset, while all of the dispersed events are preceded by the onset probably due to their finite transport time from the source region. Duration of the observed energy dispersion is consistent with our test particle simulation with the source site assumed at local midnight in the near-Earth plasma sheet. It was also found that some of the dispersed events have a long (~several tens of minutes) energy dispersion, indicating a possibility that energetic particles

occasionally could make a closed drift path around the Earth even at radial distances exceeding the radial limit of the inner magnetosphere.

Contents

Chapter 1

Introduction

1.1 General Introduction

Interplanetary space is not a vacuum but is filled with charged particles in the state of plasma. Interplanetary plasma originates in the solar corona and is called the solar wind. It flows outward at a supersonic velocity and blows against the planets. As a result, the magnetic fields of planets are deformed, and the magnetic field structure called magnetosphere is formed around each planet.

The progress of spacecraft technology made it possible to measure the space plasmas and the magnetic fields in situ, and, following the discovery of the Earth's magnetosphere, we discovered the magnetosphere of other planets in our solar system, such as Mercury, Jupiter, Saturn, Uranus, and Neptune. As shown in Figure 1-1, although they have different spatial scales, there are fundamental similarities between magnetic structures of the different magnetospheres. The similarity indicates that the magnetospheres obey similar laws of plasma physics, and thus we can understand such magnetospheres by studying the Earth's magnetosphere, the one to which we have the easiest access.

The study of The Earth's magnetosphere has progressed rapidly during the last four decades by direct observations using a number of spacecraft. Detailed analyses of the magnetospheric plasmas and fields measured in situ revealed that plasmas of solar wind origin penetrate into the magnetosphere and are then accelerated or heated primarily in the region lying along the equator called "the plasma sheet", which is almost always filled with accelerated plasmas. It was also revealed that these accelerated plasmas can be classified generally into the thermal component and the suprathermal component with regard to their energies, and correspondingly, there are different acceleration and transport processes for them. The former is a major component of the plasma in the plasma sheet and its typical energy and density are about a few keV and ~0.1 /cc, respectively. The thermal plasma plays a main role in

interaction with the ambient magnetic fields, hence their spatial distribution and global transport are closely related to the large-scale field structure of the plasma sheet. In particular, convection of this thermal plasma with magnetic field lines occurs in such a way that the spatial distribution of plasma is consistent with the field configuration. Therefore, in order to understand the structure of the magnetosphere consistently from the particle and field points of view, it is needed to investigate how plasmas are convected globally in the magnetosphere.

On the other hand, the rest (the minor component) is basically classified as a suprathermal component. This component consists of particles with energies from several tens to a few hundred keV and their abundance is negligibly small as compared to the thermal component during geomagnetically quiet times. However, it is known that their presence is significant during geomagnetically disturbed periods. In particular, during the eruptive phenomenon called substorm, explosively generated energetic particles are transported into the inner region of the magnetosphere and then generate a ring current around the Earth which significantly perturbs the geomagnetic field near the Earth. Hence we have to investigate not only the transport processes of the thermal component but also the acceleration mechanisms responsible for the generation of these energetic particles.

After all, in order to understand the dynamics of the magnetosphere comprehensively, it is essential to examine the contributions of both the thermal and suprathermal components of plasmas. Especially during substorms, we have to take energetic particles into account. In this thesis, I study their statistical and global properties by examining typical phenomena responsible for fundamental transport of each particle population. The principal mechanism causing the transport of thermal plasma in the plasma sheet is plasma convection, and we make a statistical study on it. For the suprathermal component, we study the flux enhancements of energetic particles in the magnetosphere in association with substorm activities.

For these studies, we have used particle data obtained by the GEOTAIL spacecraft. The outlook of GEOTAIL is given in Figure 1-2. GEOTAIL was launched in July, 1992 as a joint project between Institute of Space and Astronautical Science (ISAS) in Japan and NASA. In the first half of its mission time, GEOTAIL was put into a long elliptical orbit to explore the distant magnetotail. In the second orbital phase, GEOTAIL was put into a near-Earth orbit and has been surveying the near-Earth plasma sheet ($9\ R_E < R < 30\ R_E$, R_E: Earth radius ~ 6378 km). The simultaneous observation of both thermal and energetic particles carried out onboard the GEOTAIL

spacecraft enables us a statistical study using both of thermal and suprathermal data.

In this dissertation, I investigate typical magnetospheric phenomena relating to the transport processes of thermal and suprathermal components of plasmas, using the data obtained by the GEOTAIL spacecraft, and discuss the fundamental processes of plasma acceleration and subsequent transport in the magnetosphere.

1.2 The Sun, the Solar Wind, and Interplanetary Magnetic Field (IMF)

The Sun is a typical main sequence star closest to the Earth and it provides particles and fields that are responsible for electromagnetic phenomena occurring near the Earth. The Sun has an atmosphere consisting of hot fully ionized gas. Its outermost part, called the solar corona, whose temperature is about a few million K, expands steadily into interplanetary space since the solar corona cannot be in hydrostatic equilibrium because of its high temperature. This ionized gas flowing through interplanetary space is called the solar wind. The solar wind consists of protons, electrons, and other minor ion species, its composition being similar to that of the solar corona. The solar wind density and temperature decrease with increasing distance from the Sun and are about ~ 10 /cc and ~ 10^5 K near the Earth, respectively. The coronal gases obtain supersonic speeds and the solar wind arrives at the Earth with a speed of several hundred km/sec.

The Sun is a magnetic star and the solar corona is threaded with the Sun's magnetic fields. Since magnetic fields are generally frozen-in to a high conductivity media such as the solar wind, the solar wind pulls out solar corona magnetic fields away from the Sun. Interplanetary magnetic field (IMF) observed near the Earth originates in the Sun's magnetic field. The intensity of IMF is usually about several nanotesla (nT) in interplanetary space near the Earth's orbit.

1.3 The Earth's Magnetosphere

The magnetosphere is a typical magnetic structure induced around a magnetized planet by interaction of the planetary magnetic field with the stellar wind from a star close to the planet. In the case of the Earth, the stellar wind is the solar wind and the planetary magnetic field is the geomagnetic field. The basic features of the Earth's magnetosphere, deduced from many years of observations, are summarized in Figure 1-3. In this figure, the solar wind hits the geomagnetic field and deforms it, so that the

magnetic cavity (magnetosphere) as shown in Figure 1-3 is formed around the Earth. The boundary that separates the magnetosphere from interplanetary space is called the magnetopause.

The Earth's magnetosphere is not spherically symmetric; it is compressed by the solar wind on the side facing the solar wind (namely dayside), while it is elongated on the night side, forming a "magnetotail" extending more than a thousand earth radii behind the Earth. Since the solar wind is supersonic, a bow shock is formed in front of the magnetosphere as shown in Figure 1-3. The field lines in the northern (southern) hemisphere of the magnetotail are directed almost sunward (anti-sunward), and the region containing the sunward (anti-sunward) field lines is called northern (southern) lobe. Between the northern and southern lobes, there is a region filled with a hot plasma with its plasma pressure balancing the lobe magnetic pressure, called the plasma sheet.

1.4 The Open Model of the Magnetosphere and Reconnection

Spacecraft observations revealed that most of the magnetospheric phenomena are controlled by the solar wind and the associated interplanetary magnetic field (IMF). This indicates that both the solar wind plasma and IMF penetrate into the magnetosphere. In other words, the magnetosphere is partially "open" to interplanetary space, and one of the mechanisms responsible for the interaction between the solar wind and the magnetosphere is magnetic reconnection between IMF and the geomagnetic field. Incorporating two magnetic reconnection sites, *Dungey* [1961] proposed an open magnetospheric model, which has been widely accepted by researchers for the last four decades. This magnetosphere model is shown schematically as a cut along the noon-midnight meridian plane in Figure 1-4. According to this model, the magnetic reconnection between IMF and the geomagnetic field occurs on the dayside magnetopause. The magnetic reconnection creates field lines one end of which is connected to the polar region of the Earth, while another end extends into interplanetary space. They are called open field lines. This kind of field line is convected tailward around the Earth and stored in the magnetotail to form lobe magnetic fluxes. Another reconnection site is operative in the distant region of the magnetotail beyond the lunar orbit (~ 60 R_E). The field lines in the northern and southern lobes are reconnected there and the resultant closed field lines are convected earthward in the magnetosphere.

1.5 Magnetospheric Convection

1.5.1 Global Circulation of Plasma and Magnetic Fluxes

The two magnetic reconnection sites stated above induce large-scale plasma convection in the magnetosphere, which is called magnetospheric convection. The dayside reconnection transfers magnetic fluxes from the dayside magnetosphere to the magnetotail. In the magnetotail, the lobe magnetic fluxes are convected from both the northern and southern lobes toward the plasma sheet. The magnetic reconnection in the distant tail drives earthward convection of the plasma and magnetic fluxes, and transfers them through the near-Earth plasma sheet to the dayside magnetosphere. In this way, the magnetospheric convection is responsible for large-scale circulation of the plasma and magnetic flux in the magnetosphere.

1.5.2 Plasma Convection in the Near-Earth Plasma Sheet

As expected from Dungey's magnetosphere model, a sunward convection is induced in the equatorial region of the magnetosphere by reconnection occurring in the distant tail. Particularly in the near-Earth plasma sheet, this sunward (earthward) convection is induced almost always, and is primarily responsible for plasma transport to the inner magnetosphere as well as to the dayside region. In addition to the plasma transport, the earthward convection transports magnetic fluxes frozen-in to the ambient plasma. Therefore we need to examine global properties of the earthward convection such as the overall convection pattern to understand plasma and field structures in the magnetosphere.

Before direct survey of convective flows in the magnetosphere using spacecraft began, the global profile of magnetospheric convection was only inferred from the distribution of electric fields in the polar ionosphere. Because of the high electrical conductivity parallel to the field lines in the Earth's magnetosphere, such ionospheric convection pattern can be mapped to the equator along field lines and the equatorial convection pattern was inferred. The appearance of more realistic magnetic field models [e.g. *Tsyganenko*, 1989] led to more quantitative mapping between the ionosphere and the equatorial region of the magnetosphere. One of the more realistic models of the convection pattern in the near-Earth magnetotail [*Donovan and*

Rostoker, 1991] is shown in Figure 1-5. The tail plasma convection is directed generally sunward, is fairly uniform across the tail, and splits dawnward and duskward almost symmetrically as the flow approaches the Earth ($R < 10\ R_E$). It should be noted, however, that the present status of magnetospheric magnetic field models may not be realistic enough to allow a precise mapping between the ionosphere and the plasma sheet in the magnetotail, thus details of the convection pattern in the equatorial magnetosphere were still uncertain. Therefore direct satellite observations are needed to study the equatorial convection pattern in the near-Earth plasma sheet.

In the last two decades, several spacecraft were launched to study convective flows in the near-Earth plasma sheet, but none accomplished sufficiently quantitative and realistic models owing to absolute shortage of time spent on the statistical survey of plasma sheet flows. This is because a spacecraft can observe plasma flows only at a fixed point in the vast special scales of the magnetosphere at a given instant and hence a huge amount of observations are needed to survey all portions of the near-Earth plasma sheet. The GEOTAIL spacecraft has been surveying the near-Earth plasma sheet and already completed the extensive survey of the near-Earth plasma sheet for several years. Such plenty of survey data enable us to study global profiles of convective flows in the plasma sheet in detail. Using these data obtained by GEOTAIL, I have constructed a more reliable convection pattern in the near-Earth plasma sheet. I have also derived plasma flow pattern and the distribution of plasma pressure, which makes it possible to derive the associated convection electric field. These results are presented in Chapter 2 in the present thesis.

1.6 Magnetospheric Substorm

1.6.1 Near-Earth Neutral Line Model

The plasma convection has often been discussed to account for rather quasi-stationary aspect of the magnetosphere, such as the global structure of the magnetosphere. However, the magnetosphere also has a dynamic aspect yielding intermittent energy conversion. In particular, such an energy conversion process occurs sometimes very explosively and, as a result, causes global perturbation in the geomagnetic field and enhances plasma transport in the magnetosphere. This phenomenon affecting the whole magnetosphere is called substorm. One of the most accepted models for the generation of substorms is Near-Earth Neutral Line model

(NENL model) proposed by *Hones* [1977]. The temporal evolution of the plasma sheet configuration on the night side is illustrated schematically on the noon-midnight meridian plane in Figure 1-6. As shown in Figure 1-6, reconnection develops in the near-Earth plasma sheet (see the second panel of the Figure 1-6). This reconnection process converts the lobe magnetic energy explosively into the kinetic energy of the plasma in the plasma sheet and results in a large-scale transport of plasma and magnetic fluxes in the plasma sheet both in the earthward and anti-earthward (tailward) direction. The reconnection site itself is transported tailward and then the magnetosphere recovers gradually to its quiet, more relaxed state. As a result, the plasma and magnetic fluxes are transported in the earthward direction earthward of the reconnection site, while transported in the tailward direction on the tailward side of the reconnection site.

1.6.2 Energetic Particle Injection

In the course of substorms, particles are energized to energies as high as several hundred keV in the magnetotail and subsequently transported earthward with a large velocity of ~ several hundred km/sec. This energetic population is injected into the inner region of the magnetosphere, and then observed as a sudden flux enhancement of energetic particles at several tens to hundreds of keV, for example, at geosynchronous orbit. As a result, these injected energetic particles modify properties of the local particle distributions drastically, and also induce a large-scale current system providing significant perturbation even in the strong geomagnetic field near the Earth. Accordingly, the generation mechanism of these energetic particles and their transport processes in the magnetosphere are main subjects of research for understanding the magnetospheric substorm.

One of the most remarkable results obtained by geosynchronous observations is that particle flux enhancements are often observed simultaneously at different energies around local midnight, while away from the midnight, they are observed as successive flux enhancements starting from higher energies down to lower energies, that is, they are dispersed in energy [e.g., *Walker et al.*, 1976; *Baker et al.*, 1978; *Belian et al.*, 1978]. These two types of flux enhancements have been interpreted as follows: In the source region of those energetic populations, the acceleration process generates particles with different energies simultaneously and therefore they are observed with little dispersion, while away from the source region, the particles with

different energies arrive at the observation points at different times because of their difference in the transport speed caused by the energy-dependent gradient- and curvature-B drifts. Thus the conclusion was reached that energetic particles were injected around the midnight sector at the time of substorm expansion onset, and were supplied to the other local time sectors by their energy-dependent drift effects. On the other hand, the acceleration mechanisms are still controversial, and there have been various models including the ones based on the NENL model [e.g., *Baker et al.*, 1979] and the current disruption models [e.g., *Lui et al.*, 1988].

Properties of energetic particles in the near-Earth plasma sheet have attracted researcher's interests because the near-Earth plasma sheet is important as a source region of energetic particles injected into the inner magnetosphere. In order to clarify detailed transport processes of energetic particles and to inspect the validity of the above acceleration models, it is essential to examine energetic particle enhancements in the near-Earth plasma sheet on a global scale. However, the past studies made only case studies of typical events, or they have been limited to a statistical study on the general correlation with geomagnetic activities. Thus, in the present study, I shall make a statistical study on such flux enhancement events to investigate spatial and temporal characteristics of the energetic particle enhancements that occur during substorms. Taking these results into account, I shall discuss in Chapter 3 the acceleration mechanisms and global transport processes of energetic particles in the course of substorms.

1.7 Contents of This Dissertation

The aim of this dissertation is to examine global features of plasmas in the magnetosphere and to study the fundamental processes of plasma energization and transport. In order to attain this purpose, I shall utilize the plasma and magnetic field data obtained by the GEOTAIL spacecraft. In particular, by using both low energy (namely, thermal energy) and high energy particle data, I shall extend my study to a wide energy range of plasmas in the magnetosphere, and thereby discuss the global transport processes for magnetospheric plasma.

In order to do that, I pay my attention to the two typical phenomena observed in the magnetosphere. One is plasma convection in the near-Earth plasma sheet. This large-scale convection induced in the plasma sheet is primarily responsible for the plasma transport in the magnetosphere. By studying it, I can understand the global

profile of transport processes responsible for the bulk motion of the magnetospheric plasma. Another typical phenomenon is the flux enhancement of energetic particles observed in the outer magnetosphere during substorms. Because energetic populations play a significant role in the substorm-associated features observed in the magnetosphere, the study of their transport processes and also energization mechanisms provides us a key to understand temporal, but significant transport effects associated with substorms.

In Chapter 2, I study the properties of thermal ions, that is, average profiles of plasma flows and convection electric field induced by the general interaction between the magnetosphere and the solar wind. The ion bulk flows and the field structures are examined using the data obtained in the plasma sheet by GEOTAIL to construct statistically the convection flow pattern and also global profiles of the convection electric field and plasma pressure in the near-Earth plasma sheet. It is shown that the ion flow pattern is not symmetric about the noon-midnight meridian, while the convection electric field driving the ion bulk flow is symmetric in the dawn-dusk direction. Accordingly, the important conclusion is drawn that this discrepancy between ion flows and convection electric field implies the violation of the frozen-in assumption of thermal ions in the plasma sheet.

In Chapter 3, I investigate properties of energetic particles by studying flux enhancements of energetic particles in the outer magnetosphere during substorms. I examine two typical types of particle flux enhancements, that is, dispersionless and dispersed flux enhancements found in the outer magnetosphere ($R > 9\ R_E$), and show that they can be reasonably explained by assuming that these energetic particles are generated around the local midnight sector, and subsequently drift away from midnight and are supplied to whole local time sectors in the magnetosphere. Its implication for the global plasma transport associated with substorms is also discussed.

In Chapter 4, I discuss the global transport processes for both thermal and suprathermal plasmas in the magnetosphere. I also examine their relation to the state of the magnetosphere.

In Chapter 5, I summarize the present study and draw a general conclusion relating to the global plasma transport in the magnetosphere.

References

Baker, D. N., P. R. Higbie, E. W. Hones Jr., and R. D. Belian, High-resolution energetic particle measurements at 6.6 R_E: 3. Low-energy electron anisotropies and short-term substorm substorm predictions, *J. Geophys. Res., 83*, 4863, 1978.

Baker, D. N., R. D. Belian, P. R. Higbie, and E. W. Hones, High-energy magnetospheric protons and their dependence on geomagnetic and interplanetary conditions, *J. Geophys. Res., 84*, 7138, 1979.

Belian, R. D., D. N. Baker, P. R. Higbie, and E. W. Hones Jr., High-resolution energetic particle measurements at 6.6 R_E: 2. High-energy proton drift echos, *J. Geophys. Res., 83*, 4857, 1978.

Donovan, E. F., and G. Rostoker, Internal consistency of the Tsyganenko magnetic field model and the Heppner-Maynard empirical model of the electric field distribution, *Geophys. Res. Lett., 18*, 1043, 1991.

Dungey, J. W., Interplanetary magnetic field and the auroral zones, *Phys. Rev. Lett., 6*, 47, 1961.

Hones, E. W., Jr., I. D. Palmer, and P. R. Higbie, Energetic protons of magnetospheric origin in the plasma sheet associated with substorms, *J. Geophys. Res., 81*, 3866, 1977.

Lui, A. T. Y., R. E. Lopez, S. M. Krimigis, R. W. McEntire, L. J. Zanetti, and T. A. Potemra, A case study of magnetotail current sheet disruption and diversion, *Geophys. Res. Lett., 15*, 721, 1988.

Nishida, A., The GEOTAIL Mission, *Geophys. Res. Lett., 21*, 2871, 1994.

Parks, G. K., Physics of Space Plasmas An Introduction, *Addison-Wesley Publishing Company*, Redwood City, 1991.

Tsyganenko, N. A., Global quantitative models of the geomagnetic field in the cislunar magnetosphere for different disturbance levels, *Planet. Space Sci., 35*, 1347, 1987.

Tsyganenko, N. A., Magnetospheric magnetic field model with a warped tail current sheet, *Planet. Space Sci., 37*, 5, 1989.

Figure captions

Figure 1-1. Fundamental similarities in magnetospheric configurations of the planets in the solar system and some celestial objects in the Universe. (Adopted from *Parks* [1991].)

Figure 1-2. Outlook of the GEOTAIL spacecraft. (Adopted from *Nishida*, 1994.)

Figure 1-3. Three-dimensional shape of the Earth's magnetosphere. The basic particle and magnetic field features are representative of other planetary magnetospheres although the details can be different.

Figure 1-4. Magnetic field topology for the noon-midnight meridian plane in Dungey's open magnetosphere model. The Earth's closed field lines (marked by 1) are connected with the IMF (marked by 2) on the dayside. The open field lines (marked by 3 and 4) are carried by the solar wind tailward and reconnect with each other on the night side neutral line. After that, The Earth's closed field lines are conveyed sunward. (Adopted from *Lyons and Williams* [1984].)

Figure 1-5. A realistic model of the convection pattern in the near-Earth magnetotail derived by *Donovan and Rostoker* [1991]. The contour lines in the figure show the constant electric potential lines mapped from the Heppner-Maynard ionospheric electric field model using the Tsyganenko 1987 (top panel) and 1989 (bottom panel) magnetic field model [*Tsyganenko*, 1987; 1989].

Figure 1-6. Development of the near-Earth reconnection and plasmoid formation in the magnetotail. N represents the distant neutral line, and N' represents the near-Earth neutral line. This neutral line is newly formed in the near-Earth region during a substorm. (Adopted from *Hones* [1977].)

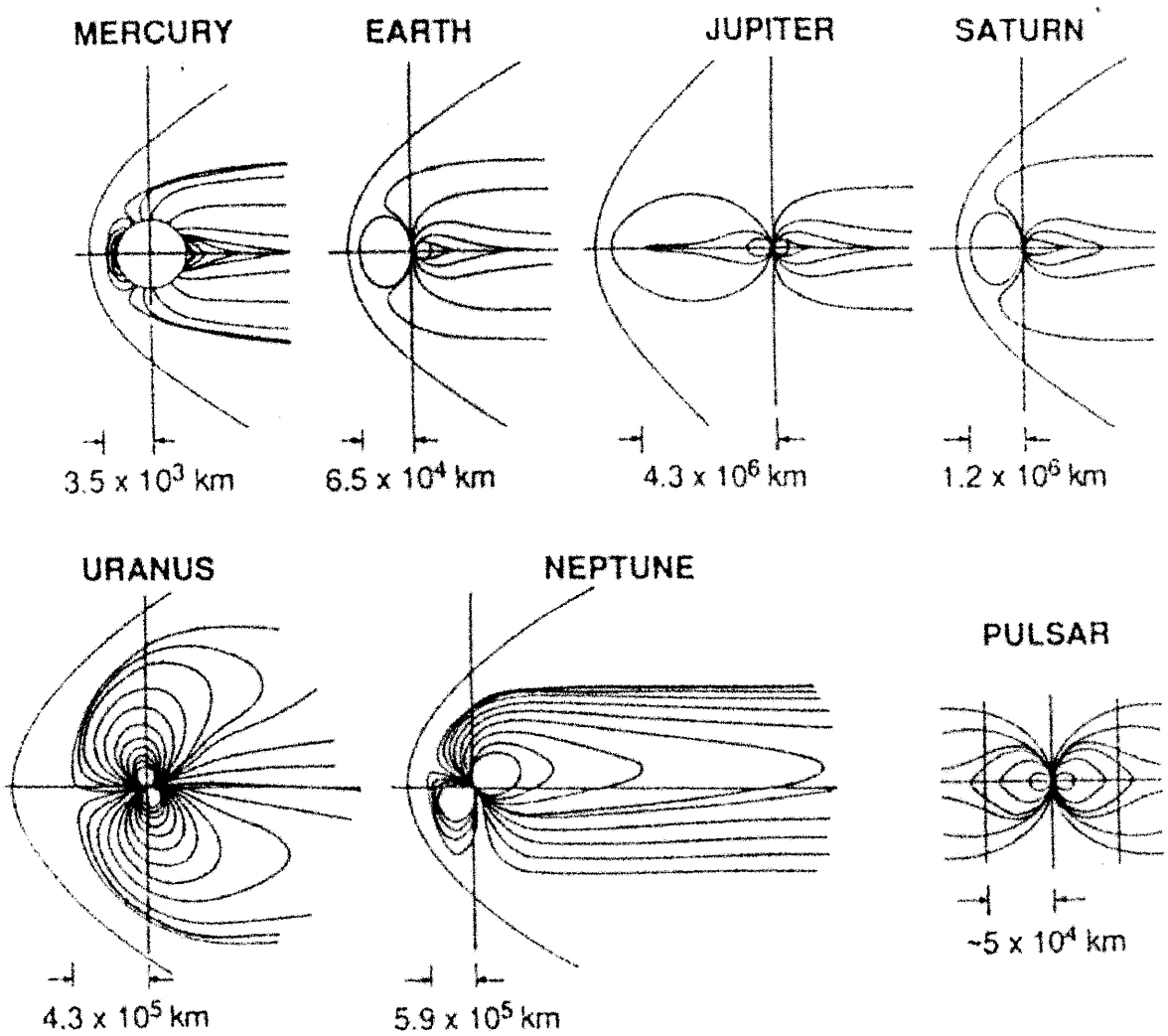
MERCURY
EARTH
JUPITER
SATURN
3.5 x 10^3 km
6.5 x 10^4 km
4.3 x 10^6 km
1.2 x 10^6 km
URANUS
NEPTUNE
PULSAR
4.3 x 10^5 km
5.9 x 10^5 km
~5 x 10^4 km

Figure 1-1

Figure 1-2

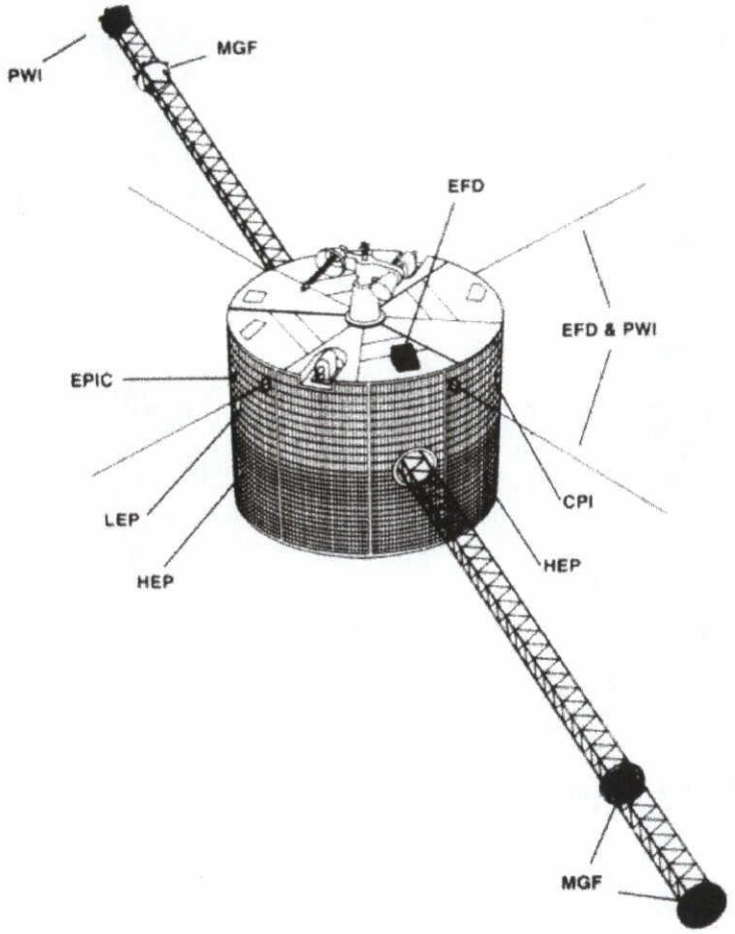

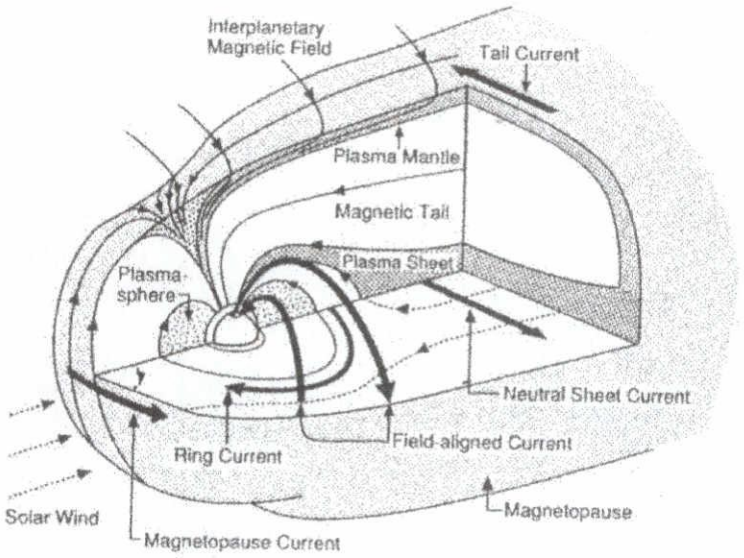
Interplanetary
Magnetic Field
Tail Current
Plasma Mantle
Magnetic Tail
Plasma Sheet
Plasma-
sphere
Neutral Sheet Current
Field-aligned Current
Ring Current
Solar Wind
Magnetopause
Magnetopause Current

Figure 1-3

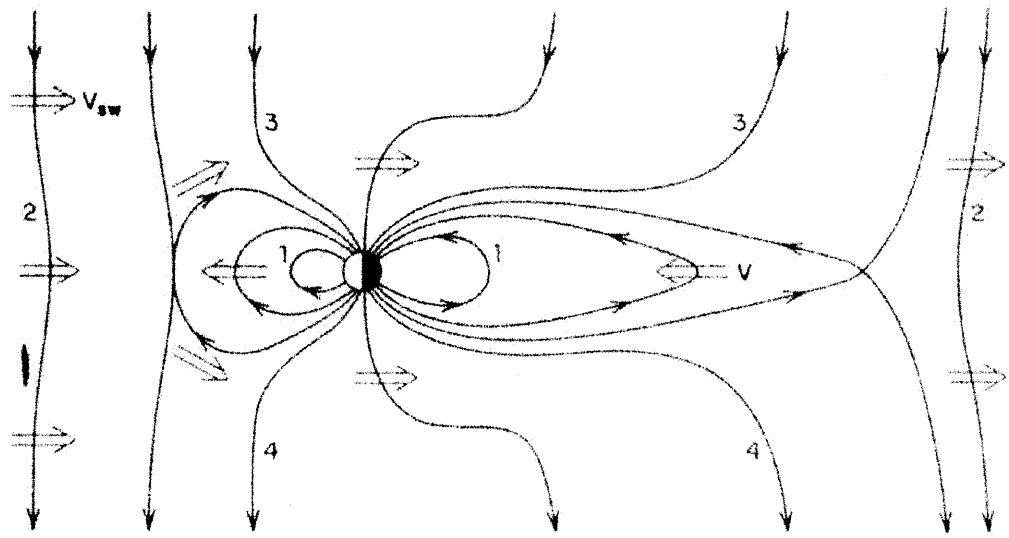

Figure 1-4

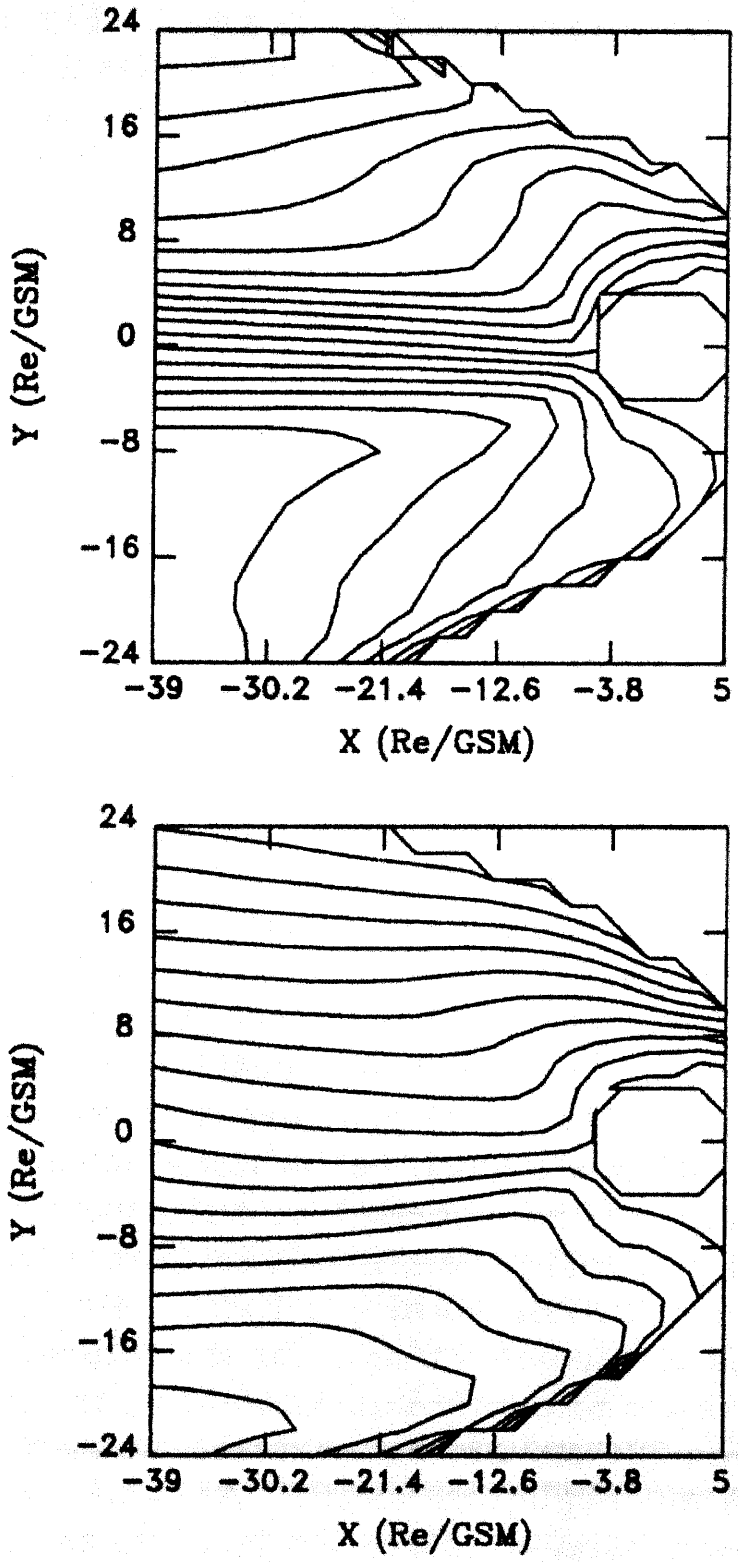
24
16
8
0
-8
-16
-24
Y (Re/GSM)
-39
-30.2
-21.4
-12.6
-3.8
5
X (Re/GSM)
24
16
8
0
-8
-16
-24
Y (Re/GSM)
-39
-30.2
-21.4
-12.6
-3.8
5
X (Re/GSM)

Figure 1-5

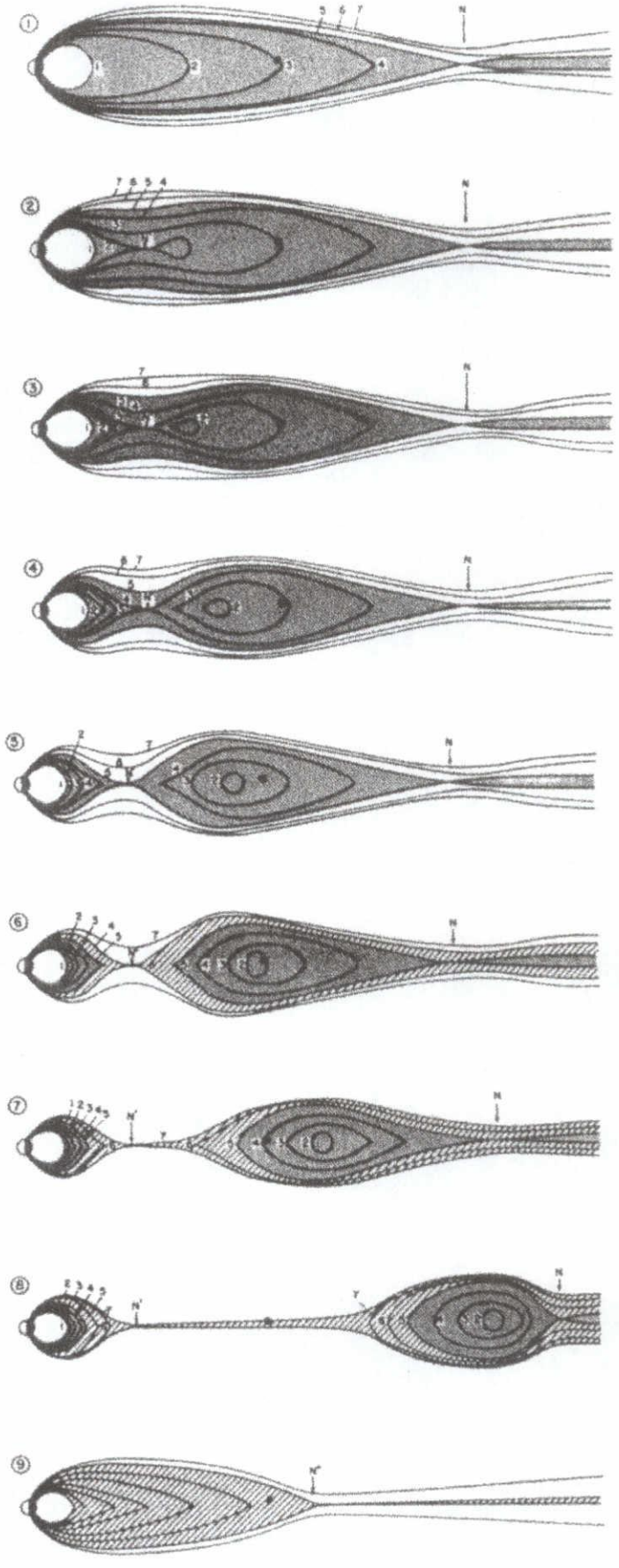

Figure 1-6

Chapter 2

Average Profile of Ion Flow and Convection Electric Field in the Near-Earth Plasma Sheet

Abstract

Two-dimensional distribution of ion flow and convection electric field in the near-Earth plasma sheet (-28 < X< 0 R_E) is obtained statistically on the basis of plasma and magnetic field measurements on board the GEOTAIL spacecraft. Our result confirms that the average ion flow in the plasma sheet has a significant duskward component in the local midnight to dusk side regions, but is directed almost sunward on the dawn side. Since this asymmetry probably resulted from the contribution of ion pressure gradient drift, we estimated the true distribution of convection electric field by correcting the observed $V \times B$ field by the observed ion pressure gradient. The convection electric field thus obtained has following characteristics: (1) In addition to the positive y component of the electric field representing the sunward convection, the electric field has a significant x-component (Ex) which has opposite signs on the dawn and dusk sides of the tail. This means that the earthward convection has a tendency to bifurcate at the midnight meridian toward dawn and dusk in a relatively symmetric way. (2) The magnitude of Ex is significant even at downtail distances of R > 15 R_E, showing that the bifurcation occurs at much greater distances than predicted by earlier models. (3) Existence of significant differences between the convection patterns of ions (deduced from ion velocity) and magnetic flux (deduced from the electric field) suggests that the frozen-in condition does not hold for ions in the near-Earth plasma sheet.

2.1 Introduction

Before direct survey of convective flows in the deep magnetosphere became available, the global profile of magnetospheric convection was inferred from the distribution of high-latitude electric fields near the Earth. *Heppner and Maynard* [1987] developed a model ionospheric convection pattern (called H-M model) at high latitudes by analyzing electric field measurements from the DE-2 satellite. Their result confirmed that anti-sunward convection dominates in the polar cap, and that, at the position where the anti-sunward convection meets the nightside auroral oval, the convection tends to bifurcate and turn either eastward or westward, thereby producing return flows to the dayside along the auroral oval. The return part of the ionospheric convection corresponds to the sunward plasma convection in the equatorial region of the magnetosphere as expected from open magnetosphere models [e.g. *Dungey*, 1961].

Because of the high electrical conductivity parallel to field lines in the Earth's magnetosphere, the ionospheric convection pattern can be mapped to the equator along field lines. *Atkinson* [1984] presented a schematic view of the equatorial projection of the ionospheric convection pattern and discussed the source regions of field-aligned currents. *Donovan and Rostoker* [1991] and *Maynard et al.* [1995] constructed more realistic convection patterns in the near-Earth magnetotail by projecting the observed electric field (H-M model) along the model magnetic field [*Tsyganenko* 1987; 1989]. According to their result for the *Tsyganenko* [1989] (T89) model, the tail plasma convection is directed generally sunward, is fairly uniform across the tail, and splits dawnward and duskward almost symmetrically as the flow approaches the Earth ($R < 10\ R_E$). It should be noted, however, that the present status of magnetospheric magnetic field models may not be realistic enough to allow a precise mapping between the ionosphere and the magnetosphere, and thus details of the convection pattern in the equatorial magnetosphere are still uncertain. It is desirable to study the equatorial convection pattern directly from satellite observations.

Direct observation of plasma flows in the near-Earth plasma sheet has been reported from instruments on board ISEE 2 and AMPTE/IRM spacecraft. Statistical studies have been made mainly for geomagnetically quiet times [*Angelopoulos et al.*, 1993; *Zhu*, 1993]. These statistics showed that the average flow in the central

plasma sheet is predominantly directed duskward at local midnight and on the dusk side, while it is weak and directed almost sunward on the dawn side. Thus a dawn-dusk asymmetry existed in the flow pattern for the central plasma sheet. The average flow speed was of the order of tens of kilometers per second. *Angelopoulos et al.*, [1993] also found that the above flow pattern was expressible as a sum of the sunward E×B drift and the duskward diamagnetic drift. In their study, the convection electric field was assumed to be directed dawn to dusk, and derived from an ensemble average of the x component of the observed flow velocity and the z component of the magnetic field, while the diamagnetic drift was calculated from the electric current estimated from the curl of a model magnetic field (T87 model, [*Tsyganenko*, 1987]). The extent of the current layer over which the diamagnetic drift was averaged was determined in such a way that the calculated flow speed agrees with the observed one. Thus their study only indicated a possibility that the observed flow pattern could be decomposed into the earthward E×B drift and the model diamagnetic drift. In order to confirm this possibility observationally, the E×B drift and the diamagnetic drift should be derived directly from actual measurements of plasma velocity, pressure, and magnetic field. This is what we aim at in the present paper.

2.2 Data and Method

For the present analysis, we use ion moments (the ion density Ni, temperature Ti, and the three components of the ion bulk velocity (Vx, Vy, Vz) obtained from the LEP instrument on board the GEOTAIL spacecraft, and the three magnetic field components (Bx, By, Bz) obtained from the MGF instrument. Detailed information on these instruments has been given by *Mukai et al.* [1994] and *Kokubun et al.* [1994], respectively. One-minute averages are used throughout. All the vector components are transformed into the Aberrated Geocentric Solar Magnetospheric (AGSM) system assuming a 4-degree aberration angle. In this coordinate system, the X-axis is rotated clockwise by 4 degree from the Sun-Earth line so that the X-axis is aligned with the nominal solar wind direction in the Earth's rest frame, that is, the central axis of the magnetotail. The sign convention for the X-axis is such that it is positive sunward. The Y-axis is defined as the vector product of the X direction and the Earth's dipole moment, and the Z-axis completes the right handed Cartesian coordinates.

We identified the plasma sheet measurements by the presence of a hot, tenuous plasma, which is operationally defined to be of ion density less than 1.0 /cc and ion

temperature exceeding 1.0 keV. We restricted ourselves to the central portion of the plasma sheet by additionally requiring either that the magnetic field elevation angle (the angle between the B vector and the X-Y plane) was larger than 30 degree or that the absolute value of Bx was smaller than half the lobe field intensity estimated from the T89 model for Kp=2. We analyzed only the central portion of the plasma sheet defined in this way to avoid the contamination from the plasma sheet boundary layer, which may have different characteristics from the main body of the plasma sheet.

Figure 2-1 shows the GEOTAIL orbit on the X-Y plane during Oct. 1994 to Dec. 1997. The thick dashed curve in the figure shows the nominal magnetopause in the equatorial plane. In the present study, the extent of our analysis is limited in x coordinate to $0 > X_{AGSM} > -28\ R_E$, where GEOTAIL had a good coverage of the plasma sheet, and in y coordinate to $|Y_{AGSM}| < 18\ R_E$ to avoid magnetopause crossings. The analyzed region is shown by the black rectangle in Figure 2-1. We divided this rectangular region into 14×18 bins each having a $2\ R_E \times 2\ R_E$ area. Observed quantities were first averaged in each X-Y bin and then a low-pass spatial filter was applied in such a way that a weighted mean of 3×3 bins was assigned to the bin at the center. The weight ratio was 2:1 between the central bin and each of the surrounding eight bins. During the period Oct. 1994 to Dec. 1997, a total of 499,676 individual data points (1-min values) were available in the central plasma sheet, with an average of 3084 measurements for one X-Y bin. In order to maintain the reliability of statistics, only those X-Y bins for which more than 500 data points were classified as the central plasma sheet were utilized for statistics.

2.3 Results

2.3.1 Ion flow pattern

Figure 2-2 shows the distribution of ion flow vectors in the analyzed area. Ion velocities plotted here have been obtained assuming that all detected ions are protons [*Mukai et al.*, 1994]. It is apparent that the average flow has a positive X component, i.e., is directed sunward, everywhere in the region studied here. The magnitude of Vx decreases with increasing X, indicating that the sunward flow obtained above is generally decelerated as the flow approaches the Earth. At the midnight meridian, for example, the magnitude of Vx amounts to 110 km/s at $X = -25\ R_E$ but decreases to only 20 km/s at $x = -12\ R_E$. It is also apparent that the ion flow has a significant y

component (Vy) which is asymmetrically distributed around the midnight meridian, as has been pointed out by *Angelopoulos et al.*[1993]. Vy is large and pointed duskward from local midnight to the dusk flank, but is small and pointed dawnward on the dawn side. The dawnward component on the dawn side is so small that the flow does not deviate much from the sunward direction. On the other hand, the duskward component on the dusk side is comparable to, or even exceeds the sunward component, leading to a large deviation of flow vectors from the sunward direction. Both dawnward and duskward components become small in magnitude at the tail flanks.

2.3.2 Ion pressure distribution and pressure gradient drift

Although the average flow vectors shown in Figure 2-2 constitute a systematic flow pattern, individual velocity data sampled in each bin have large variance (standard deviation) about the mean values shown in the figure. Therefore the plasma sheet flow pattern obtained above should be interpreted to be averages over relatively large velocity variations inherent to the plasma sheet flow, as was pointed out by *Angelopoulos et al.* [1993].

Our goal in the present paper is to derive the average distribution of convection electric field in the near-Earth plasma sheet. At first, it may seem easy to estimate the convection electric field from the vector product of V and B, both of which can be derived from our GEOTAIL measurements. However, as has been pointed out earlier, both the pressure gradient drift and the E×B drift contribute to the ion bulk velocity observed. Therefore, prior to obtaining the equatorial distribution of the electric filed, we should first study the distribution of ion pressure on the X-Y plane. Figure 2-3 shows the X and Y dependence of ion pressure for a few representative X and Y ranges. The ion pressure has been derived as a product Pi = Ni k Ti, where Ni and Ti are the observed ion density and temperature, respectively, and k is the Boltzmann constant. The ion density and temperature have been averaged for the same set of data points as used for the statistics of flows. The top panel shows the X dependence of Pi for the midnight and an off-midnight Y range, i.e., $|Y| < 2\ R_E$ and $8 < |Y| < 10\ R_E$, respectively. The ion pressure is an increasing function of X both near and away from the midnight meridian [*Spence et al.*, 1989; Angelopoulos et al., 1993]. At the midnight meridian ($|Y| < 2\ R_E$), the ion pressure gradient is greatly enhanced close to the Earth, while it is only gradually increased in the region away from the midnight meridian. The bottom panel of Figure 2-3 shows the y-dependence of the ion pressure

for two representative X positions, i.e. -16 R_E <X< -14 R_E (shown as a dotted line) and -24 R_E <X< -22 R_E (shown as a solid line). It is clearly seen that the ion pressure in the plasma sheet is peaked around local midnight (with a possible shift toward dawn for the X interval of -16 R_E <X< -14 R_E), and decreases gradually toward the dawn and dusk flanks for both X ranges.

Once the ion pressure distribution is obtained, the pressure gradient drift $V_{\nabla P}$ can be estimated from the observed values of ion density and magnetic field (not shown). For example, at the position X = -15 R_E in Figure 2-3, the maximum values of $\partial P_i / \partial X$ and $\partial P_i / \partial Y$ are about 0.031 nPa/R_E (at midnight) and 0.011 nPa/R_E (at Y= 3 R_E), respectively. From the ion density of 0.3 /cc and the Bz component of 5.7 nT for both bins, we get $V_{\nabla P\,x}$ = 6.3 km/s and $V_{\nabla P\,y}$ = 18 km/s. The Y-component of the pressure gradient drift $V_{\nabla P\,y}$ obtained at midnight provides 45 % of the duskward component of the average ion flow velocity (~40 km/s) obtained at the same location in Figure 2-2. On the other hand the X-component, $V_{\nabla P\,x}$, obtained at Y = 3 R_E provides only 12 % of the sunward component of the average ion flow velocity (~55 km/s) obtained at the same bin.

2.3.3 Convection electric field

Now we can derive the average electric field vectors by correcting the ion flow vectors obtained in Figure 2-2 for the two-dimensional pressure gradient whose cuts have been presented in Figure 2-3. From the ion equation of motion, assuming a quasi-steady state ($\partial V / \partial t \sim 0$) and also assuming that the convective derivative term is negligible, the average electric field can be calculated according to the formula

$$<E> \;=\; -<V \times B> + \nabla <Pi> / e<Ni>,$$

where V, B, Pi, Ni, and e are ion bulk velocity, magnetic field, ion thermal pressure, ion density, and the electron charge, respectively. The brackets (< >) in the formula shows that the observed quantities are averaged for each X-Y bin and then low-pass filtered. The pressure gradient at each bin is evaluated by numerical differentiation using the centered difference scheme. In the present study, only the X and Y components of the electric field are discussed because the spatial coverage of the spacecraft in the Z direction is not enough to derive statistically significant pressure gradient in the Z direction. We use the $\nabla <Pi>/e<Ni>$ term as an approximation to

its exact counterpart $<\nabla Pi / e Ni>$.

The resultant electric field vectors are plotted in Figure 2-4. As expected, the average electric field vectors in the central plasma sheet have a positive Y-component (Ey) everywhere in the plotted region indicating the presence of the sunward convection in the plasma sheet. The sunward convection is strongest (Ey = 0.2 mV/m) at local midnight and becomes weak away from the midnight meridian toward dawn and dusk.

It is found that, in addition to Ey, the electric field has a significant x-component (Ex). Ex is positive (directed earthward) on the dawn side and is negative (directed tailward) on the dusk side, indicating that the convection flow tends to bifurcate with one branch deviating duskward and the other branch deviating dawnward, avoiding the Earth. We should note, however, that a significant Ex component exists not only near the Earth, but also at considerable distances down the tail ($X<-15\ R_E$) in the region not far from the midnight meridian (around $|Y| < 5\ R_E$, for example). This result indicates that the convection toward the Earth begins to bifurcate at positions much farther away from the Earth than expected from the past studies [e.g. *Maynard et al.*, 1995].

Figure 2-5 shows quantitatively how much the V×B term and the pressure gradient term in formula (1) contribute to the average electric field shown in Figure 2-4. Figure 2-5a and Figure 2-5b show contributions of the two terms at $X = -15\ R_E$ to Ex and Ey, respectively. Figure 2-5a shows that the x component of the V×B term (represented by a solid line) is large and negative for local midnight to dusk side regions, but is almost zero on the dawn side. This asymmetry is consistent with the dawn-dusk asymmetry of the ion flow pattern noted before (see Figure 2-2). However, this asymmetry is largely compensated by the X-gradient of the ion pressure given by a dashed line. The x component of the pressure gradient is always positive so that it partially cancels the x component of the V×B term in the dusk to midnight regions and augments it on the dawn side. As a result of the summation of these two terms, the resultant Ex (dotted line) has opposite signs but similar magnitudes on the dawn and dusk sides of the midnight meridian, producing a rough mirror symmetry (precisely speaking, antisymmetry) about the midnight meridian. On the other hand, as can be seen from Figure 2-5b, Ey (dotted line) is dominated by the V×B term (solid line). The magnitude of Ey is almost constant for the y range of $-15< Y < 10\ R_E$, and becomes small near the tail flanks, particularly on the dusk side. Summing up, the global distribution of the electric field vectors is fairly mirror-symmetric about the

midnight meridian with the Ex component having opposite signs on the dawn and dusk sides.

2.3.4 E×B drift pattern

Two-dimensional distribution of the E×B drift vectors obtained from the calculated E vectors is given in Figure 2-6. X and Y components of the E×B drift are evaluated at the tail mid plane by dividing the observed <Ey> and <Ex> by <Bz>, respectively, assuming that the magnetic field has only the Z component at the tail mid plane. Note that this evaluation involves another approximation that <Ex/Bz> is replaced by <Ex>/<Bz>. As expected from the electric field distribution obtained in Figure 2-4, the E×B drift vectors are directed sunward everywhere in the analyzed region. The beginning of the bifurcation of the sunward flow is already evident at x = -28 R_E. The E×B drift vectors have rough mirror symmetry about the midnight meridian in contrast to the asymmetric ion flow pattern shown in Figure 2-2. Since the E×B drift corresponds to the transport of magnetic flux, a significant difference exists between the global convection patterns of ions and magnetic flux.

2.4 Discussion

It should be stressed that our results represent gross features of the plasma sheet for which dynamical and spatially localized characteristics inherent to the plasma sheet have been largely smoothed out. As noted in the past studies [*Baumjohann et al.*, 1989, *Angelopoulos et al.*, 1993], ion flows observed in the plasma sheet tend to be random and highly time-variable in both magnitude and direction even during geomagnetically quiet times. Thus an instantaneous snapshot of the ion flow pattern would not be as systematically ordered as the one shown in Figure 2-2 is. The convection pattern derived in this paper should be interpreted as representing an ensemble average (or a long-time average) of such highly variable flows. Although individual flows may appear to be random and have no preferred direction on a relatively short time-scale, they constitute a systematic flow pattern on a longer time-scale. From this point of view, the average profiles derived in our statistical study reflect the essence of such a long time-scale convection pattern.

The average electric field profile derived in the present study is important for the transport of particles and magnetic flux in the magnetotail. It is interesting to

compare our result with the tail convection pattern inferred from ionospheric observations [*Rostoker*, 1991; *Maynard et al.*, 1995]. The ionospheric convection pattern projected onto the tail equatorial plane by these authors indicated that a dawn-to-dusk electric field is dominant in the tail, a fact that has been supported by our study. A striking difference exists between the pattern inferred from low-altitude observations and the one observed in-situ (our result) regarding the Ex component of the electric field. In both results, the Ex component is directed sunward on the dawn side and anti-sunward on the dusk side, indicating that the sunward convection flow is bifurcated near the midnight meridian. Projection of low-altitude observations suggests that the region where the Ex component becomes significant is restricted to the near-Earth region ($R<10\ R_E$). On the other hand, our result indicates that the Ex component is comparable in magnitude to the Ey component not only in the near-Earth region but also at larger distances of $>25\ R_E$ as seen in Figure 2-4. The discrepancy between our result and the tail convection pattern inferred from ionospheric measurements probably implies that the T89 magnetic field model used in the projection process maps the nightside portion of the ionospheric convection much nearer to the Earth than reality. It is noted that both Donovan and Rostoker and Maynard et al. used the T89 model for a relatively large Kp value (Kp=4), for which the magnetic field in the magnetotail is more dipolar than usual so that the field line from the fixed point in the ionosphere is mapped to the equatorial plane closer to the Earth than usual.

The average ion flow pattern in Figure 2-2 shows a clear dawn-dusk asymmetry: ion flow vectors have a significant duskward component both on the dusk side and around local midnight but have only a small dawnward component on the dawn side. *Angelopoulos et al.* [1993] showed that the observed flow pattern may be explained as a sum of the sunward E×B drift and the duskward diamagnetic drift. In showing this, they estimated the diamagnetic drift by taking the curl of the model magnetic field [Tsyganenko,1987] and dividing it by the measured ion density. Further, the convection electric field (excluding the corotation part) was assumed to be directed dawn to dusk and was estimated from the polynomial fit to the earthward convection speeds measured at $X < -10\ R_E$ and the measured magnetic field. They showed that the observed and the model flow patterns are similar. However, since the E×B drift at $X < -10\ R_E$ (excluding corotation) was assumed to be purely sunward in their model, they did not discuss the deviation of E×B drift from the x direction. The average electric field obtained in our analysis shows that the E×B drift itself has a significant

Y component at X <-10 R_E. Since this component of the E×B drift tends to cancel the pressure gradient drift on the dawn side and augment it on the dusk side, the dawn-dusk asymmetry of the observed flow pattern naturally arises in our model, while the origin of asymmetry was not apparent in the model of Angelopoulos et al. [1993].

We have not mentioned the dependence of the convection pattern on geomagnetic activity in the present paper. It has been shown that bursty flows in the plasma sheet tend to occur more frequently during geomagnetically active times [e.g. *Angelopoulos et al.*, 1989]. Large electric field values accompanying such fast flows may result in a larger mean electric field for disturbed times than for quiet times. However, evidence has been presented that the plasma sheet is for the most part characterized by randomly varying slow flows, and that the fast flows mentioned above are much rarer than slow flows [*Huang and Frank*, 1986; *Baumjohann et al.*, 1989]. In addition, our preliminary studies (not shown here) show that the qualitative aspect of the average flow pattern does not depend on the Kp index. This topic is being investigated and will be discussed in a separate paper.

Our analysis presented in this paper has shown that a significant difference exists between convection patterns of ions and magnetic flux in the near-Earth portion of the magnetotail. (Compare Figure 2-2 with Figure 2-6.) This fact indicates that the frozen-in condition is violated even for thermal ions as analyzed here. The frozen-in condition is not satisfied because the pressure gradient term is comparable to the V×B term in the ion momentum equation. Particularly, the presence of the radial pressure gradient in the near-Earth plasma sheet leads to an imbalance between E and V×B in the X direction and gives rise to a difference in the Y-component of ion/magnetic flux transport. Figure 2-6 shows that magnetic flux, while being convected earthward, is transported towards dawn and dusk in a symmetric way. On the other hand, the ion flow pattern presented in Figure 2-2 indicates that the averaged motion of ions is deflected duskward significantly so that the frozen-in condition is not satisfied in the plasma sheet.

References

Angelopoulos, V., W. Baumjohann, C. F. Kennel, F. V. Coroniti, M. G. Kivelson, R. Pellat, R. J. Walker, H. Luhr, and G. Paschmann, Bursty bulk flows in the inner central plasma sheet, *J. Geophys. Res., 97*, 4027, 1992.

Angelopoulos, V., C. F. Kennel, F. V. Coroniti, R. Pellat, H. E. Spence, M. G. Kivelson, R. J. Walker, W. Baumjohann, W. C. Feldman, J. T. Gosling, and C. T. Russell, Characteristics of ion flow in the quiet state of the inner plasma sheet, *Geophys. Res. Lett., 20*, 1711, 1993.

Atkinson, G., Thick Current Sheets in the Renovated Model of the Magnetosphere, *J. Geophys. Res., 89*, 8949, 1984.

Baumjohann, W., G. Paschmann, C. A. Cattell, Average plasma properties in the central plasma sheet, *J. Geophys. Res., 94*, 6597, 1989.

Dungey, J. W., Interplanetary magnetic field and the auroral zones, *Phys. Rev. Lett. 6*, 47, 1961.

Donovan, E. F., and G. Rostoker, Internal consistency of the Tsyganenko magnetic field model and the Heppner-Maynard empirical model of the electric field distribution, *Geophy. Res. Lett, 18*, 1043, 1991.

Heppner, J. P., and N. C. Maynard, Empirical high-latitude electric field models, *J. Geophys. Res., 92*, 4467, 1987.

Huang, C. Y., and L. A. Frank, A statistical study of the central plasma sheet: Implications for substorm models, *Geophy. Res. Lett., 13*, 652, 1986.

Kokubun, S., T. Yamamoto, M. H. Acuna, K. Hayashi, K. Shiokawa, and H. Kawano, The GEOTAIL magnetic field experiment, *J. Geomagn. Geoelectr., 46*, 7, 1994.

Maynard N. C., F. D. William, and J. B. William, Mapping ionospheric convection patterns to the magnetosphere, *J. Geophys. Res., 100*, 1713, 1995.

Mukai, T., S. Machida, Y. Saito, M. Hirahara, T. Terasawa, N. Kaya, T. Obara, M. Ejiri, and A. Nishida, The low energy particle (LEP) experiment onboard the GEOTAIL satellite, *J. Geomagn. Geoelectr., 46*, 59, 1994.

Spence, H. E., M. G. Kivelson, R. J. Walker, and D. J. McComas., Magnetotail plasma pressures in the Midnight Meridian: Observations, *J. Geophys. Res., 94*, 5264, 1989.

Tsyganenko, N. A., Global quantitative models of the geomagnetic field in the cislunar magnetosphere for different disturbance levels, *Planet. Space Sci., 35*, 1347, 1987.

Tsyganenko, N. A., A magnetospheric magnetic field model with a warped tail current

sheet, *Planet. Space Sci., 37*, 5, 1989.

Zhu, X., Magnetospheric convection pattern and its implications, *J. Geophys. Res., 98*, 291, 1993.

Figure captions

Figure 2-1. GEOTAIL orbit on the X-Y plane during Oct., 1994 – Dec., 1997. The black dashed curve is the nominal magnetopause in the equatorial plane. The black rectangle shows the area for which the statistical study is made.

Figure 2-2. Average ion flow pattern in the plasma sheet on the X-Y plane.

Figure 2-3. Average profiles of ion kinetic pressure P_i in the plasma sheet.

Figure 2-4. The electric field vectors (Ex, Ey) calculated from both the average V×B values and the pressure gradient for each X-Y bin.

Figure 2-5. Y-variations of (a) the x-components and (b) y-components of the V×B term, pressure gradient term, and the resultant electric field evaluated in the bin of X = -15 Re.

Figure 2-6. E×B drift vectors in the X-Y plane calculated from the electric field shown in Figure 2-4.

Figure 2-1

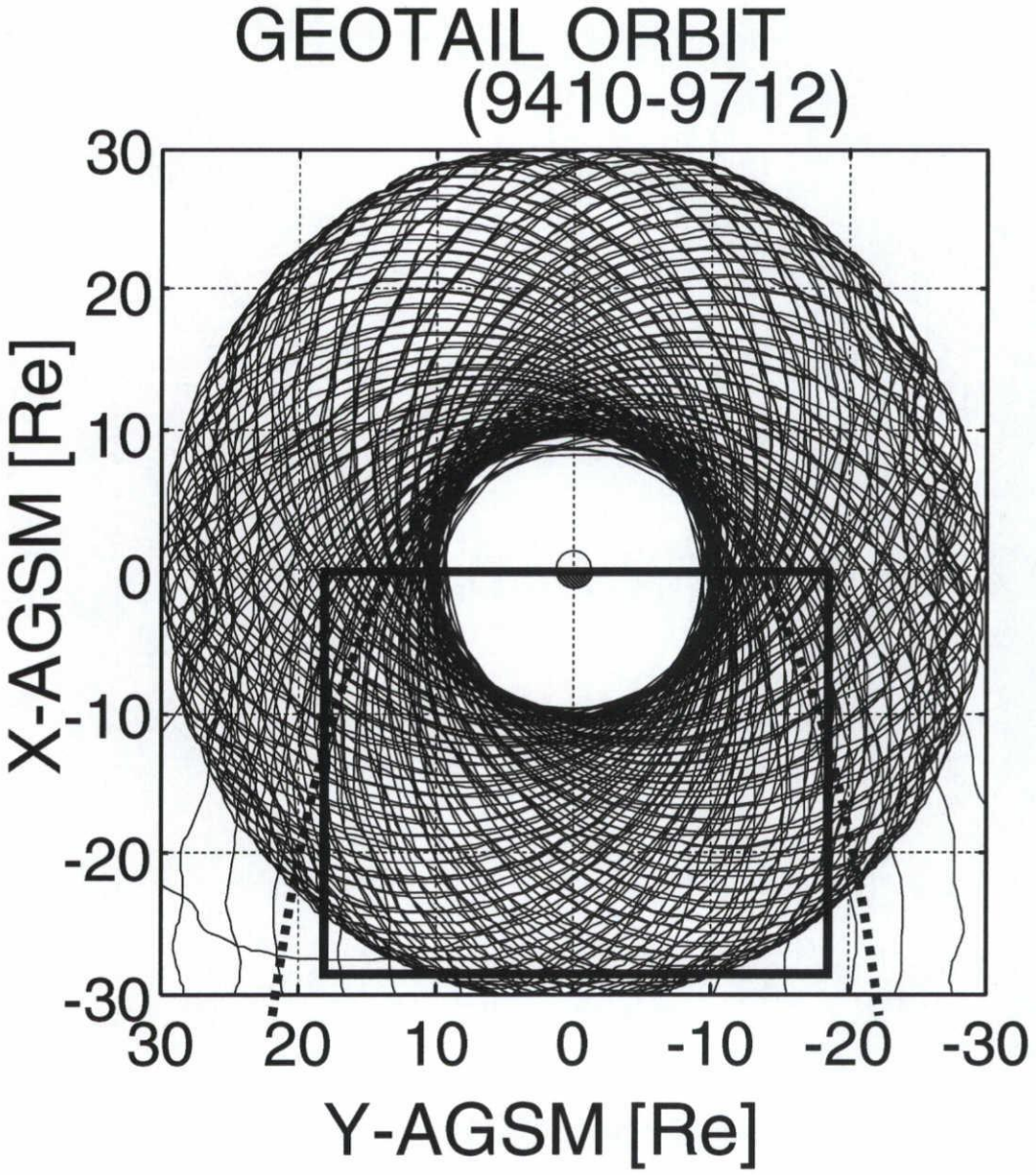
GEOTAIL ORBIT
(9410-9712)
30
20
10
0
-10
-20
-30
X-AGSM [Re]
30
20
10
0
-10
-20
-30
Y-AGSM [Re]

Figure 2-2

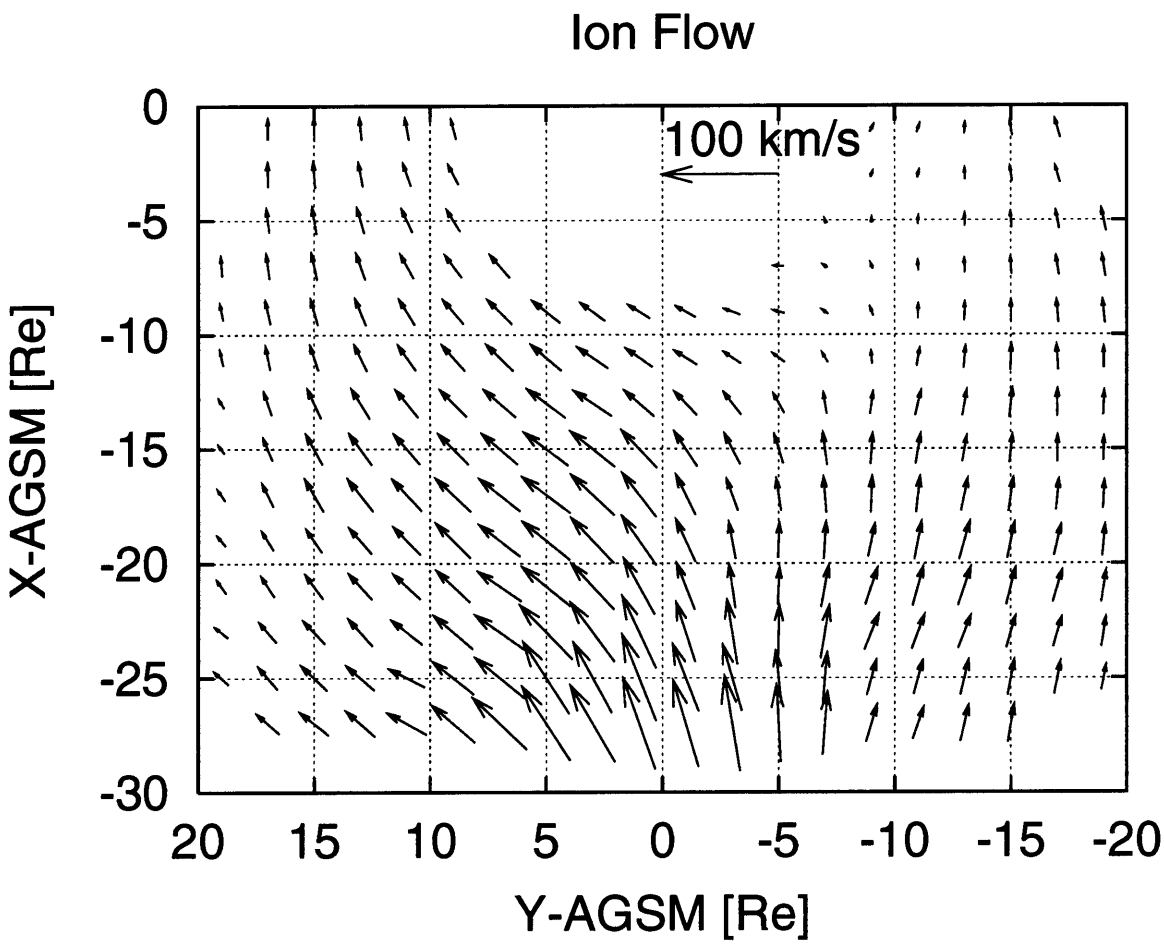
Ion Flow
100 km/s
0
-5
-10
-15
-20
-25
-30
X-AGSM [Re]
20
15
10
5
0
-5
-10
-15
-20
Y-AGSM [Re]

Figure 2-3

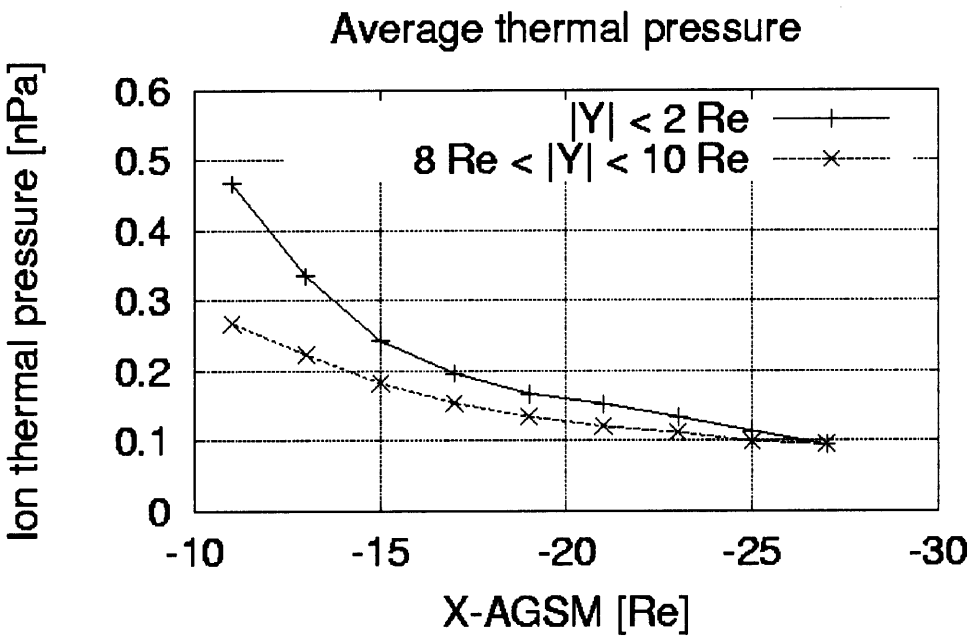
Average thermal pressure
Ion thermal pressure [nPa]
0.6
0.5
0.4
0.3
0.2
0.1
0
|Y| < 2 Re
8 Re < |Y| < 10 Re
-10
-15
-20
-25
-30
X-AGSM [Re]

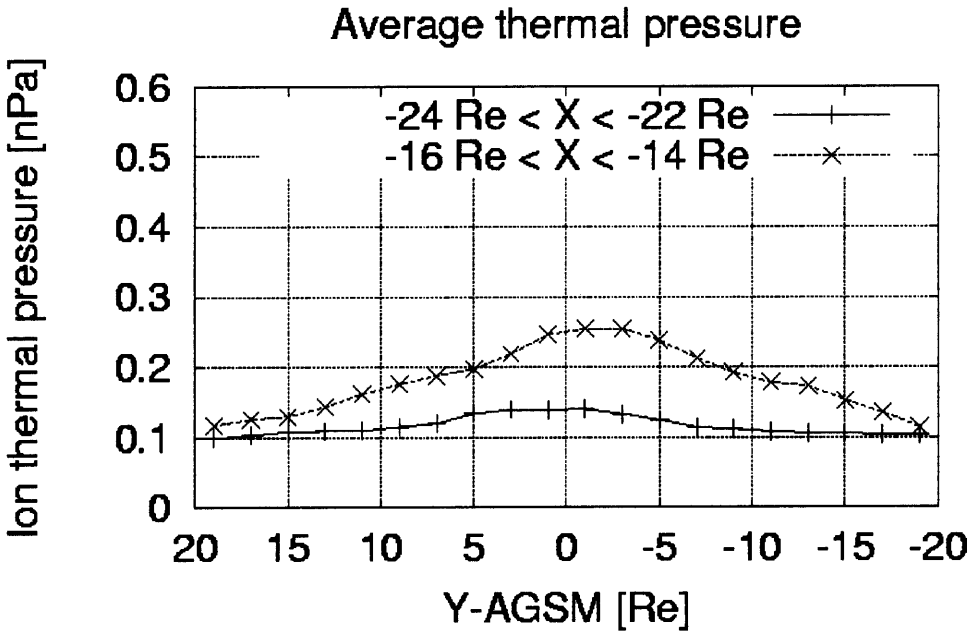
Average thermal pressure
Ion thermal pressure [nPa]
0.6
0.5
0.4
0.3
0.2
0.1
0
-24 Re < X < -22 Re
-16 Re < X < -14 Re
20
15
10
5
0
-5
-10
-15
-20
Y-AGSM [Re]

Figure 2-4

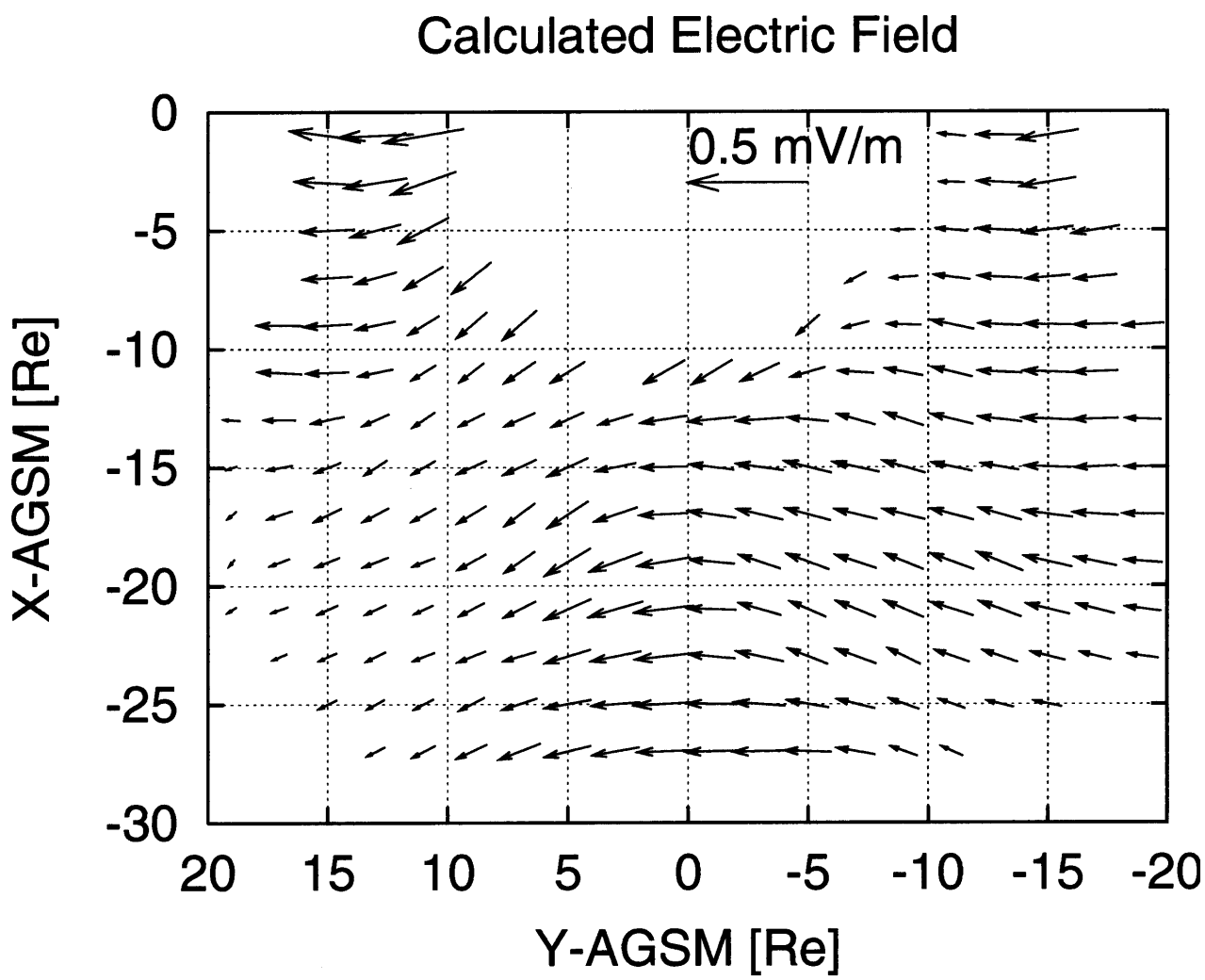
Calculated Electric Field
0.5 mV/m
0
-5
-10
-15
-20
-25
-30
X-AGSM [Re]
20
15
10
5
0
-5
-10
-15
-20
Y-AGSM [Re]

Figure 2-5a

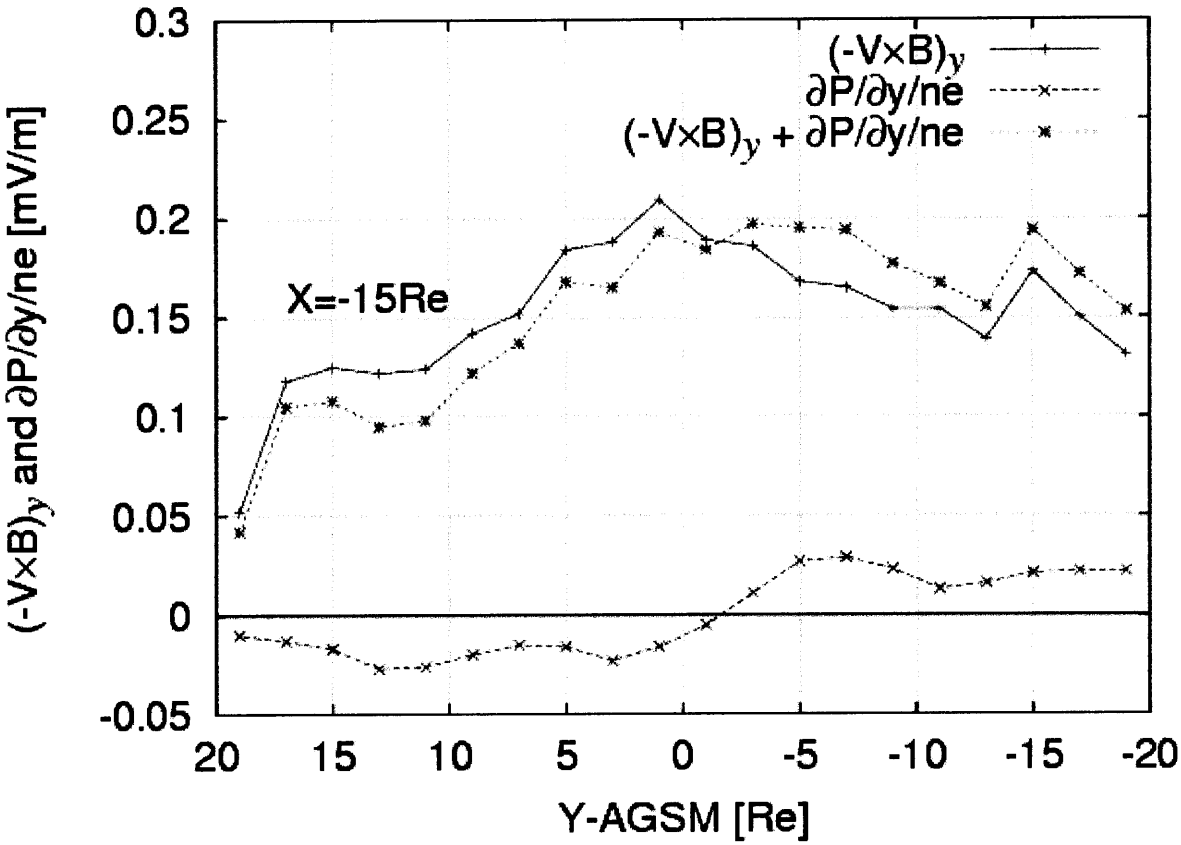

Figure 2-5b

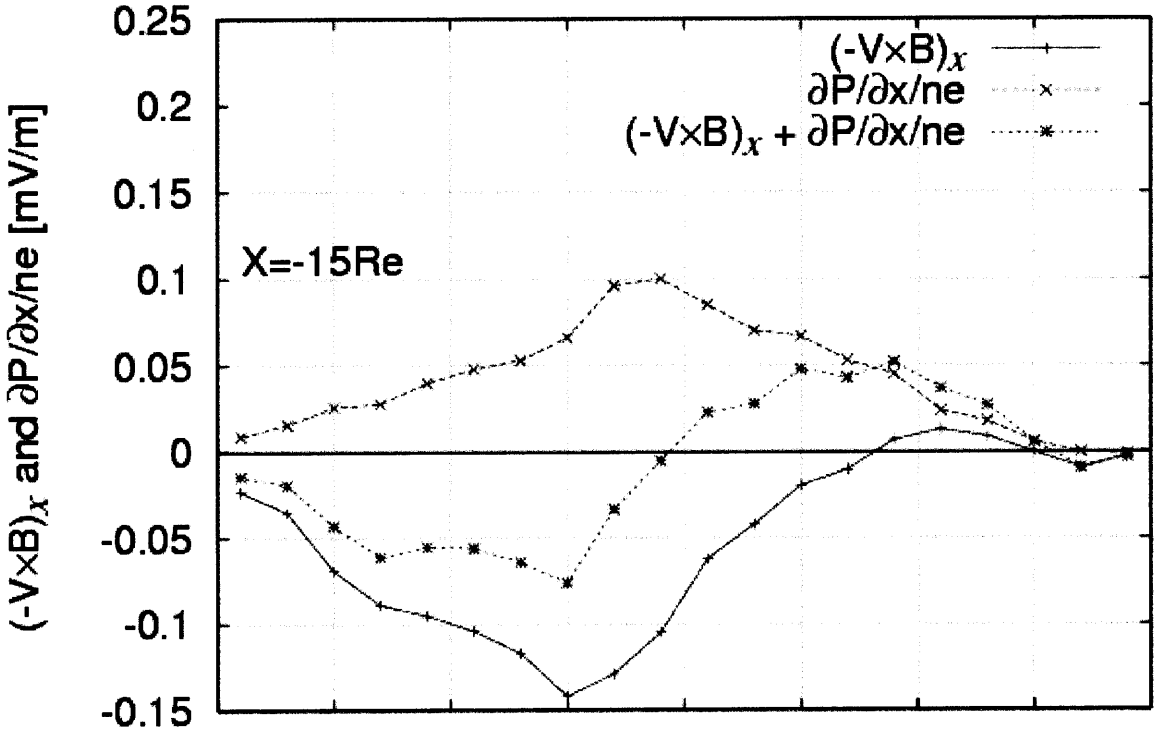

Figure 2-6

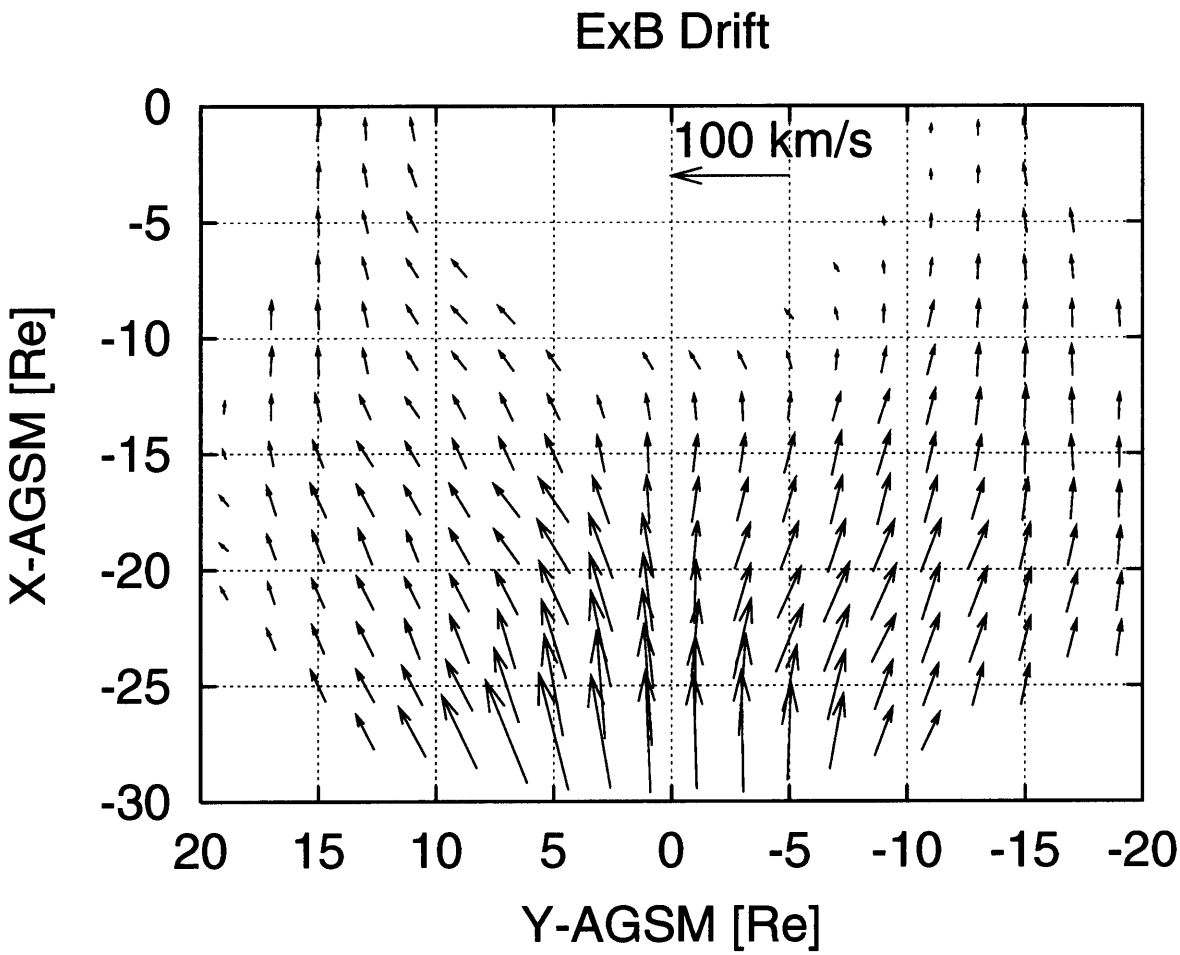
ExB Drift
100 km/s
0
-5
-10
-15
-20
-25
-30
X-AGSM [Re]
20
15
10
5
0
-5
-10
-15
-20
Y-AGSM [Re]

Chapter 3

Flux Enhancement of Energetic Particles in the Near-Earth Region: GEOTAIL-HEP Observation.

Abstract

We have found that both the energy-dispersed and the dispersionless flux enhancements of energetic (>40keV) particles are frequently observed far away (R>9 R_E) from the Earth, which are similar to the ones observed in association with substorm activities at geosynchronous orbit. Using energetic particle data obtained by the HEP-LD instrument onboard the GEOTAIL spacecraft, we studied spatial and temporal characteristics of these flux enhancement events and also examined their correlation with substorm activities. It was found that the dispersed events of energetic ions are distributed preferentially on the dusk side and are very rare on the dawn side, while most of the dispersed electron events are found on the dawn side with few events found on the dusk side. It is also noted that the dispersed events are relatively rare around the noon and midnight meridian. On the other hand, the dispersionless events can be found only on the night side and are mostly distributed within R < 15 R_E from the Earth. A detailed analysis shows that ion dispersionless events are found more frequently than the electron events and that the ion events are found both around local midnight and in the evening sector but that the electron events are found only in the post-midnight sector. Since the dispersionless and dispersed characteristics of the flux enhancements imply that their source site is nearby and that they are transported far away from the source, respectively, it is interpreted that energetic particles forming such flux enhancements are generated on

the night side, and then drift azimuthally westward or eastward, to reach the observation points. We also examined their correlation with substorm activities and found that almost all (96%) of the dispersionless and dispersed events are associated with substorms. The dispersionless flux enhancements in the plasma sheet proper occur within +/- 2 minutes of the corresponding substorm onset determined by ground magnetograms, while all of the dispersed events are preceded by the onset owing to their finite transport time from the source region. Time scales of the observed energy dispersions are consistent with our test particle simulation result with the source site assumed at local midnight. It was also found that some of the dispersed events have a long (~ several ten minutes) energy dispersion, indicating a possibility that energetic particles occasionally can follow a closed drift path around the Earth at radial distances further away from the inner magnetosphere.

3.1 Introduction

It is well known that energetic particles with energies of a few tens to several hundred keV are generated in the plasma sheet and then injected into the inner magnetosphere during a magnetospheric substorm [e.g., *Lui et al.*, 1987 and references therein]. These energetic populations are observed directly by the spacecraft as a sudden flux enhancement of energetic particles within a certain range of energy. To reveal the generation mechanism of these energetic particles and also their transport processes in the magnetosphere is one of the most important subjects of magnetospheric physics.

A large number of studies on substorm injection have been made primarily on the basis of observations made at geosynchronous orbits in the last three decades. It was revealed by many authors that the particle population injected into geosynchronous distance consists mainly of electrons and protons with energies more than 25 keV [e.g., *Walker et al.*, 1976; *Baker et al.*, 1978; *Belian et al.*, 1978]. These injections in the night side magnetosphere are associated with the substorm expansion onset [*Konradi*, 1967; *Belian et al.*, 1981]. It was also found that the flux enhancements caused by these injections have different shapes depending on the distance from the injection source [*Lanzerotti et al.*, 1967; 1971; *Pfitzer and Winckler*, 1969]. In the vicinity of the source region, particle fluxes increase simultaneously for different energies (dispersionless flux enhancement), while flux enhancements occur successively from higher to lower energies, being dispersed in energy, owing to their energy-dependent drift from the source to the observation point, which is referred to as a dispersed flux enhancement. Because gradient- and curvature-B drifting particles corresponding to a dispersed flux increase can go around the Earth at geosynchronous altitude, it is observed that the injected population passes the satellite many times as drift echoes. These two injection features were interpreted by means of the injection boundary model [*McIlwain*, 1974; *Mauk and McIlwain*, 1974], which is assuming a injection source region with double-spiral shaped boundaries where particle fluxes are suddenly enhanced simultaneously over a wide energy range. Recently, *Birn et al.* [1997a] made a statistical study on dispersionless injections at geosynchronous orbit and refined the above injection boundary model. They showed that the injection boundary is not identical for ions and electrons but displaced against each other in the dawn-dusk direction.

Observational studies have been made also for energetic particles in the

magnetotail. *Sarris et al.*, [1976] analyzed energetic proton data obtained in the plasma sheet and found field-aligned proton beams with short durations (~ a few minutes) called impulsive bursts. They also found that these impulsive bursts are closely associated with the substorm onset. There are other energetic particle enhancements observed in the plasma sheet that were found to be clearly associated with substorm and/or plasma sheet recovery [*Hones et al.*, 1976]. These observational results were incorporated into the model proposed by *Baker et al.* [1979] where particles are energized within a brief interval (~ 1 min) by magnetic reconnection in the vicinity of the magnetic neutral line at the substorm onset, and then injected into the inner magnetosphere. Subsequently, the injected energetic population leaks out to the near-Earth plasma sheet as the plasma sheet expands in the substorm recovery phase. On the other hand, *Lui et al.* [1988] indicated a possibility that energetic particles associated with substorms are accelerated by the turbulent inductive electric field associated with the current disruption in the near-Earth plasma sheet. *Birn et al.* [1997b] performed a global MHD simulation of magnetosphere including the near-Earth reconnection, and calculated test particle trajectories in the above field to reveal detailed characteristics of acceleration processes with the injected energetic particles. Their results indicate that energetic particles are effectively accelerated by the inductive electric field in the near-Earth region, rather than by magnetic reconnection itself.

Flux enhancement events found in the outer magnetosphere ($R > 9R_E$) frequently show either a clear dispersionless or dispersed signature similar to those observed at geosynchronous distance. In the present study, we concentrate ourselves on these characteristic flux enhancements of energetic particles, because these dispersionless and dispersed features provide us import information about the location of the acceleration site and also the transport processes from the source site. This kind of enhanced flux events has been reported in the past studies [*Lui et al.*, 1988; *Fennell et al.*, 1998], however, the past studies were mainly concerned with the case study of a typical event. Thus, in the present study, we will make a statistical study on such flux enhancement events to investigate general properties of flux enhancements of energetic particles in the outer magnetosphere. In order to discuss the above models, we need to examine spatial and temporal distributions of the enhanced flux regions in detail, utilizing their dispersionless or dispersed features. Taking these results into account, we will discuss the acceleration mechanism and the global transport process of energetic particles in the outer magnetosphere during substorm.

3.2 Data and Instrument Characteristics

In the present paper, we use energetic particle measurements obtained by the HEP-LD instrument [*Doke et al.*, 1994] onboard the GEOTAIL spacecraft. HEP-LD is a spectrometer for energetic particles employing time-of-flight(T) and energy(E) detection systems to determine both the particle's mass and energy. Because the amount of the raw data with the full resolution in (E,T) is too large to be transmitted fully, the obtained data are summed in various bins and compressed into several data types by the onboard data processor and then transmitted down to the ground station. Among several data transmission modes supported by HEP-LD, we used the mode called EDIS. This mode provides us three dimensional (3 polar directions and 16 azimuthal spin sectors) particle fluxes with 11 energy channels in the range of 80 keV – 4 MeV for ions and 30 keV – 400 keV for electrons with the time resolution of 24 sec. In this mode, each incident particle is counted by the onboard system without mass identification so that the accumulated particle fluxes for each energy channel contain both ions and electrons in the specified energy range. This is because the EDIS mode is designed to measure particle fluxes solely on the basis of SSD counts (without the time-of-flight information) to avoid relatively low efficiency of the time-of-flight detection.

When the HEP-LD data transmission is operated in the EDIS mode, the scientific data of the time-of-flight measurement is not transmitted to the ground station. Even in this mode, however, the time-of-flight detection is still operating onboard the spacecraft and we can obtain some information in the engineering section of the data. This engineering data includes output from hardware counters which count the total number of incident particles and also, among all of the incident particles, the number of particles whose time-of-flight are successfully measured. Since the post-launch calibration of the instrument revealed that the onboard time-of-flight detection system has no sensitivity to incident electrons, while is sensitive to ions, this fact suggests that we can estimate incident flux ratio of ions to the entire incident particles by comparing the above two counter outputs. We analyzed statistically the correlation between the above two counter outputs and empirically developed a method by which we can estimate a ratio of ion flux to the total amount of particle flux (the detailed information on this estimation method is described in *Hayashi*, 1998). Thus using this

ratio, we can classify each observation interval (24 sec) as an "ion-dominant interval" or "electron-dominant interval" by inquiring whether the ion fluxes dominates the total flux or not. To avoid ambiguity, we excluded the time intervals where ion abundance is comparable to electron. In addition to the energetic particle data, we used the low energy particle and magnetic field data obtained by the LEP instrument [*Mukai et al.*, 1994] and the MGF instrument [*Kokubun et al.*, 1994] , respectively.

3.3 Case study

First of all, we will show an example each for the dispersionless and dispersed flux enhancements of energetic particles observed by GEOTAIL. These events demonstrate typical characteristics of flux enhancements that will be studied later statistically. Using these typical examples, we will discuss basic features of variations in energetic particle fluxes and also their correlation to substorm activity in detail.

3.3.1 Event 1 (June 21, 1996)

Figure 3-1 shows the energy-time spectrogram, the differential fluxes for the lowest five energy channels, and pitch angle anisotropies of energetic particles in the first, fourth, and fifth panel, respectively, observed with HEP during 11:00UT-15:00UT on June 21. Also shown are ion and electron energy spectra obtained by the LEP instrument (second and third panel, respectively) with the ion bulk velocity components, density, and temperature (6th and 8th panel) derived from the LEP observation, and Bx- and Bz-components of the magnetic field (7th panel). Because the analysis of ion flux ratio described in the previous section shows that this time interval is on the whole classified as an ion-dominant interval, the plotted energetic particle fluxes represent energetic ion fluxes. As seen from high (>1 keV) ion temperature derived by LEP, GEOTAIL was within the near-Earth plasma sheet during this time interval. At 11:51UT, GEOTAIL observed an abrupt flux enhancement of energetic ions without any energy-dispersion in the energy range from 80 keV up to about 500 keV. It is also seen that the dispersionless flux increase is associated with a fast earthward flow (~250 km/s) and sharp increase in the Bz component of the magnetic field. Such association of fast flows and Bz dipolarization is common to almost all dispersionless flux enhancements studied here.

Since energetic particles in the near-Earth plasma sheet are subject to energy-dependent azimuthal drift, a dispersionless characteristic of the flux increases indicates that these energetic ions were observed before they had time to drift any appreciable distances from the acceleration site. Presumably they were produced very close to the observation point. Examining a temporal variation in flux reveals that the dispersionless flux enhancement has no coherent feature in the pitch angle anisotropy, and that the flux intensity as well as the pitch angle anisotropy is highly time-varying during the interval of flux enhancement. These features are consistent with the past studies made on the sudden flux enhancement of energetic particles associated with the dipolarization or current disruption [e.g. *Lui et al.,* 1988].

After the temporal decay of the enhanced energetic ion fluxes, a second flux enhancement started gradually from the higher energy channels beginning at 12:26UT, successively toward the lowest energy channel reaching E = 88 keV at 12:48UT, producing a clear energy-dispersion with a time scale of ~ 40 min. Because the motion of energetic particles along the field line is too fast to be dispersed much in energy, the dispersed arrivals should be interpreted as a result of the time-of-flight effect caused by energy-dependent drifts perpendicular to the magnetic field. Hence such separate arrivals in different energies imply that energetic particles constituting the second enhancement had already drifted a distance long enough to be dispersed appreciably in energy. This fact indicates that these dispersed energetic particles are not a locally accelerated population but a population which had been generated at some other place and then drifted to the spacecraft position. Another interesting characteristic of the dispersed energetic population is that its particle flux is enhanced more in the direction of the magnetic field than normal to it, as shown in the fifth panel of Figure 3-1. This pitch angle anisotropy occurred for most of the long dispersion events found in the present study and hence these dispersed populations are composed mainly of particles with small pitch angles.

When these energetic particle events occurred in the magnetotail, a clear substorm activity was seen on the ground as shown in Figure 3-2. The top panel of Figure 3-2 shows ground magnetometer data taken at College (CMO) on the same day and the bottom panel shows Pi2 pulsation activity during 10:00UT – 12:00UT recorded at KAKIOKA (a low latitude station). It is evident from these panels that a moderate substorm activity was initiated with the expansion onset at 11:37UT as determined from a Pi2 onset in the bottom panel. Thus the dispersionless flux enhancement in Figure 3-1 took place 14 min. after the substorm onset, and is followed by the

dispersed enhancements. A somewhat large time delay of flux increase from the substorm onset was probably caused by the fact that the spacecraft was situated fairly off-equator in the plasma sheet.

3.3.2 Event 2 (Dec. 9, 1996)

Next we will present an example of the dispersed flux enhancement of energetic ions typically observed away from the midnight sector. Figure 3-3 shows, in the same format as Figure 3-1, the plasma and field profile during the interval 12:00UT – 16:00UT on December 9, 1996, when GEOTAIL was located in the evening sector of the magnetosphere. Also shown in Figure 3-4 are (top panel) magnetic field data from the 210° magnetic meridian stations [*Yumoto et al.*, 1996], and (bottom panel) Pi2 pulsation activities observed at KAKIOKA. Again our estimation of ion flux ratio reveals that the energetic particles observed during this interval consisted predominantly of ions. A visual inspection of Figure 3-4 enables us to identify at least two substorm sequences during this time interval: the first substorm occurred at about 13:00UT, and the second one became activated at 14:30UT. In association with the two substorms, multiple flux enhancements were clearly seen in the HEP energy range from 13:04UT and 14:32UT, respectively. It is noted that these flux enhancements were dispersed in energy for relatively short durations of a few minutes. In addition to the high energy range, the energy dispersions appeared to extend down to the LEP energy range (< 40 keV), even though the low energy tails of the dispersions were less discernible probably owing to their merging with the pre-existing population. Examining the temporal correlation with the corresponding substorm onsets in detail, we found that the delay in the arrival times of multiple flux increases, relative to the onsets of the corresponding substorms, is about a few minutes and thus consistent with the time required for 200 keV protons to drift from local midnight to the location of the spacecraft. Therefore it can be interpreted that ions constituting these dispersed flux enhancements came from the local midnight region where energetic particles had been generated in close association with a substorm onset as indicated previously in Event 1. The fact that flux enhancements observed at dusk consisted of multiple dispersed populations implies that multiple accelerations of energetic particles occurred at local midnight even for a single substorm, and the resultant multiple energetic populations were observed as a series of dispersed flux enhancements after their duskward transport with the energy-dependent drift.

3.4 Statistical study

The GEOTAIL spacecraft has been surveying the near-Earth region (9 R_E < R < 30 R_E) of the magnetosphere for several years. Figure 3-5 shows the GEOTAIL orbit on the X-Y (namely, equatorial) plane during the period Apr., 1996 – May, 1998, when the EDIS data of the HEP-LD instrument were available. We visually inspected our data plots for this time interval, and identified 63 (53 ion and 10 electron) dispersionless and 200 (136 ion and 64 electron) dispersed flux enhancement events, respectively. Using these data sets, we performed a statistical study to obtain the spatial distribution and temporal properties of the dispersionless and dispersed flux enhancements. Their correlation with substorm activities was also examined in detail.

3.4.1 Spatial distribution of the events

In Figure 3-6a (top panel), we show the locations of the spacecraft on the X-Y plane for the intervals when the dispersionless and dispersed flux enhancements were observed. In the figure, red asterisks and small blue circles represent the dispersed and dispersionless events, respectively. Superimposed are the nominal magnetopause position (green curve), the geosynchronous orbit (blue circle), and the spacecraft's perigee altitude of ~ 9 R_E (violet circle). We see that the dispersed flux enhancements are observed in all local time sectors. A careful examination of their local time distribution reveals that the dispersed events are distributed rather uniformly between the spacecraft's perigee, namely the inner edge of the spacecraft coverage, and the nominal magnetopause in the evening sector, while are relatively rare near the magnetopause in the morning sector. Since the orbital coverage of GEOTAIL is good near the magnetopause as well as well inside the magnetopause, this dawn-dusk asymmetry implies a difference in the transport path of energetic particles between the dawn and dusk flanks. On the other hand, the dispersionless flux enhancements are found only on the night side and are distributed around the midnight sector in the near-Earth plasma sheet. It is also seen that most of both the dispersed and dispersionless events are located inward of about R = 15 R_E. These results imply that the acceleration yielding such energetic particles occurs frequently at the locations

earthward of X = -15 R_E around local midnight. In Figure 3-6b (bottom panel), we show a plot which represents occurrence frequencies of the dispersed (black open rectangles) and dispersionless (red solid bars) events as a function of local time. Here the occurrence frequency is normalized by the time GEOTAIL spent in each local time sector. The occurrence frequency of dispersed flux enhancements shows a blunt peak in the morning and evening sectors, respectively, and becomes small toward the local midnight, where the dispersionless flux enhancements have the maximum occurrence. This result is consistent with the interpretation that energetic particles are generated near the midnight meridian and become dispersed in energy as they drift towards dawn and dusk away from midnight.

The above interpretation implies that ions and electrons should have different local time dependences because the direction of azimuthal drift is opposite for ions and electrons. Figure 3-7a, 3-7b present the local time profiles of the event occurrence for energetic ions and electrons separately. As seen clearly from Figure 3-7a, the ion and electron dispersed events are dominant on the dusk and dawn side, respectively, consistent with the direction of their azimuthal drift motion. The distribution of dispersed events for ions and electrons is almost exclusive to each other; The distribution has a peak in the evening and morning sector for ions and electrons, respectively. It is also noted that some dispersed events are found in the unfavorable sectors both for ions and electrons. We found that all of these events showed rather flat energy-dispersion with a long time, i.e., a few to several tens of minutes. This fact suggests that energetic particles can go around the Earth completely forming a closed drift path at a distance of R ~ 10 R_E; the time scale of these dispersions is comparable to the drift period of a few hundred keV protons and electrons around the Earth under the influence of gradient and curvature drifts. This result will be discussed in detail later.

The dispersionless events illustrated in Figure 3-7b also show the same tendency of local time distribution as the dispersed events. On the other hand, unlike the dispersed events, the local time distributions of ions and electrons are overlapped around the midnight sector. These results are quite similar to those of dispersionless injections observed at geosynchronous orbit [e.g. *Birn et al.*, 1997a]. However, it is of interest that the ion dispersionless events have a significantly larger rate of occurrence than the electron events. In addition, the similar unbalance in the occurrence frequency can be seen (but less markedly) between ions and electrons dispersed events. These facts appear to indicate that electrons tend to obtain less

energy as compared to ions in the course of the acceleration process that causes for the dispersionless flux enhancements.

3.4.2 Substorm correlation

In order to examine whether the above events are associated with substorm activity, we checked if at least one of the following two substorm signatures was observed: (1) a clear bay-like decrease in the H-component of the geomagnetic field at high latitude ground stations and (2) a clear positive bay signature at mid-latitude stations. The substorm activities identified with the above criteria can include weak activities, like pseudo breakups or small substorms that are localized both latitudinally and longitudinally, as well as fully developed substorms. In the present study, we examined all such activities with various magnitudes to examine the substorm association, because even small activities appear to be correlated one-to-one with the earthward flow bursts or with plasma heating phenomena in the tail plasma sheet as reported in the past study [e.g., *Angelopoulos et al.*, 1996, *Ieda et al.*, 2001]. In Table 1, we showed the number of substorm-associated events as well as the total event number for ions and electrons. We see that almost all of both the dispersed and dispersionless events are closely correlated with the substorm activity. These statistical results strongly indicate that these flux increases of energetic particles in the near-Earth plasma sheet take place in association with substorms. It is also noted that, even though they are very rare, there exist a certain number of flux enhancement events with no substorm signature. These events may be interpreted to be caused to the plasma heating associated with flow bursts in the plasma sheet: It was reported that fast earthward flows can occur even during quiet times and be accompanied by energetic particles [*Angelopoulos et al.*, 1994; 1996].

Next we will examine temporal correlation of the flux enhancements with the substorm onset in detail. In particular, the timing analysis for the dispersionless events is very important because the dispersionless characteristics directly reflect the on-site generation of energetic particle fluxes. In this analysis, however, we must carefully interpret the dispersionless features by considering the motion of the plasma sheet relative to the spacecraft. This is because plasma sheet boundary crossings caused by quick expansions of the plasma sheet filled with energetic particles also lead to apparently the same observational feature, namely the dispersionless flux increase. Hence we separate the dispersionless events into two groups, "Lobe-to-PS events" and

"PS-throughout events", by considering whether the flux increases were observed as the spacecraft enters the plasma sheet from the lobes, or the spacecraft was in the plasma sheet proper throughout the events, respectively. Events in the plasma sheet but with large Bx component of the magnetic field are classified as Lobe-to-PS events to avoid events near the plasma sheet boundary.

Figure 3-8 shows a local time dependence of the time delay of the dispersionless flux enhancement from the corresponding substorm onset. Here we plotted only events during which the onset time could be determined from Pi2 pulsation activity at the low-latitude ground stations of Kakioka (KAK) and Hermanus (HER). In the figure, open circles and triangles denote Lobe-to-PS events and PS-throughout events, respectively. A negative value of the time delay means that the flux enhancement precedes the substorm onset. It is shown again that the dispersionless events are localized around the midnight sector. As seen from Figure 3-8 for Lobe-to-PS events, the values of time delay are scattered from around zero to more than ten minutes, while PS-throughout events were observed within the time difference of ~2 minutes from the substorm onset, except one event with a large (~11 min) time delay. Also seen is that the time delay from the substorm onsets for PS-throughout events appears to be rather uniformly distributed in local time. Even though some flux enhancement events precede the Pi2 pulsation, this fact does not necessarily mean energetic particle generation prior to substorm onset. It should be taken into account that the identification of Pi2 pulsation onsets has a potential uncertainty of a few minutes due to latitudinal and azimuthal propagation properties of the pulsation waves [*Uozumi et al.*, 2000]. Hence, from the result of PS-throughout events, we can only say that energetic particles forming the dispersionless flux enhancements are generated "almost simultaneously" with substorm onsets within an accuracy of a few minutes.

On the other hand, Lobe-to-PS events can be observed not only at the onsets but also even much later (~10 min) than the corresponding substorm onsets, and such large time differences cannot be explained by the temporal uncertainty of the onset determination due to the wave propagation time. Instead, as stated above, these events can be reasonably interpreted as the rapid entry of the spacecraft into the plasma sheet caused by the expansion of the plasma sheet itself associated with the substorm expansion onset. The thin plasma sheet that exists prior to the onsets is known to expand in the north-south direction at the substorm onsets. Therefore the plasma sheet entry of the spacecraft, namely observation of apparent dispersionless features, can be delayed depending on the pre-onset positions of the spacecraft relative

to the plasma sheet.

On the contrary, the dispersed events do not appear to be correlated with the corresponding substorm onsets, as shown in Figure 3-9. Red pluses and green crosses in Figure 3-9 represent the dispersed events for ions and electrons, respectively. As seen from the figure, time delays of the dispersed events are distributed from 0 min. to several tens of minutes at any local time sector. This result is not surprising but would be reasonably interpreted by the multiple dispersed flux enhancements as noted in Event 2. We have shown observationally that even a single onset of substorm could produce multiple populations of energetic particles in an intermittent manner. Such multiple ejections of energetic particles at local midnight would lead to the observation of dispersed flux enhancements with time delays of several tens of minutes from substorm onset at local time sectors away from midnight.

3.4.3 Spatial characteristics of time scale of energy-dispersion

Energy-dispersed features of energetic flux enhancements give us important information on the transport of energetic particles from their source region to the observation points. Past studies showed that energetic particles with energies of several tens of keV or larger are subject to gradient and curvature drifts in the magnetosphere [e.g. *Reeves et al.,* 1991]. Since the gradient and curvature drift speeds increase with particle's energies, the drifting particles having different energies get dispersed in space and then arrive at the observation point in the order of decreasing energy after they travel a finite distance on their drift path from the source region. Since the separation of drifting particles is expected to become larger as they travel longer on their drift path, the difference of their arrival times, that is, the time scale of energy dispersion is a measure of the distance from the source region of energetic particles measured along their drift path. In this section, we will investigate the local time dependence of the time scale of energy-dispersion to examine transport processes of energetic particles in the magnetosphere during substorm activity. However, the magnetic field as well as the electric field of the magnetosphere is very complicated and hence particle trajectories cannot be obtained analytically. Therefore, we will first perform a numerical simulation of energetic particle drifts in the model magnetospheric electric and magnetic field to understand basic properties of particle trajectories in the magnetosphere. Then we will compare the numerical estimates with the observational results obtained earlier in this study.

3.4.3.1 Numerical tracing of energetic particle drifts

In order to examine characteristics of particle drift paths in the magnetosphere, we made a drift path calculation in the model electric and magnetic field. As a model field, we adopted a Volland-Stein type electric field with the shaping factor of 2 [*Volland*, 1973] and the Tsyganenko 1989 magnetic field model for Kp=3 [*Tsyganenko*, 1989]. Trajectories of particle drifts were traced three-dimensionally by solving the equation of guiding center motion both perpendicular and parallel to the magnetic field [e.g., *Northrop* 1963],

$$u_{\perp} = \frac{\vec{e_1}}{B} \times (-\vec{E} + \frac{\mu}{q} \nabla B + \frac{m}{q} u_{\parallel}^2 \frac{\partial \vec{e_1}}{\partial s}) \quad (1)$$

$$m du_{\parallel} / dt = -\mu \frac{\partial B}{\partial s} + m \vec{u_{\perp}} \cdot \frac{d \vec{e_1}}{dt} \quad (2),$$

where $u_{\perp}$ and $u_{\parallel}$ describe the guiding center motion perpendicular or parallel to the magnetic field, respectively, $\vec{e_1}$ is the unit vector of the magnetic field, and μ represents the magnetic moment which is conserved throughout each drift trajectory. $\partial / \partial s$ denotes a derivative along a local field line. In Formula (1), gradient and curvature drift terms (the second and third term, respectively) are proportional to the perpendicular and parallel kinetic energy, respectively, which cause dispersed drift speeds in energy. These two terms depend also on the electric charge of particles so that ions and electrons drift in the opposite direction to each other. On the other hand, the E×B drift term (the first term) depends neither on charge nor on energy. The electron trajectory is calculated by reversing the direction of the ion gradient and curvature drifts in the azimuthal direction. This simplification leads to the same equatorial projection of trajectory as the one with real electron mass, but wrong bouncing period along the filed line [*Takahashi and Iyemori*, 1989].

In Figure 3-10a, we show the calculated three-dimensional trajectory of the guiding center of a proton with an initial energy of 100 keV and with a 15 degree pitch angle at the starting point of calculation (X=-9 R_E, Y=Z=0). Figure 3-10b is the equatorial projection of the 3-D trajectory on the X-Y plane. It is seen that the proton

drifted azimuthally westward around the Earth, bouncing between the northern and southern hemisphere along the magnetic field line. As a result, the test proton makes a closed drift path around the Earth and comes back to the proximity of the start point. A detailed examination of the interrelationship between different drift components revealed that the gradient and curvature drift components contribute predominantly to the azimuthal drift motion. It is also found that the resultant closed drift path is nearer the Earth on the dusk side, while it expands outward on the dawn side, which is due to a small contribution from the E×B drift. The calculation for an electron path (not shown) with the same initial condition revealed that the shape of the electron trajectory is anti-symmetric to that of the proton trajectory about the noon-midnight meridian, as expected from the charge dependence of gradient and curvature drifts. These results are in qualitative agreement with the past studies [*Takahashi and Iyemori*, 1989; *Reeves et al.*, 1991].

Next we will demonstrate the dependence of the drift trajectory on the particle pitch angle. Figure 3-11 shows the proton drift paths mapped to the equatorial plane along the field line, and the red, green, and blue curves are the mapped drift paths of protons with the start point of X= -7, -9, -11 R_E, Y=Z=0, respectively. Three curves with the same color represent the trajectories for pitch angle of 15, 45, 90 degrees.

To understand general properties of the pitch angle dependence of trajectories, we first focus on the three trajectories starting at X = -7 R_E illustrated with red curves. Among three red curves, the most inward one with a fairly circular shape is the one for 15 degree pitch angle, and the ellipse-like trajectory just outside of it corresponds to the 45 degree pitch angle case, and the most outward trajectory reaching the post-noon magnetopause is for 90 degree pitch angle. It is found that particles with smaller pitch angles can take more inward paths even if they started to drift at the same downtail distance on the nightside. This pitch angle dependence can be seen for all of the cases with different starting point distances. This effect is due to the difference in trajectory between gradient drift and curvature drift in the magnetosphere. Because, in the near-Earth magnetosphere, the radius-of-curvature vector of the magnetic field is directed almost radially at all local time sectors, the curvature drift is always pointed in the almost azimuthal direction and thus results in a fairly circular drift path for the curvature drift-dominant particles with small pitch angles. On the other hand, the intensity of the model magnetic field in the equatorial region is not azimuthally uniform but shows a clear asymmetry in the noon-midnight direction due to the field compression by the solar wind on the dayside. Therefore

contour lines of the constant field intensity in the equatorial region tend to be off-centered, and even cross the magnetopause on the dayside [*Roederer*, 1970]. This fact means that the gradient drift-dominant particles with pitch angles near 90 degree tend to pass a more radially outward region on the dayside than on the nightside. It is also noted that gradient-drifting particles may directly reach the magnetopause if their starting points on the nightside are more distant than the geosynchronous orbit. These results are consistent with drift path calculations performed in the past studies [*Reeves et al.*, 1991].

3.4.3.2 Comparison between the numerical estimates and the observation

Now we can compare quantitatively simulation results and the observation results. Figure 3-12 shows the local time dependence of the time scale of energy dispersion for dispersed ion (red pluses) and electron (green crosses) events, respectively. Here the time scale of energy dispersion is defined as the time difference between the flux increases in the energy channels of 312 keV and 88 keV. In addition, we theoretically estimate the time scale of dispersion by back-tracing drift motions of particles at the above two energies at R=9 R_E at a given local time to the midnight sector. The difference in the time that is needed for particles with different energies (312 keV and 88 keV) to drift from midnight to a given local time is considered as a time scale of dispersion. For this estimation, we considered ions and electrons with the pitch angle of 45 degree to take the effects of both the gradient and curvature drifts into account. The estimated time scale for each local time is shown in Figure 3-12 by red and green lines for protons and electrons, respectively.

In Figure 3-12, the distributions of the ion and electron dispersed events are almost exclusive of each other, being centered on the dusk and dawn side, respectively, showing the same result as Figure 3-7b. It is also seen that most of the dispersed events show fairly short (< 10 minutes) dispersions and that the time scale of dispersion tends to become larger away from the midnight. A comparison between the observation result and the numerical estimate shows that, for the most part, the observed time scale of dispersion is consistent with the estimated one at all local time sectors. These results strongly support our interpretation that both ions and electrons contributing to the observed dispersion were generated at local midnight and then drifted to the observed locations.

A surprising fact is that part of the dispersed events shows substantially long (~

a few to several tens of minutes) dispersions. It is also seen from Figure 3-12 that these events with a long dispersion are found at any local time sector for both ions and electrons. Thus these features cannot be explained by the effect of the charge-dependent drift from the midnight region; they rather indicate that particles forming the dispersion have drifted from somewhere much further than the midnight sector. We can interpret such a long dispersion as a result of particle's trip around the Earth before the observation. If energetic particles go around the Earth and thereby drift a sufficiently long path, they get further dispersed in energy. Hence observations require that energetic particles with energies of a few hundred keV make a closed drift path around the Earth in the magnetospheric field configuration. According to the drift path calculation shown in Figure 3-11, we see that such a closed drift path can be realized outward of the geosynchronous distance if drifting particles have small pitch angles (see the case of 15 degree pitch angle with the starting point of X = -9 R_E in Figure 3-11).

The pitch angle dependence is actually observed as a parallel pitch angle anisotropy of particle fluxes in Event 1 shown in Figure 3-1. As stated previously, a dispersed increase in particle fluxes parallel to the magnetic field directly indicates that the enhanced fluxes consist of particles with small pitch angles. In addition to the event study, a statistical study for these dispersed events with long energy-dispersion has been made and the result is shown in Figure 3-13. In the figure, the ratio of particle fluxes perpendicular and parallel to the magnetic field is plotted against local time for the dispersed events whose time is longer than 20 min. Here the pitch angle anisotropy is derived by averaging over each dispersion the ratio of particle fluxes with pitch angles more than and less than 45 degree. Thus the anisotropy index more/less than unity indicates perpendicular-/parallel-enhanced fluxes of energetic particles, respectively, referring to the direction of local magnetic field line. It is seen from Figure 3-13 that most of the dispersed events having a long dispersion show a parallel pitch angle anisotropy on the nightside. As shown by the present simulation results, only energetic particles with small pitch angles can go around the Earth and then get back to the night side region. Thus the dispersed flux enhancements on the nightside can be reasonably interpreted as a result of energetic particles drifting with small pitch angles on a closed path around the Earth. On the other hand, the anisotropy index indicates an isotropic feature or even perpendicular-enhanced characteristics for events observed on the dayside, indicating a significant contribution from particle flux perpendicular to the magnetic field. This result implies that

energetic particles with large pitch angles as well as those with small pitch angles have access to the dayside magnetosphere along their closed drift paths. According to the simulation, it is expected that those particles with large pitch angles would be the ones which started on the nightside much nearer to the Earth. It should be remembered that the drift path for large pitch angle particles expands outward on the dayside and hence particles that were in the inner region on the nightside can go out to the region on the dayside where GEOTAIL was located. Therefore, such dispersed events observed on the dayside would be a mixture of particles with large pitch angles from the inner magnetosphere and those with small pitch angles from the nightside magnetosphere.

3.4 Summary and Discussion

We found that flux enhancements of energetic particles with clear energy-dispersed features are observed in the outer magnetosphere ($R > 9R_E$) following the corresponding substorm onset. In addition to our observation, it has been reported that, during substorms, the ion composition sensors on the POLAR satellite (placed in a polar orbit) observed ion populations drifting around the Earth over wide L and energy ranges of L ~4-8 R_E (L: geocentric distance mapped to the equator) and a few keV to hundreds of keV, independent of the mass and charge of the ions [*Fennell et al.*, 1998]. Taking observations made at different radial distances into account, it is concluded that the region of such enhanced energetic particles extends spatially from the inner magnetosphere of $R \sim 4\ R_E$ to the outer magnetosphere ($R \sim 10\ R_E$). However, in the inner region, energetic particles can go around the Earth many times and result in multiple drift echoes because of the steady dipole-like magnetic field there [*Fennell et al.*, 1998]. On the other hand, such multiple drifting echoes are hardly observed, or at most only the first drift echo is seen in the outer magnetosphere. The reason for it would be that only particles with small pitch angles can make a closed drift path around the Earth at radial distances further away from the geosynchronous orbit and such particles would be lost to the high latitude ionosphere due to the collision with the neutral atmosphere. Of course, energetic particles with large pitch angles, which are steadily confined between magnetic mirrors of both hemispheres, would readily reach the flank magnetopause and be lost from the magnetosphere. As a result, the drifting echoes of energetic particles would rapidly decay in the outer magnetosphere.

In Figure 3-6a, we showed that the dispersionless flux enhancement of energetic

particles occurs mostly around the midnight sector within a downtail distance of 15 R_E. Since the dispersionless feature indicates that the observation point is close to the source site of energetic particles, this fact indicates that the acceleration site should be much closer to the Earth than the nominal reconnection site in the plasma sheet ($-30 < X < -20$ R_E) [*Nagai et al.*, 1998]. Thus this result does not support the Baker model [*Baker et al.*, 1979] in which particles are accelerated by the near-Earth reconnection and then injected into the inner magnetosphere. Instead, our result is rather consistent with the acceleration with an inductive electric field as proposed by *Birn et al.* [1997b]. They suggested that energetic particle acceleration is due to the temporarily evolving electric field localized around the midnight sector somewhat earthward of the near-Earth reconnection site. They performed a global MHD simulation of the near-Earth magnetic reconnection for substorms, and then, using the resultant dynamical electric and magnetic field, they calculated trajectories of test particles. Their most remarkable result is that ions tend to be accelerated more efficiently around $X = -12$ R_E due to the inductive electric field associated with depolarization of the magnetic field, rather than in the vicinity of the magnetic reconnection point around $X = -20$ R_E. The region of enhanced inductive electric field found in their simulation is consistent with the acceleration site expected from the observed dispersionless flux enhancements in the present study. In addition to this spatial correspondence between the simulation and the observation, as stated in Case study 1, most of the dispersionless events analyzed in the present study are accompanied by a significant increase in the northward (Bz) component of the magnetic field. The similar Bz increase is seen in the simulation of Birn et al. and is interpreted to be responsible for the generation of the inductive electric field. Therefore we suggest that energetic particles contributing to the enhanced flux would have been accelerated by the same mechanism demonstrated by Birn et al.

In relation to the acceleration mechanism stated above, temporal variations of enhanced particle fluxes during dispersionless events provide information about their acceleration processes. The present observation of dispersionless flux enhancements revealed that a dispersionless flux enhancement consists of intermittent flux increases with short durations of ~ minutes and that their pitch angle distributions are randomly varying or fairly uniform with no preferential direction of anisotropy. Similar features were obtained in the past study on a dispersionless flux enhancement associated with the disruption of the near-Earth cross-tail current [*Lui et al.*, 1988], where energetic particle fluxes as well as the local magnetic field exhibit a highly

turbulent feature. Hence these observational results are suggestive of a possibility that not only a simple adiabatic betatron acceleration by the increase of field intensity, which is expected to result in a perpendicular-enhanced pitch angle distribution, but also some localized transient nonadiabatic acceleration works efficiently in the above region. For such an acceleration mechanism, *Birn et al.* [1997a] proposed an acceleration process where equatorially trapped particles experience the succession of the Speiser type acceleration [*Speiser*, 1963] under the inductive electric field and thereby gain energy repeatedly in a stepwise fashion. However, as shown in their test particle simulation, this mechanism tends to generate particles with large pitch angles, and thus is not consistent with the observed flux enhancements in the present study that show no preferential pitch angle anisotropy. Thus in order to explain the observations by this mechanism, an additional physical process responsible for the rapid pitch angle scattering of the accelerated particles is needed. In contrast to the near-Earth plasma sheet, the injection at geosynchronous distances shows a clear pitch angle anisotropy where large pitch angle particles are dominant. This can be reasonably understood because, around geosynchronous orbit, the Speiser type acceleration does not work effectively due to the large magnetic field intensity, and instead, the adiabatic betatron acceleration becomes dominant. Therefore, the primary acceleration process for the injected particles shifts from the nonadiabatic to adiabatic processes as particles are injected from the near-Earth plasma sheet into the geosynchronous distance.

One of the important statistical results in the present study is that electron flux enhancement events are relatively rare as compared to ion events. In particular, the dispersionless electron events were found to be substantially less frequent than the ion ones, suggesting that the corresponding acceleration mechanism does not work effectively for electrons. This would be considered as a reasonable result if you assumed the nonadiabatic acceleration processes discussed above to be responsible for the dispersionless flux enhancements in the near-Earth plasma sheet ($R > 9R_E$). This kind of nonadiabatic energization is achieved generally by violating particle's gyromotion around the field line and thereby making them drift in the direction of local electric field. In the proximity of the neutral sheet in the near-Earth plasma sheet, characteristic length of the curvature of field lines can be comparable to the gyroradius for ions with energies ~ a few tens of keV and thus ions at these energies can easily stray out of their gyromotion and gain energies efficiently from the inductive electric field. On the other hand, electron gyroradius is much smaller and

electrons tend to behave adiabatically. *Birn et al.* [1998] examined electron trajectories in the region of the strong inductive electric field and found that the adiabatic betatron energization caused by the sunward E×B drift plays a more important role on the electron acceleration. Because the betatron acceleration is more effective closer to the Earth where the gradient of the field intensity becomes steeper, it is expected that electrons are accelerated efficiently in the inner region ($R < 9\ R_E$). Therefore it is suggested that the acceleration site (precisely speaking, the tailward edge of the acceleration site) for electrons is shifted closer to the Earth than that for ions. This radial displacement of the acceleration region between ions and electrons can explain not only the rare observation of dispersionless electron events around the midnight sector, but also the absence of dispersed electron events around the dawn flank region as shown in Figure 3-7b, because energetic electrons are expected to start drifting from the region closer to the Earth than ions, and thus they drift toward the more sunward magnetopause.

The difference in the radial distance of the acceleration region between ions and electrons may cause an imbalance between the abundance of the injected energetic ions and electrons in the inner magnetosphere. Generally in the magnetosphere, once a particle is accelerated to high energies, it starts to drift azimuthally away from the acceleration site and thereby deviates greatly from the transport path expected from E×B drift. Actually the test particle simulation performed by *Birn et al.* [1997b] demonstrated that accelerated ions are ejected duskward from the acceleration site at the midnight. Therefore, in the course of the acceleration process associated with injection, energized ions drift away before electrons begin to be accelerated and thus it is difficult for the energized ions to penetrate as radially inward as the electrons that have not been accelerated yet. This may result in a relatively small abundance of injected energetic ions as compared to energetic electrons in the inner magnetosphere. *Friedel et al.* [1996] studied the energetic particle injection events around $R \sim 6\ R_E$ using particle data obtained at the CRRES satellite and indicated that, at the CRRES orbit, dispersionless ion injections are in general less clear and tend to occur more frequently in the higher energy channels. This result seems to be consistent with the above suggestion derived from the present study, because the small abundance of injected energetic ions would lead to a less clear flux enhancement of ions. In addition, if part of ions are trapped deeply in the acceleration region and transported to the inner magnetosphere together with electrons, the ions are subject to acceleration for a longer time and thus expected to be energized to higher energies than electrons.

Here it is interesting to discuss the spatial extent of the injection region and its relationship with that of injection events observed at geosynchronous orbit. As shown in Figure 3-6a, the dispersionless flux enhancements are found not only at midnight but also at local time sectors significantly away from midnight. In addition to the dispersionless events away from the midnight, Figure 3-6b shows that, even in the midnight sector, the dispersed events are also found with almost the same probability as the dispersionless events. These results suggest two important characteristics of the acceleration region in the near-Earth plasma sheet. One is that the acceleration site of injected energetic particles can be formed not only in the midnight sector but also at the local time sectors away from the midnight. This means that energetic particles can be injected into regions significantly away from the midnight sector in the inner magnetosphere. Another characteristic is that the acceleration site is fairly localized in the azimuthal direction so that the dispersed signatures can be observed only when the acceleration site shifts azimuthally from local midnight. This azimuthally localized acceleration site is consistent with the region of large inductive electric field shown in the MHD simulation performed by *Birn et al.* [1997b]. It should be also noted that the past studies at geosynchronous orbit [e.g., *Friedel et al*, 1996; *Birn et al.*, 1997a] reported the existence of significantly off-midnight dispersionless injections and such an injection can be explained by the off-midnight acceleration of energetic particles in the near-Earth plasma sheet shown in the present study.

Finally, we interpret our result of flux enhancements in the outer magnetosphere in the light of the past studies closer to the Earth and summarize energization and subsequent global transport of energetic particles in the magnetosphere in association with substorms. Our interpretation is shown schematically in Figure 3-14. Here we illustrate on the X-Y plane temporal evolution of the region of enhanced energetic ions (red hatched region) and electrons (green hatched region) just after the substorm expansion onset and a few tens of minutes after the onset on the left and right panels, respectively. Also shown are the nominal magnetopause (solid curve), the spacecraft's perigee distance (dotted circle of R = 9 R_E), and geosynchronous orbit (the innermost solid circle). As shown in the left panel, during a substorm, energetic particles with energies from several tens to hundreds of keV are generated around local midnight almost simultaneously with the substorm expansion onset. The acceleration region is associated with the region of depolarization (shaded region) and slightly displaced in the dawn-dusk direction for ions and electrons. According to the past studies in the inner magnetosphere [e.g., *Barfield et al*, 1977, *Friedel et al*, 1996], the sunward edge

of the enhanced flux region can extend to geocentric distance of 4-5 R_E. On the other hand, its tailward edge is mostly located around R = 15 R_E, which is significantly earthward of the near-Earth reconnection site. As shown in the present study, the tailward edge of the acceleration region for electrons tends to be formed more earthward and thus electrons are primarily accelerated and start drifting in inner regions as compared to ions. Subsequently, the energetic ions and electrons generated at the midnight sector start to drift duskward and dawnward, respectively, and are transported into the dawn and dusk flanks on a time scale of ~several minutes. Since energetic particles with energies of ~ hundreds of keV are primarily subject to gradient- and curvature-B drift whose speed depends on particle's energy, the energetic population get dispersed in energy in the course of their azimuthal transport. The energetic particles drift on separate drift paths depending also on their pitch angles; those with larger pitch angles, that is, nearer 90 degree, tend to trace outer paths and reach the magnetopause at more tailward positions. It should be noted that electrons are accelerated in and then start to drift from the region closer to the Earth than ions. Thus energetic electrons are supplied into more sunward regions along their drift path, as shown in the right panel of Figure 3-14. In particular, particles with small pitch angles can make a closed drift path around the Earth, i.e., go longitudinally around the Earth via the dayside magnetosphere and return to the midnight sector.

A few tens of minutes after the onset (the right panel), energetic ions and electrons spread out over the dusk and dawn side magnetosphere, respectively, and further, particles with small pitch angles still drift into the opposite sides of the magnetosphere, then get back to the midnight sector and merge into the newly accelerated population there. This drifting population is observed as a fully dispersed flux enhancement due to their long drift path they have drifted on. The drift path calculation in the present study showed that only particles with small pitch angles can return to the midnight region in the near-Earth plasma sheet (R > 9R_E), while those with large pitch angles reach the flank magnetopause and be lost into the magnetosheath. Hence well dispersed flux enhancements found on the night side are mostly composed of energetic particles with small pitch angles, showing parallel pitch angle anisotropy. On the other hand, particles with large pitch angles starting from the inner magnetosphere also have access to the dayside magnetosphere near the magnetopause along their closed drift path expanding sunward on the dayside. Thus energetic population with long dispersion found on the dayside consists of small pitch

angle particles coming from the night side plasma sheet and also of large pitch angle particles originating in the inner magnetosphere. Since generally flux intensity of energetic particles is larger closer to the Earth, the dispersed flux enhancements on the dayside are dominated by the particles of the near-Earth origin, resulting in isotropic or even perpendicular pitch angle anisotropy.

References

Angelopoulos, V., C. F. Kennel, F. V. Coroniti, R. Pellat, M. G. Kivelson, R. J. Walker, C. T. Russel, W. Baumjohann, W. C. Feldmann, and J. T. Gosling, Statistical characteristics of bursty bulk flow events, *J. Geophys. Res., 99*, 21257, 1994.

Angelopoulos, V., F. V. Coroniti, C. F. Kennel, M. G. Kivelson, R. J. Walker, C. T. Russel, R. L. McPherron, E. Sanches, C.-I. Meng, W. Baumjohann, G. D. Reeves, R. D. Belian, N. Sato, E. Friis-Christensen, P. R. Sutcuiffe, K. Yumoto, and T. Harris, Multipoint analysis of a bursty bulk flow event on April 11, 1985, *J. Geophys. Res., 101*, 4967, 1996.

Baker, D. N., P. R. Higbie, E. W. Hones Jr., and R. D. Belian, High-resolution energetic particle measurements at 6.6 R_E: 3. Low-energy electron anisotropies and short-term substorm predictions, *J. Geophys. Res., 83*, 4863, 1978.

Baker, D. N., R. D. Belian, P. R. Higbie, and E. W. Hones, High-energy magnetospheric protons and their dependence on geomagnetic and interplanetary conditions, *J. Geophys. Res., 84*, 7138, 1979.

Barfield, J. N., S. E. DeForest, D. J. Williams, Simultaneous observations of substorm electrons: Explorer 45 and ATS 5, *J. Geophys. Res., 82*, 531, 1977.

Belian, R. D., D. N. Baker, P. R. Higbie, and E. W. Hones Jr., High-resolution energetic particle measurements at 6.6 R_E: 2. High-energy proton drift echos, *J. Geophys. Res., 83*, 4857, 1978.

Belian, R. D., D. N. Baker, E. W. Hones Jr., P. R. Higbie, S. J. Bame, and J. R. Asbridge, Timing of energetic proton enhancements relative to magnetospheric substorm activity and its implication for substorm theories, *J. Geophys. Res., 86*, 1415, 1981.

Birn, J., M. F. Thomsen, J. E. Borovsky, G. D. Reeves, D. J. McComas, and R. D. Belian, Characteristic plasma properties during dispersionless substorm injections at geosynchronous orbit, *J. Geophys. Res., 102*, 2309, 1997a.

Birn, J., M. F. Thomsen, J. E. Borovsky, G. D. Reeves, D. J. McComas, R. D. Belian, and M. Hesse, Substorm ion injections: Geosynchronous observations and test particle orbits in theree-dimensional dynamic MHD fields, *J. Geophys. Res., 102*, 2325, 1997b.

Birn, J., M. F. Thomsen, J. E. Borovsky, G. D. Reeves, D. J. McComas, R. D. Belian, and M. Hesse, Substorm electron injections: Geosynchronous observations and test particle simulations, *J. Geophys. Res., 103*, 9235, 1998.

Doke, T., M. Fujii, M. Fujimoto, K. Fujiki, T. Fukui, F. Gliem, W. Guttler, N. Hasebe, T. Hayashi, T. Ito, K. Itsumi, T. Kashiwagi, J. Kikuchi, T. Kohno, S. Kokubun, S. Livi, K. Maezawa, H. Moriya, K. Munakata, H. Murakami, Y. Muraki, H. Nagoshi, A. Nakamoto, K. Nagata, A. Nishida, R. Rathje, T. Shino, H. Sommer, T. Takashima, T. Terasawa, S. Ullaland, W. Weiss, B. Wilken, T. Yamamoto, T. Yanagimachi, and S. Yanagita, The Energetic Particle Spectrometer HEP onboard the GEOTAIL Spacecraft, *J. Geomagn. Geoelectr., 46*, 713, 1994

Fennell, J. F., M. W. Chen, J. L. Roeder, W. K. Peterson, K. J. Trattner, R. Friedel, S. Livi, M. Grande, C. Perry, T. A. Fritz, and R. Sheldon, Multiple discrete-energy ion features in the inner magnetosphere: Polar observations, in *Physics of Space Plasmas, 15*, 395, MIT Press, Cambridge, MA, 1998.

Friedel, R. H. W., A. Korth, and G. Kremser, Substorm onsets observed by CRRES: Determination of energetic particle source regions, *J. Geophys. Res., 101*, 13137, 1996.

Hones, E. W., Jr., I. D. Palmer, and P. R. Higbie, Energetic protons of magnetospheric origin in the plasma sheet associated with substorms, *J. Geophys. Res., 81*, 3866, 1976.

Ieda, A., D. H. Fairfield, T. Mukai, Y. Saito, S. Kokubun, K. Liou, C. –I. Meng, G. K. Parks, and M. J. Brittnacher, Plasmoid ejection and auroral brightenings, *J. Geophys. Res., 106*, 3845, 2001

Kokubun, S., T. Yamamoto, M. H. Acuna, K. Hayashi, K. Shiokawa, and H. Kawano, The GEOTAIL magnetic field experiment, *J. Geomagn. Geoelectr., 46*, 7, 1994.

Konradi, A., Proton events in the magnetosphere associated with magnetic bays, *J. Geophys. Res., 72*, 3829, 1967.

Lanzerotti, L. J., C. S. Roberts, and W. L. Brown, Temporal variations in the electron flux at synchronous altitudes, *J. Geophys. Res., 72*, 5893,, 1967.

Lanzerotti, L. J., C. G. Maclennan, and M. F. Robbins, Proton drift echoes in the magnetosphere, *J. Geophys. Res., 76*, 259, 1971.

Lui, A. T. Y., R. W. McEntire, and S. M. Krimigis, Evolution of the ring current during two geomagnetic storms, *J. Geophys. Res., 92*, 7459, 1987.

Lui, A. T. Y., R. E. Lopez, S. M. Krimigis, R. W. McEntire, L. J. Zanetti, and T. A. Potemra, A case study of magnetotail current sheet disruption and diversion, *Geophys. Res. Lett., 15*, 721, 1988.

Mauk, B. H., and C. E. McIlwain, Correlation of Kp with the substorm-injected plasma boundary, *J. Geophys. Res., 79*, 3193, 1974.

McIlwain, C. E., Substorm injection boundaries, in *Magnetospheric Physics*, edited by B. M. McCormac, p. 143, D. Reidel, Norwell, Mass., 1974

Mukai, T., S. Machida, Y. Sato, M. Hirahara, T. Terasawa, N. Kaya, T. Obara, M. Ejiri, and A. Nishida, The low energy particle (LEP) experiment onboard the GEOTAIL satellite, *J. Geomagn. Geoelectr., 46*, 59, 1994.

Nagai, T., M. Fujimoto, Y. Saito, S. Machida, T. Terasawa, R. Nakamura, T. Yamamoto, T. Mukai, A. Nishida, and S. Kokubun, Structure and dynamics of magnetic reconnection for substorm onsets with Geotail observations, *J. Geophys. Res., 103*, 4419, 1998.

Northrop, T. G., *The adiabatic motion of charged particles*, Interscience Publishers, New York, 1963.

Pfitzer, K. A., and J. R. Winckler, Intensity correlations and substorm electron drift effects in the outer radiation belt measured with the Ogo 3 and ATS 1 satellites, *J. Geophys. Res., 74*, 5005, 1969.

Reeves, G.D., R. D. Belian, and T. A. Fritz, Numerical tracing of energetic particle drifts in a model magnetosphere, *J. Geophys. Res., 96*, 13997, 1991.

Roederer, J. G., *Dynamics of Geomagnetically Trapped Particles*, Springer-Verlag, New York, 1970.

Sarris, E. T., S. M. Krimigis, and T. P. Armstrong, Observations of magnetospheric bursts of high-energy protons and electrons at 35 R_E with Imp 7, *J. Geophys. Res., 81*, 2341, 1976.

Speiser, T., Particle trajectories in model current sheets, 1, Analytical solutions, *J. Geophys. Res., 70*, 4219, 1965.

Takahashi, S., and T. Iyemori, Three-dimensional tracing of charged particle trajectories in a realistic magnetospheric model, *J. Geophys. Res., 94*, 5505, 1989.

Tsyganenko, N. A., Magnetospheric magnetic field model with a warped tail current sheet, *Planet. Space Sci., 37*, 5, 1989.

Uozumi, T., K. Yumoto, H. Kawano, A. Yoshikawa, J. V. Olson, S. I. Solovyev, and E. F. Vershinin, Characteristics of energy transfer of Pi 2 magnetic pulsations: Latitudinal dependence, *Geophys. Res. Lett., 27*, 1619, 2000.

Volland, H., A semiempirical model of large-scale magnetospheric electric fields, *J. Geophys. Res., 78*, 171, 1973.

Walker, R. J., K. N. Erickson, R. L. Swanson, and J. R. Winckler, Substorm-associated particle boundary motion at synchronous orbit, *J. Geophys. Res., 81*, 5541, 1976.

Yumoto, K. and the 210° MM magnetic observation group, The STEP 210° magnetic

meridian network project, *J. Geomagn. Geoelectri., 48*, 1297, 1996.

Figure captions

Figure 3-1. HEP energy-time spectrograms, differential fluxes for the lowest five energy channels, and pitch angle anisotropies of energetic particles in the first, fourth, and fifth panel, respectively, observed by HEP during 11:00UT-15:00UT on June 21. Also shown are ion and electron energy spectra obtained by LEP (second and third panel, respectively) with ion bulk velocities, density, temperature (6th and 8th panel) derived from the LEP observation, and Bx- and Bz-components of the magnetic field (7th panel).

Figure 3-2. (Top) ground magnetometer data on June 21, 1996 observed at College (CMO) and (bottom) Pi2 pulsation activity during 10:00UT – 12:00UT at KAKIOKA (a low latitude station). It is evident from Figure 3-2 that a moderate substorm activity was initiated with the expansion onset at 11:37UT as determined from a Pi2 onset in the bottom panel.

Figure 3-3. The plasma and field profile during 12:00UT – 16:00UT on December 9, 1996, in the same format as Figure 3-1. During this time interval, GEOTAIL was located at the evening sector in the magnetosphere.

Figure 3-4. (Top) magnetic field data of the 210° magnetic meridian stations [*Yumoto et al.*, 1996], and (bottom) Pi2 pulsation activities observed at KAKIOKA. A visual inspection of this data enables us to identify, at least, two substorm sequences during 12:00UT – 16:00UT: the first substorm occurred at about 13:00UT, and the second one became activated at 14:30UT.

Figure 3-5. GEOTAIL orbit on the X-Y (namely, equatorial) plane during Apr., 1996 – May, 1998, where the EDIS data of the HEP-LD instrument were available.

Figure 3-6a. The locations of the spacecraft on the X-Y plane when the dispersionless and dispersed flux enhancements were observed. In the figure, red asterisks and small blue circles represent the dispersed and dispersionless events, respectively. Also superimposed are the nominal magnetopause (green curve), geosynchronous orbit (blue circle), and the spacecraft's perigee altitude of ~ 9 R_E (violet circle).

Figure 3-6b. The occurrence frequencies of the dispersed (black open rectangles) and dispersionless events (red solid bars). Here the occurrence frequency is normalized by the satellite residence time for each local time sector.

Figure 3-7. The local time profiles of the occurrence frequencies for (a) dispersed and (b) dispersionless ions and electrons, respectively.

Figure 3-8. The local time dependence of the time delays of the dispersionless flux enhancements from the corresponding substorm onsets. Here we plotted only events during which the onset times could be determined from Pi2 pulsation activities on the low-latitude ground stations of Kakioka (KAK) and Hermanus (HER). In the figure, open circles and triangles denote Lobe-to-PS events and PS-throughout events, respectively. In the figure, a negative value of the time delay means that a flux enhancement precedes a substorm onset.

Figure 3-9. The local time dependence of the time delays of the dispersed flux enhancements from the corresponding substorm onsets. Red pluses and green crosses in the figure represent the dispersed events for ions and electrons, respectively.

Figure 3-10. (a) The calculated three-dimensional trajectory of the guiding center of a proton with an initial energy of 100 keV and 15 degree pitch angle at the starting point of calculation (X=-9 R_E, Y=Z=0), and (b) is its equatorial projection of the 3-D trajectory on the X-Y plane.

Figure 3-11. The proton drift paths mapped to the equatorial plane along the field line ,and the red, green, and blue curves are the mapped drift paths of protons with the start point of X= -7, -9, -11 R_E, Y=Z=0, respectively. Each three curves for each color represent the trajectories for pitch angle of 15, 45, 90 degree.

Figure 3-12. The local time dependence of the time scale of energy dispersions for dispersed ion (red pluses) and electron (green crosses) events, respectively. Here the time scale of energy dispersions is defined as the time difference between the flux increases in the energy channels of 312 keV and 88 keV. Also shown are the estimated time scale of dispersions by back-tracing drift motions of particles at the above two energies at R=9 R_E at a given local time to the midnight sector.

Figure 3-13. The ratios of particle flux intensities between perpendicular and parallel to the magnetic field are plotted against local time for the dispersed events whose time scales of dispersions are longer than 20 min. Here a pitch angle anisotropy is derived by averaging over each dispersion the ratio of intensity of particle fluxes with pitch angles between more than and less than 45 degree.

Figure 3-14. Schematic diagrams of energization and subsequent global transport of energetic particles in the magnetosphere in association with a substorm, which is deduced from the present study as well as the past studies.

Table 1. The number of substorm-associated events as well as the total event number for dispersionless/dispersed ions and electrons.

Figure 3-1

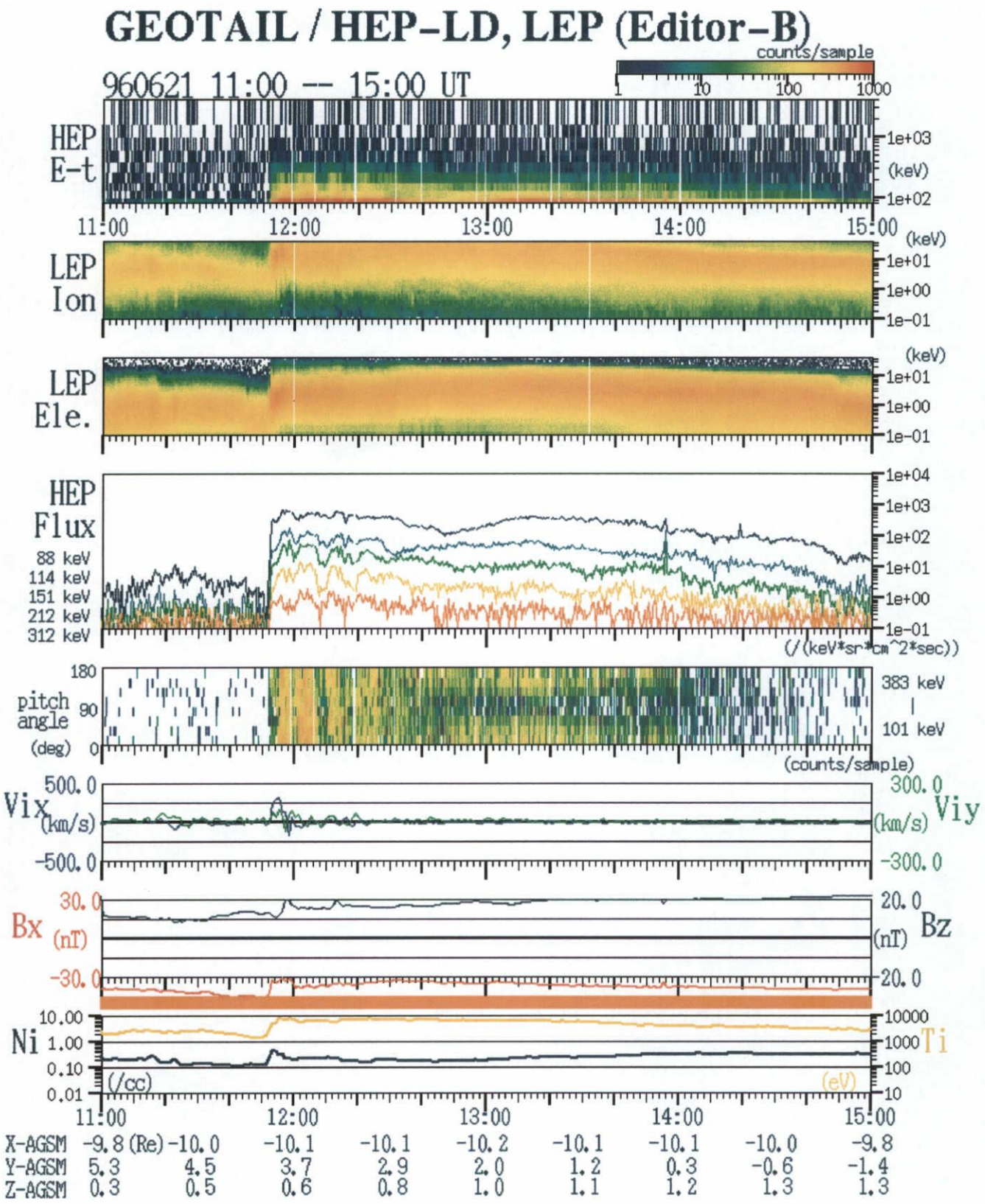
GEOTAIL / HEP-LD, LEP (Editor-B)
960621 11:00 -- 15:00 UT
counts/sample
1
10
100
1000
HEP
E-t
1e+03
(keV)
1e+02
11:00
12:00
13:00
14:00
15:00
(keV)
LEP
Ion
1e+01
1e+00
1e-01
(keV)
LEP
Ele.
1e+01
1e+00
1e-01
HEP
Flux
88 keV
114 keV
151 keV
212 keV
312 keV
1e+04
1e+03
1e+02
1e+01
1e+00
1e-01
(/(keV*sr*cm^2*sec))
180
pitch
angle
90
(deg)
0
383 keV
101 keV
(counts/sample)
500.0
Vix
(km/s)
-500.0
300.0
(km/s)
Viy
-300.0
30.0
Bx
(nT)
-30.0
20.0
(nT)
Bz
-20.0
10.00
Ni
1.00
0.10
0.01
(/cc)
10000
1000
Ti
100
10
(eV)
11:00
12:00
13:00
14:00
15:00
X-AGSM -9.8 (Re) -10.0 -10.1 -10.1 -10.2 -10.1 -10.1 -10.0 -9.8
Y-AGSM 5.3 4.5 3.7 2.9 2.0 1.2 0.3 -0.6 -1.4
Z-AGSM 0.3 0.5 0.6 0.8 1.0 1.1 1.2 1.3 1.3

Figure 3-2

960621 CMO

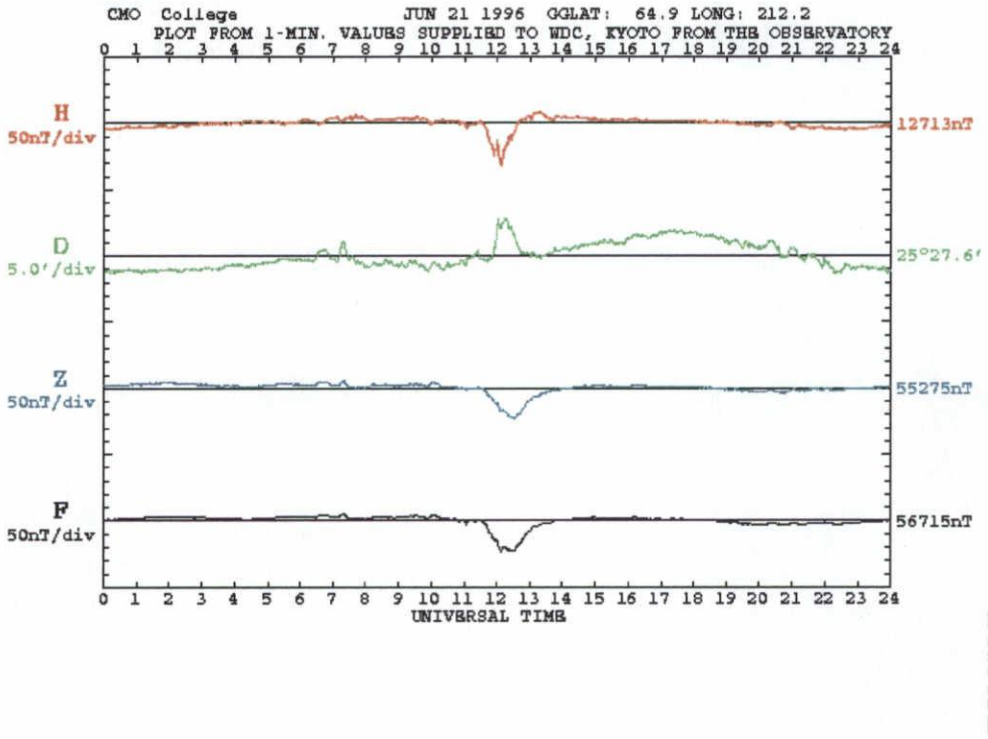

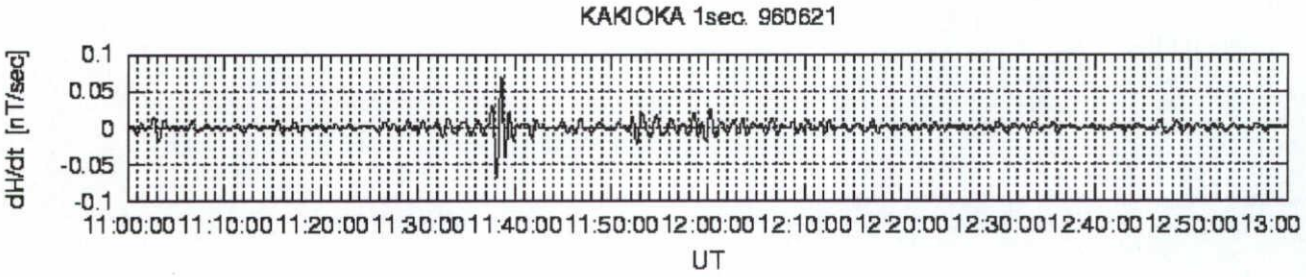

Figure 3-3

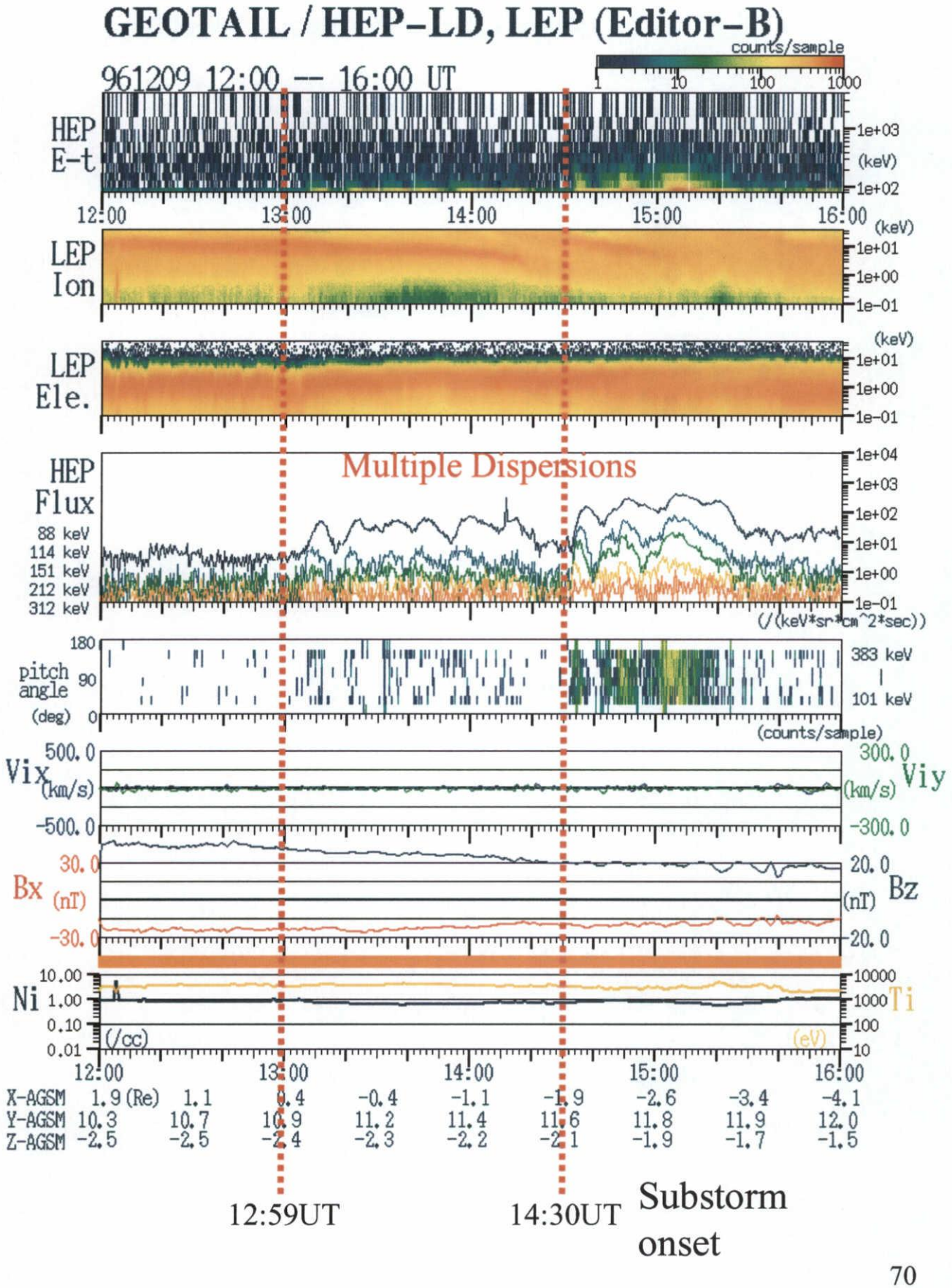
GEOTAIL / HEP-LD, LEP (Editor-B)
961209 12:00 -- 16:00 UT
counts/sample
1
10
100
1000
HEP
E-t
1e+03
(keV)
1e+02
12:00
13:00
14:00
15:00
16:00
LEP
Ion
(keV)
1e+01
1e+00
1e-01
LEP
Ele.
(keV)
1e+01
1e+00
1e-01
HEP
Flux
Multiple Dispersions
88 keV
114 keV
151 keV
212 keV
312 keV
1e+04
1e+03
1e+02
1e+01
1e+00
1e-01
(/(keV*sr*cm^2*sec))
pitch
angle
(deg)
180
90
0
383 keV
101 keV
(counts/sample)
Vix
(km/s)
500.0
-500.0
Viy
300.0
-300.0
Bx
(nT)
30.0
-30.0
Bz
20.0
-20.0
Ni
10.00
1.00
0.10
0.01
(/cc)
Ti
10000
1000
100
10
(eV)
12:00
13:00
14:00
15:00
16:00
X-AGSM 1.9 (Re) 1.1 0.4 -0.4 -1.1 -1.9 -2.6 -3.4 -4.1
Y-AGSM 10.3 10.7 10.9 11.2 11.4 11.6 11.8 11.9 12.0
Z-AGSM -2.5 -2.5 -2.4 -2.3 -2.2 -2.1 -1.9 -1.7 -1.5
12:59UT
14:30UT
Substorm
onset

Figure 3-4

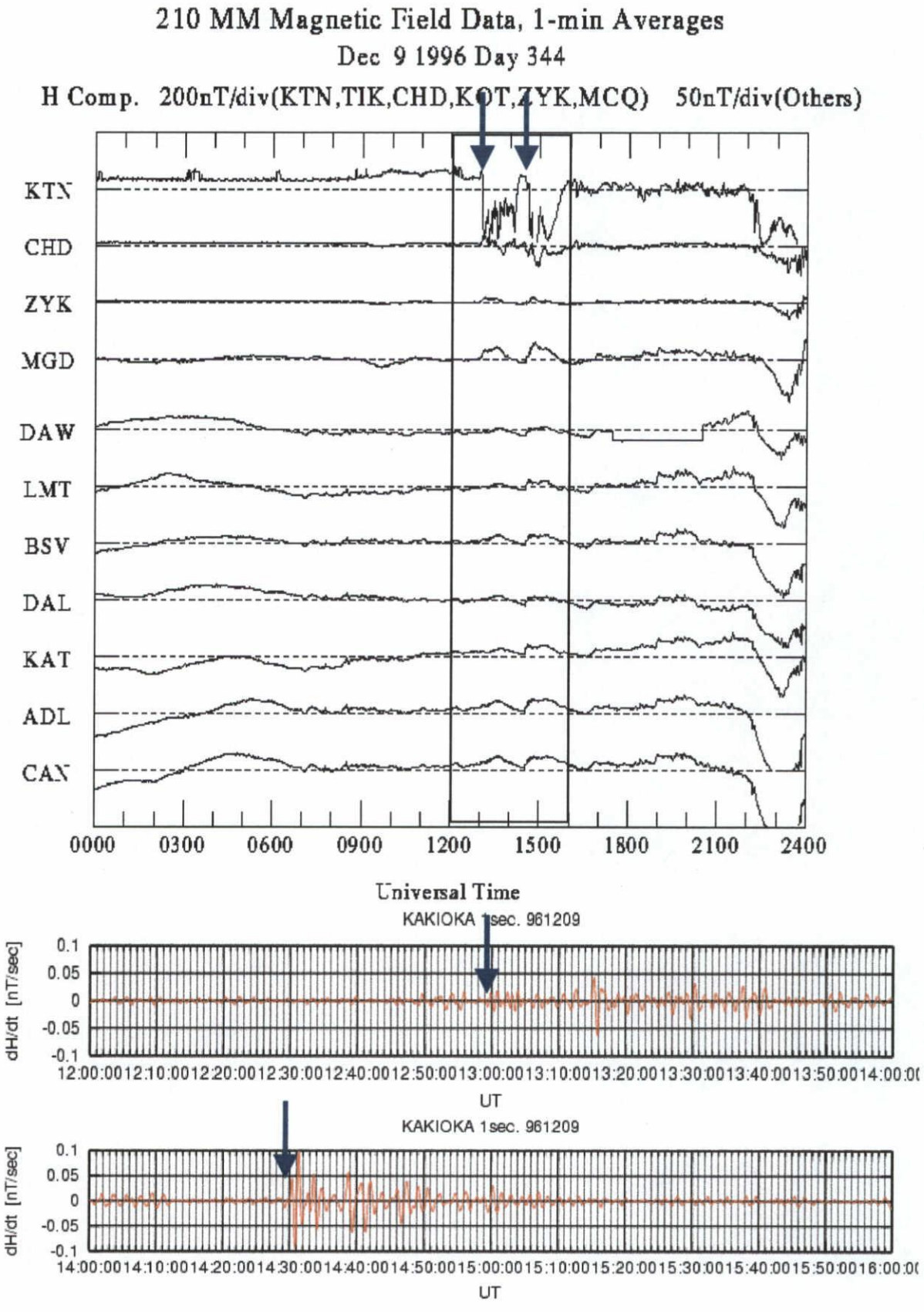
210 MM Magnetic Field Data, 1-min Averages
Dec 9 1996 Day 344
H Comp. 200nT/div(KTN,TIK,CHD,KOT,ZYK,MCQ) 50nT/div(Others)
KTN
CHD
ZYK
MGD
DAW
LMT
BSV
DAL
KAT
ADL
CAN
0000
0300
0600
0900
1200
1500
1800
2100
2400
Universal Time
KAKIOKA 1sec. 961209
dH/dt [nT/sec]
0.1
0.05
0
-0.05
-0.1
12:00:0012:10:0012:20:0012:30:0012:40:0012:50:0013:00:0013:10:0013:20:0013:30:0013:40:0013:50:0014:00:0(
UT
KAKIOKA 1sec. 961209
dH/dt [nT/sec]
0.1
0.05
0
-0.05
-0.1
14:00:0014:10:0014:20:0014:30:0014:40:0014:50:0015:00:0015:10:0015:20:0015:30:0015:40:0015:50:0016:00:0(
UT

Figure 3-5

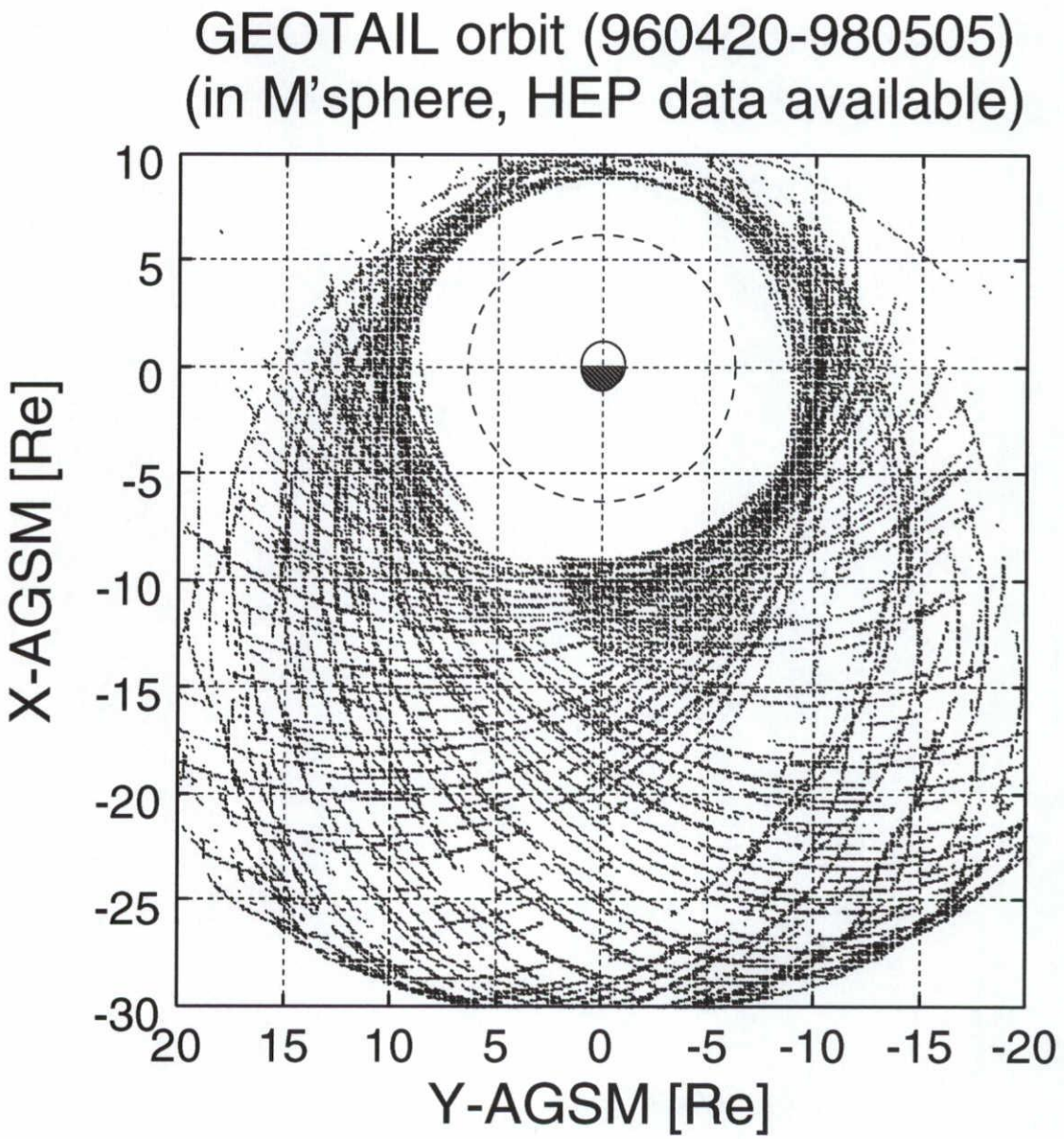
GEOTAIL orbit (960420-980505)
(in M'sphere, HEP data available)
X-AGSM [Re]
Y-AGSM [Re]
10
5
0
-5
-10
-15
-20
-25
-30
20
15
10
5
0
-5
-10
-15
-20

Figure 3-6a

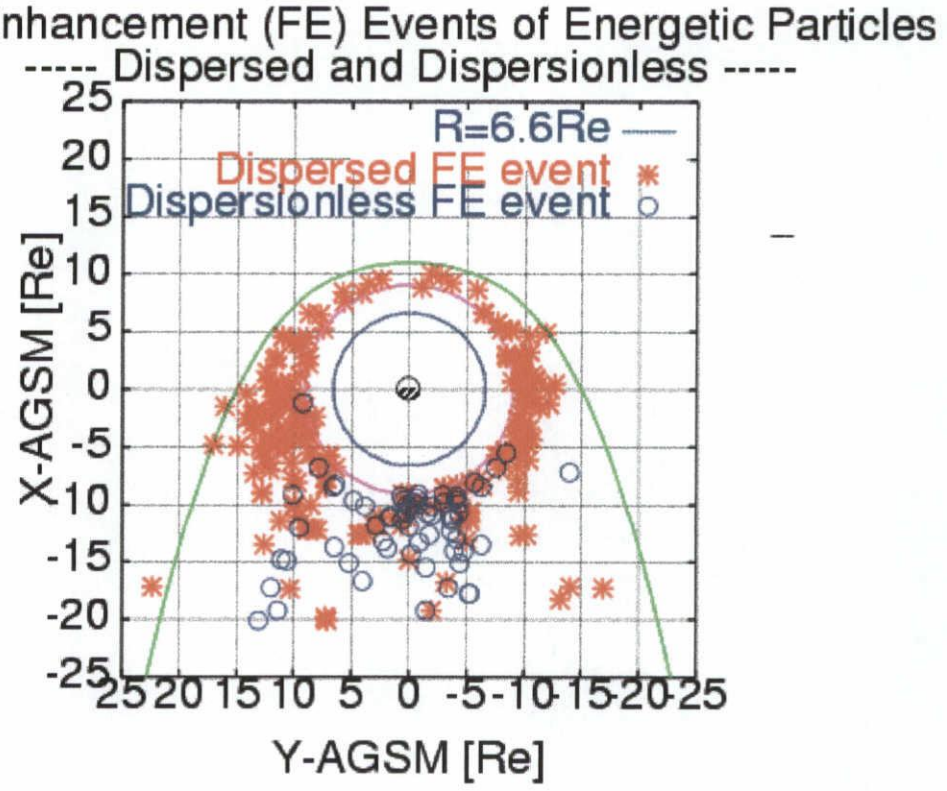

Figure 3-6b

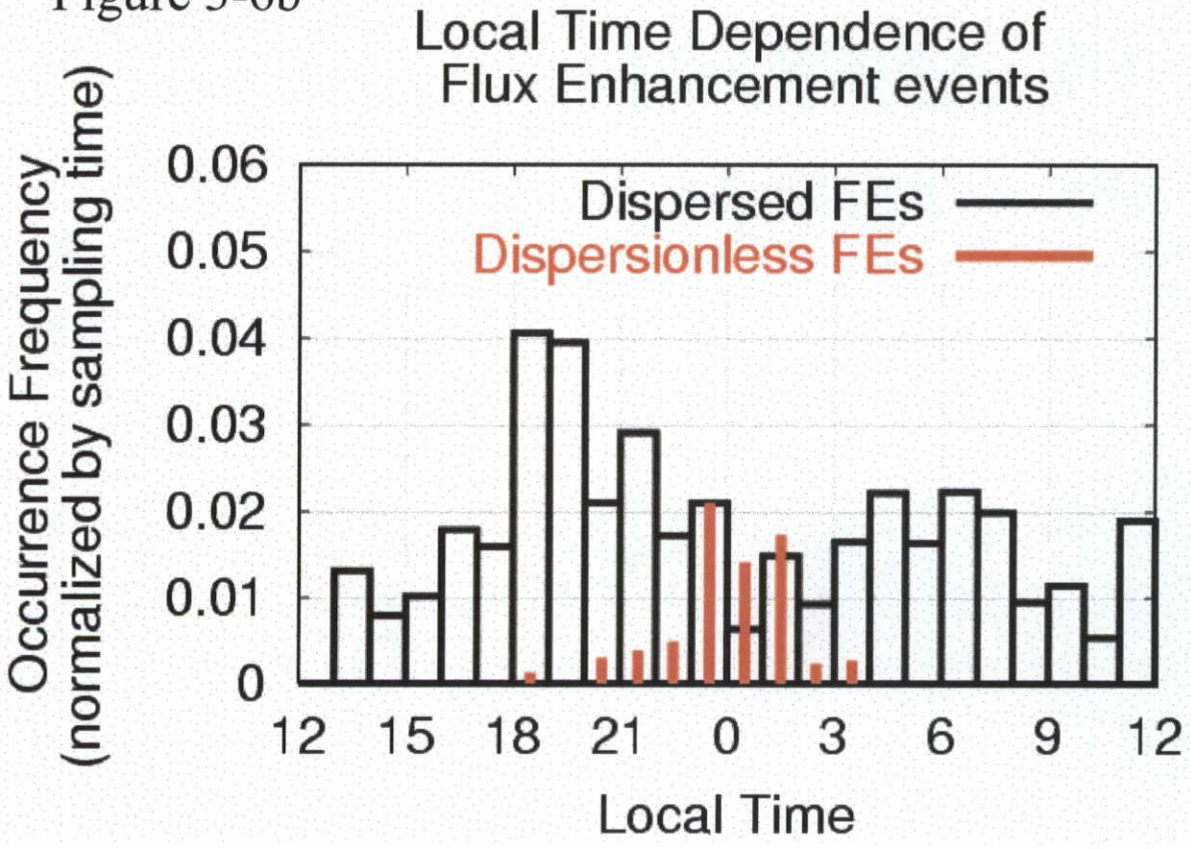

Figure 3-7a

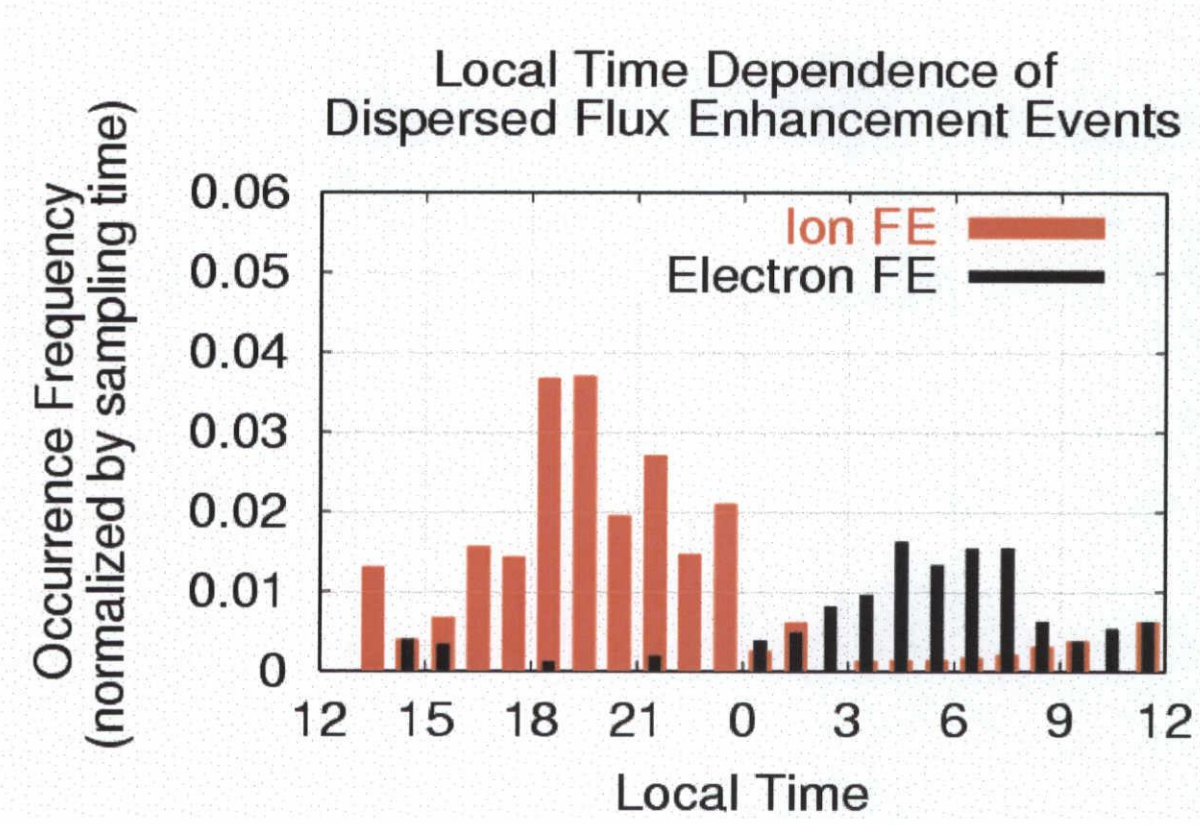
Local Time Dependence of
Dispersed Flux Enhancement Events
Occurrence Frequency
(normalized by sampling time)
0.06
0.05
0.04
0.03
0.02
0.01
0
Ion FE
Electron FE
12
15
18
21
0
3
6
9
12
Local Time

Figure 3-7b

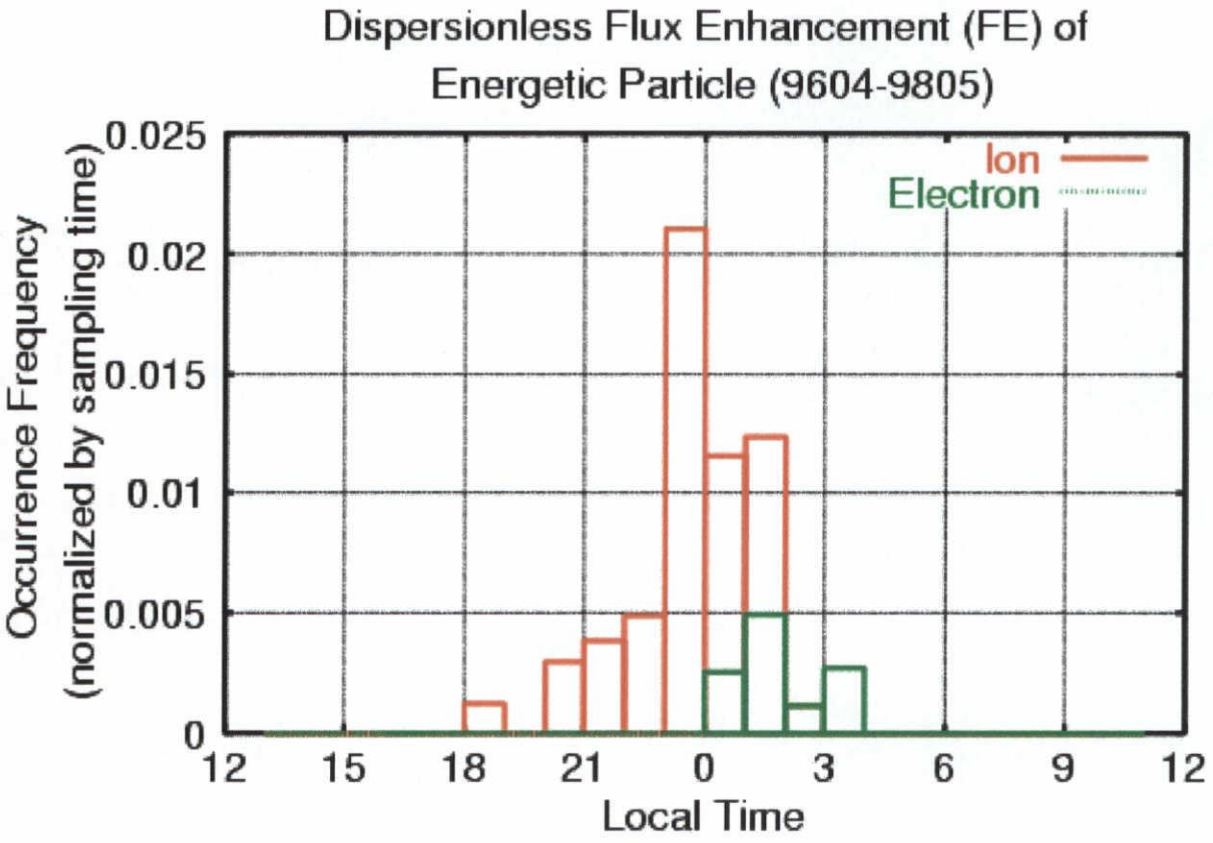
Dispersionless Flux Enhancement (FE) of
Energetic Particle (9604-9805)
Occurrence Frequency
(normalized by sampling time)
0.025
0.02
0.015
0.01
0.005
0
Ion
Electron
12
15
18
21
0
3
6
9
12
Local Time

Table 1

		substorm-associated	No substorm signatures	total
Dispersionless event	Ions	51 (96%)	2	53
	Electrons	10 (100%)	0	10
Dispersed events	Ions	130 (96%)	6	136
	Electrons	55 (86%)	9	64

Figure 3-8

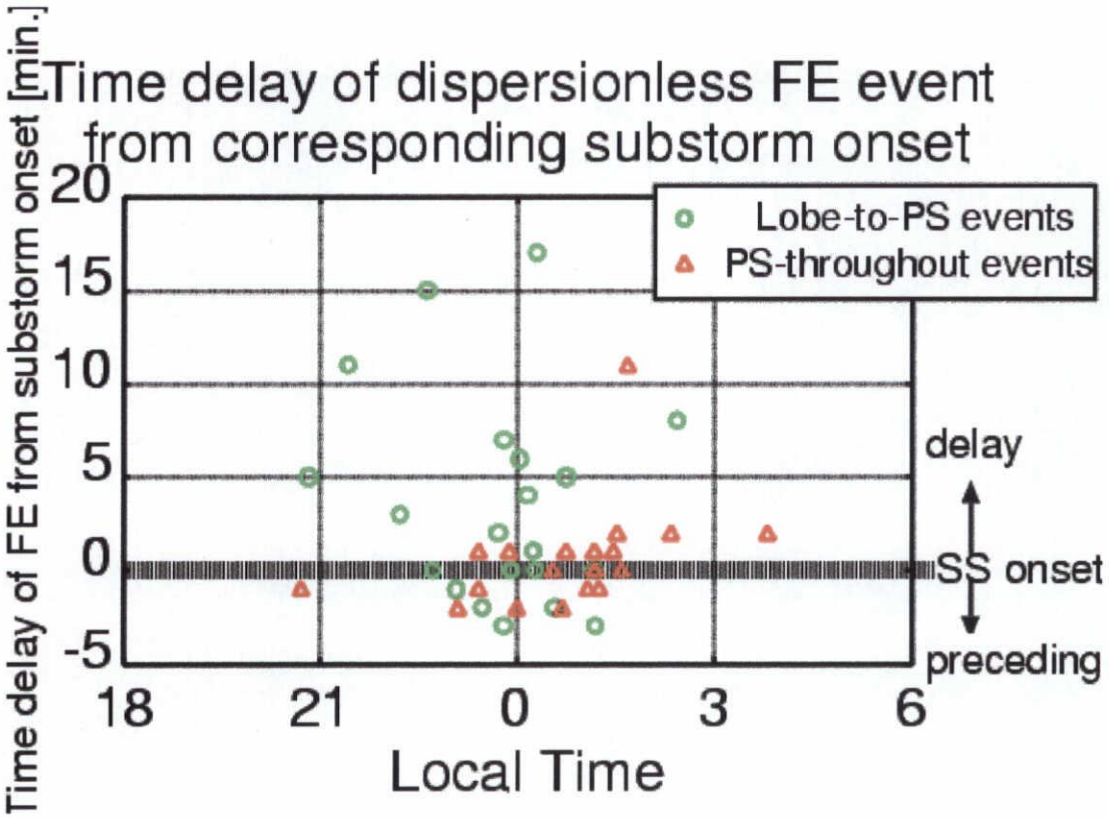
Time delay of dispersionless FE event
from corresponding substorm onset
Time delay of FE from substorm onset [min.]
20
15
10
5
0
-5
18
21
0
3
6
Local Time
Lobe-to-PS events
PS-throughout events
delay
SS onset
preceding

Figure 3-9

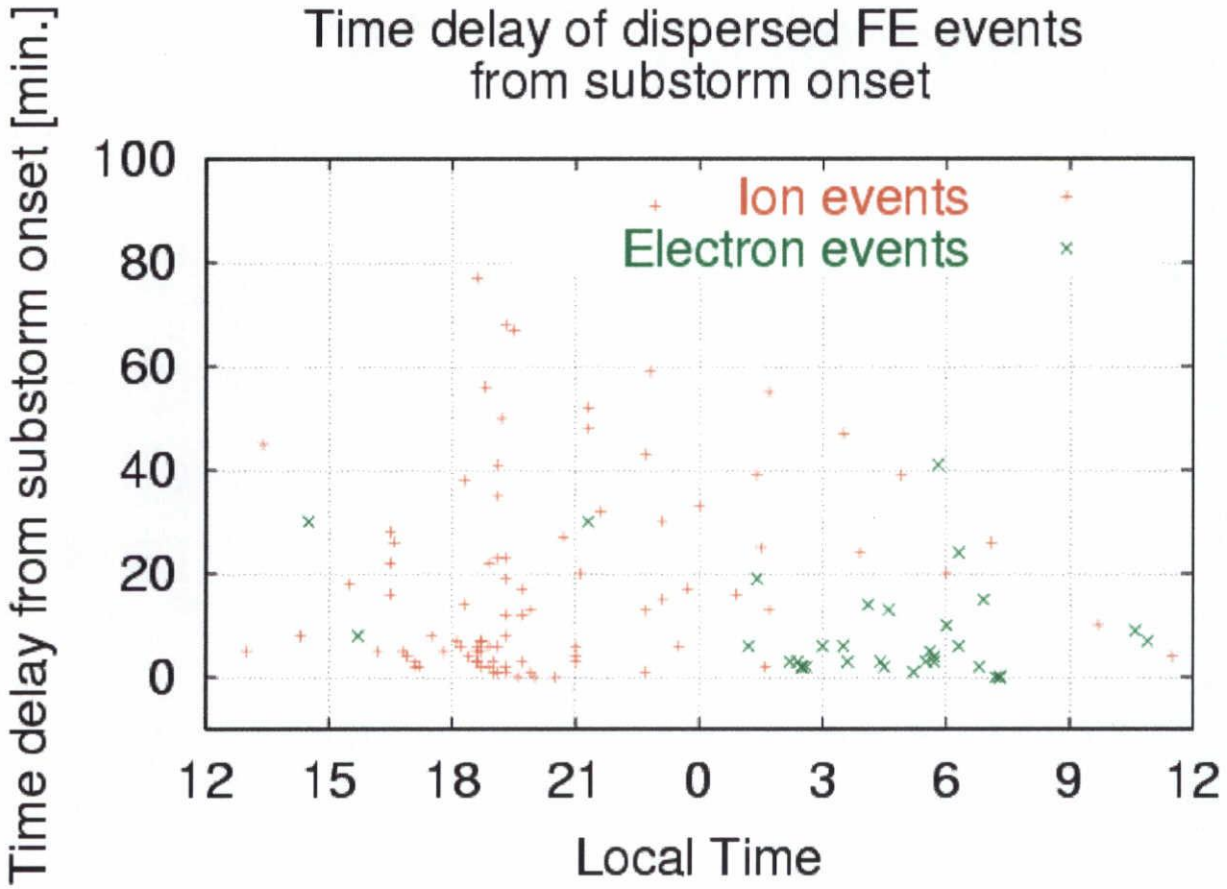
Time delay of dispersed FE events
from substorm onset
Ion events
Electron events
Time delay from substorm onset [min.]
100
80
60
40
20
0
12
15
18
21
0
3
6
9
12
Local Time

Figure 3-10a

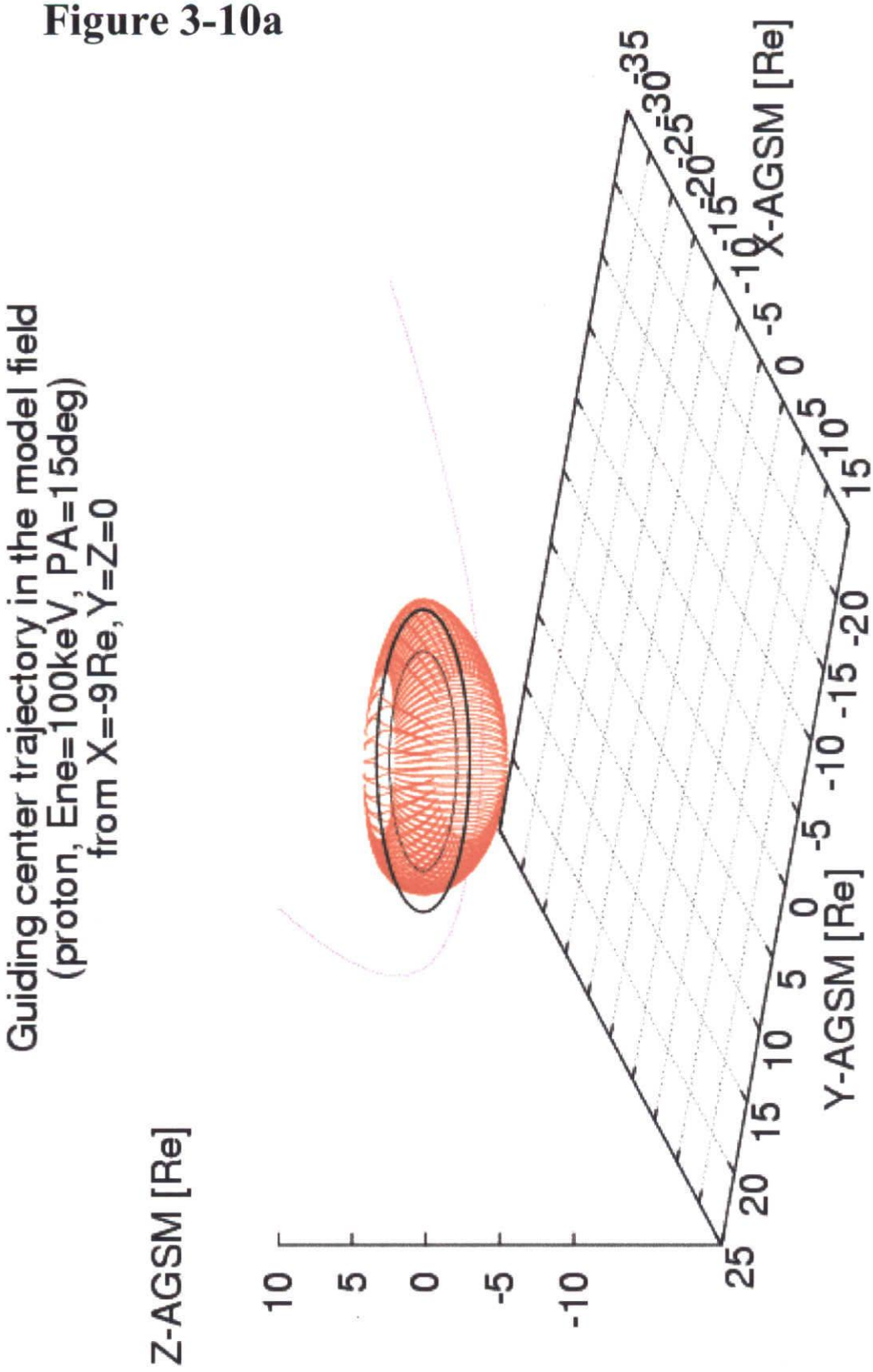
Guiding center trajectory in the model field
(proton, Ene=100keV, PA=15deg)
from X=-9Re, Y=Z=0
Z-AGSM [Re]
10
5
0
-5
-10
25
20
15
10
5
0
-5
-10
-15
-20
Y-AGSM [Re]
15
10
5
0
-5
-10
-15
-20
-25
-30
-35
X-AGSM [Re]

Figure 3-10b

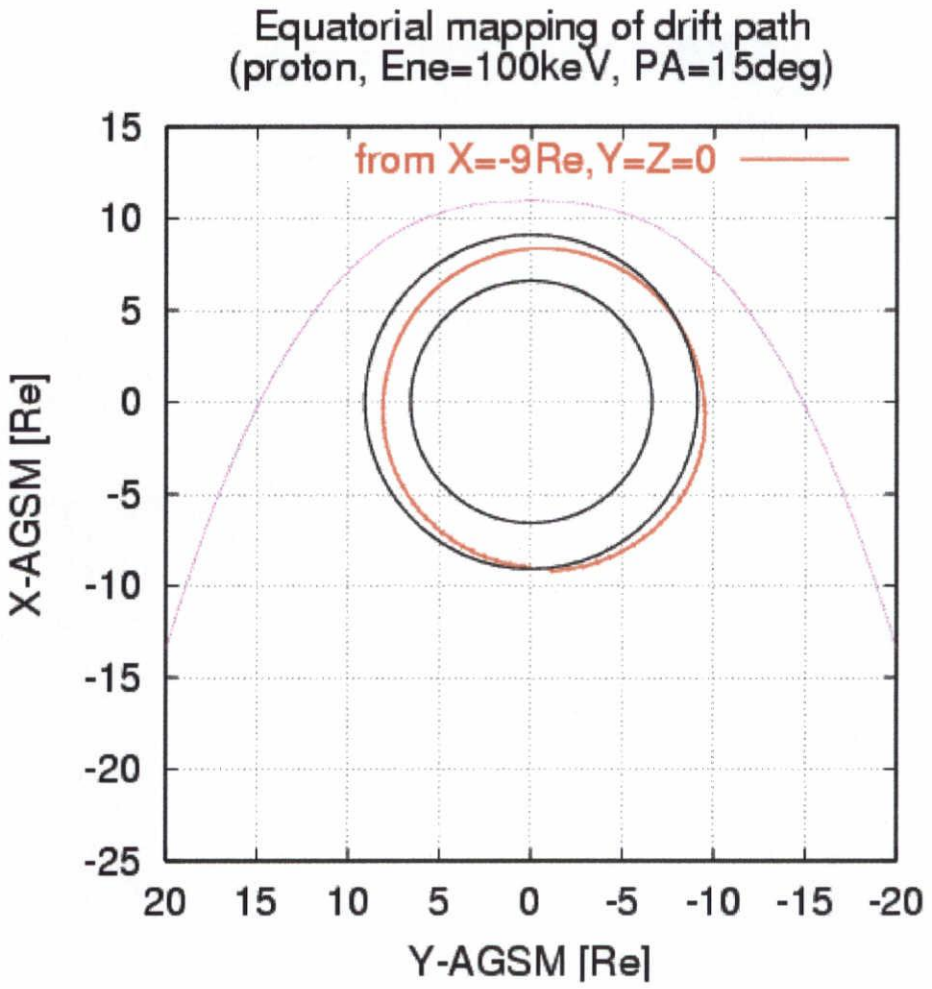
Equatorial mapping of drift path
(proton, Ene=100keV, PA=15deg)
from X=-9Re, Y=Z=0
X-AGSM [Re]
Y-AGSM [Re]
15
10
5
0
-5
-10
-15
-20
-25
20
15
10
5
0
-5
-10
-15
-20

Figure 3-11

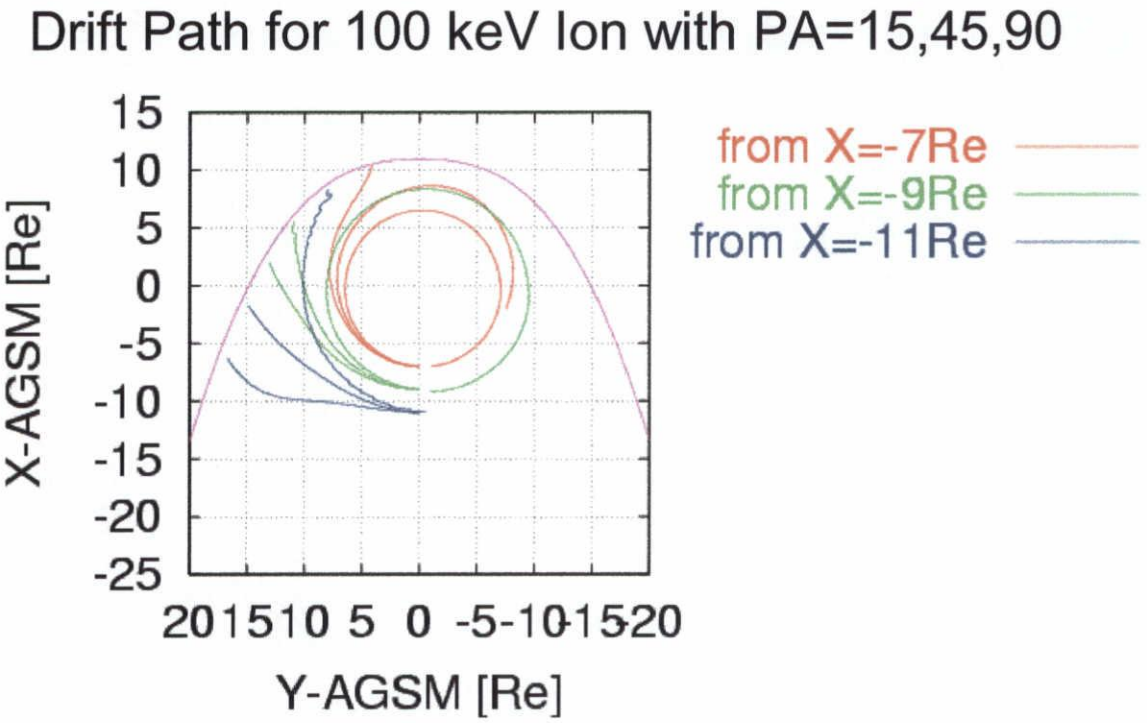
Drift Path for 100 keV Ion with PA=15,45,90
X-AGSM [Re]
Y-AGSM [Re]
15
10
5
0
-5
-10
-15
-20
-25
20 15 10 5 0 -5 -10 -15 -20
from X=-7Re
from X=-9Re
from X=-11Re

Figure 3-12

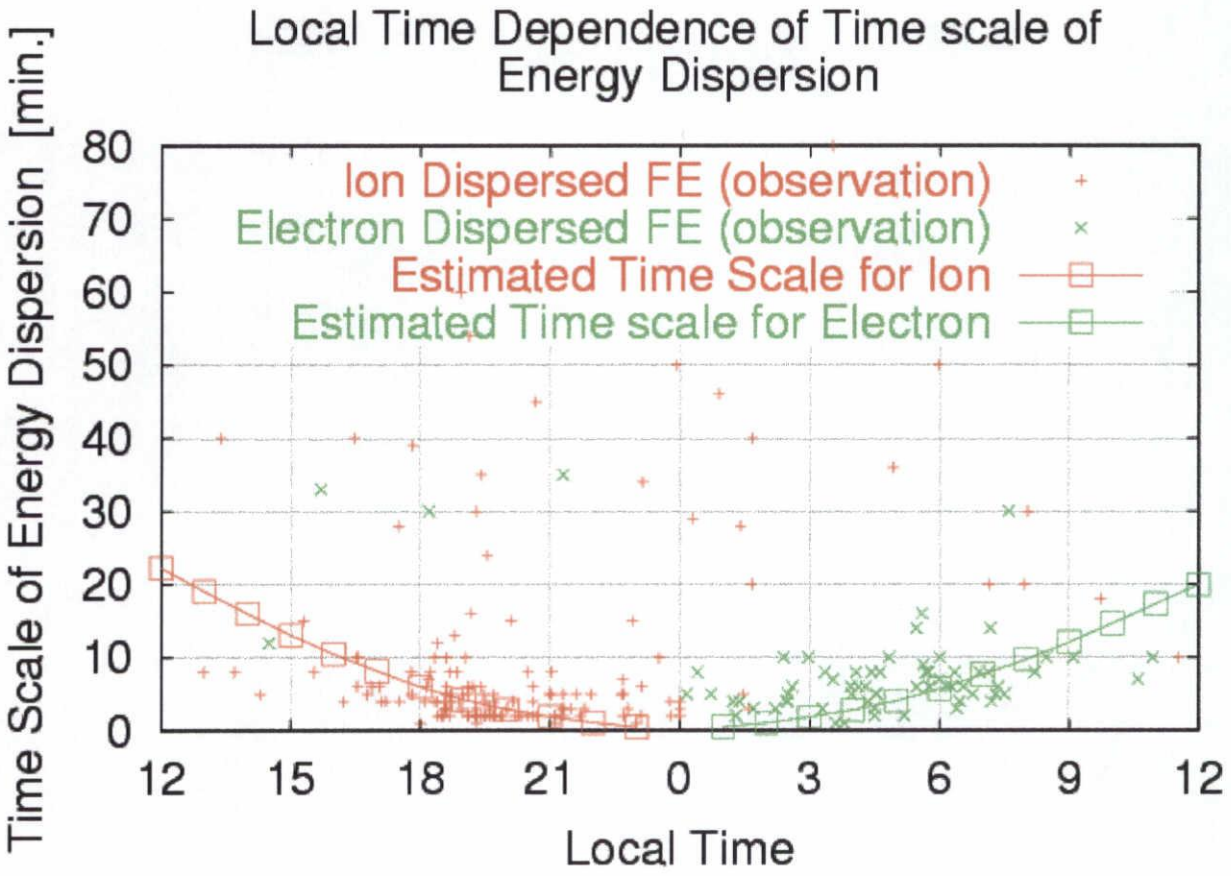
Local Time Dependence of Time scale of Energy Dispersion
Time Scale of Energy Dispersion [min.]
Local Time
Ion Dispersed FE (observation)
Electron Dispersed FE (observation)
Estimated Time Scale for Ion
Estimated Time scale for Electron
0
10
20
30
40
50
60
70
80
12
15
18
21
0
3
6
9
12

Figure 3-13

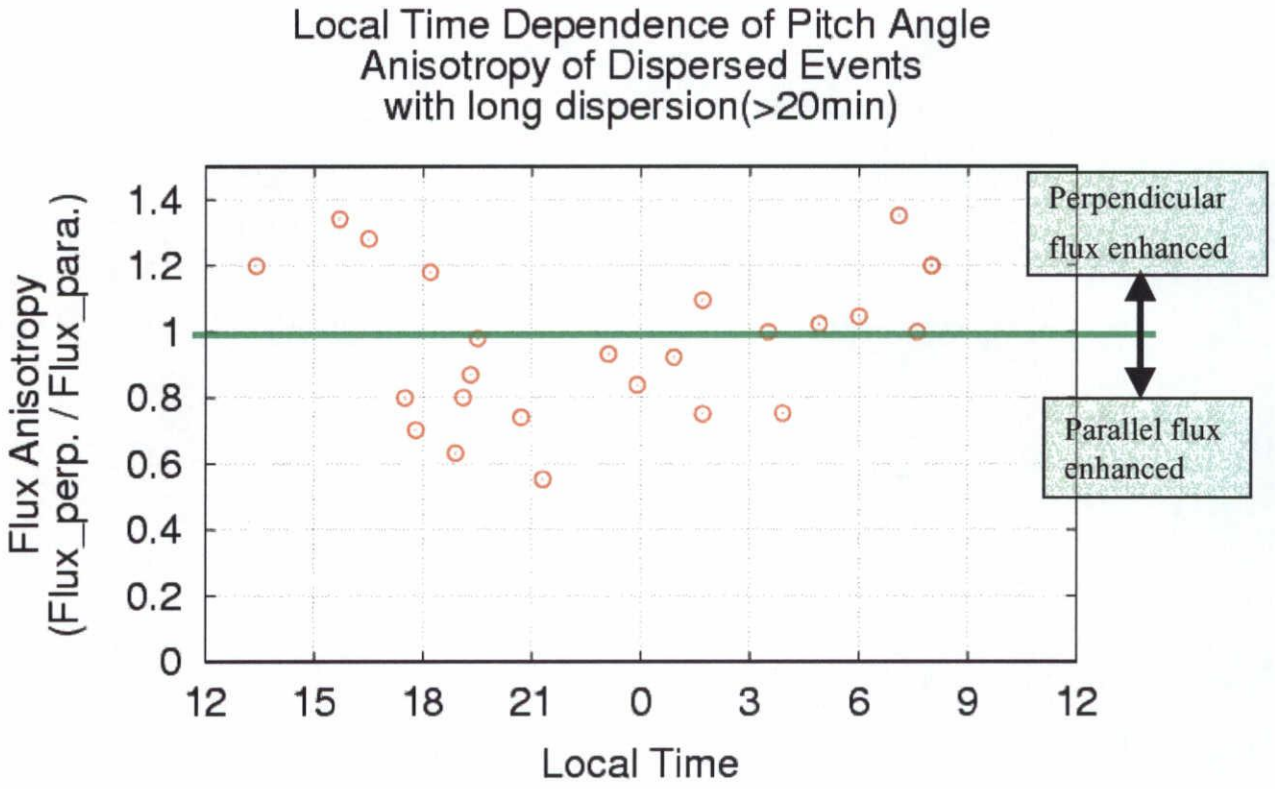
Local Time Dependence of Pitch Angle
Anisotropy of Dispersed Events
with long dispersion(>20min)
Flux Anisotropy
(Flux_perp. / Flux_para.)
1.4
1.2
1
0.8
0.6
0.4
0.2
0
12
15
18
21
0
3
6
9
12
Local Time
Perpendicular
flux enhanced
Parallel flux
enhanced

Figure 3-14

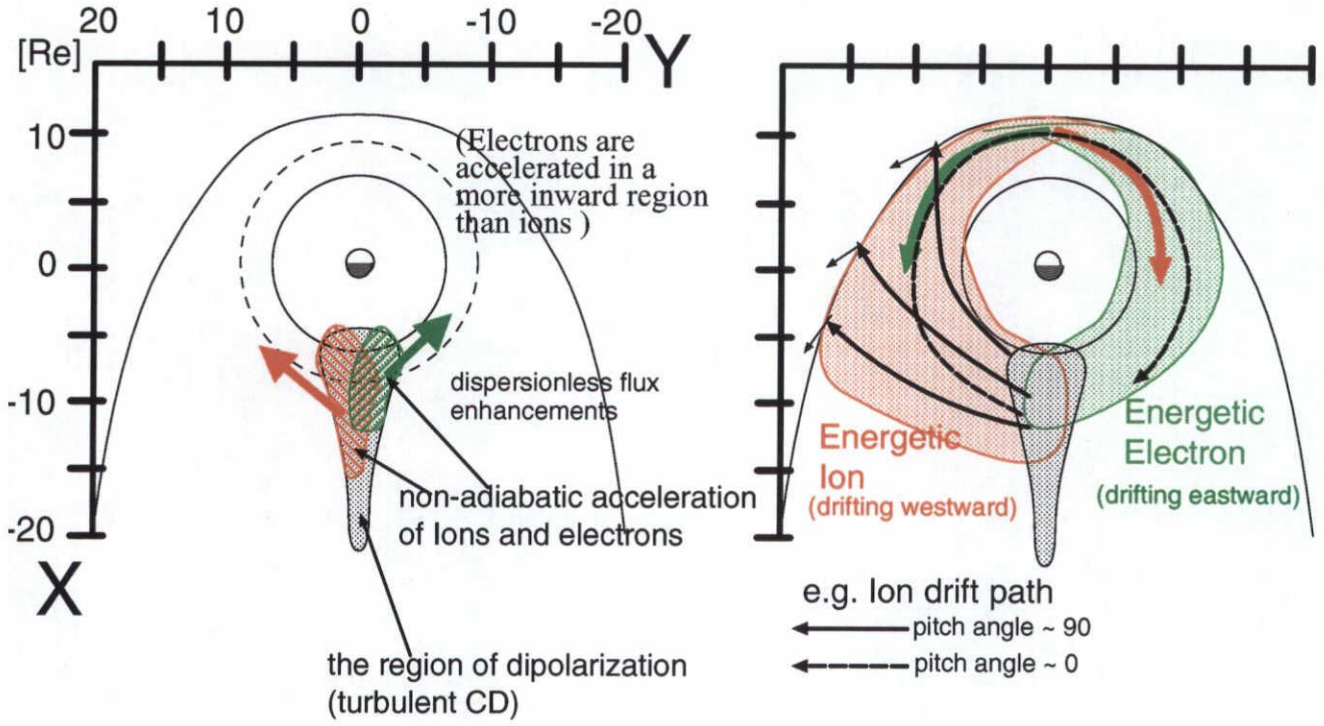

At substorm onset → A few tens of minutes after the onset

Chapter 4

General Discussion

I have studied both thermal and suprathermal components of plasma in the near-Earth plasma sheet by examining large-scale phenomena typical for each component, such as ion convection in the near-Earth plasma sheet and flux enhancements of substorm-associated energetic particles. What I found from these studies is that acceleration and transport processes are much different between the thermal and suprathermal populations.

The plasma in the near-Earth plasma sheet consists mainly of the thermal component with density and temperature of ~ 10^{-1} /cc and ~ a few keV, respectively, and the thermal component plays a significant role in the interaction with ambient electric and magnetic fields. We have shown in Chapter 2 that not only the E×B drift caused by the convection electric field but also the ion pressure gradient drift contribute to ion transport in the near-Earth plasma sheet, and, as a result, the ion flow vectors, which are generally directed earthward, have a significant duskward component especially around the midnight region and on the dusk side. On the other hand, the convection of magnetic fluxes determined by the E×B drift is mainly directed earthward, and it bifurcates near the Earth towards dawn and dusk in a fairly symmetric way. The significant difference in the convection pattern that exists between ions and magnetic flux means that the frozen-in condition is not satisfied even for large-spatial-scale transport phenomena such as the plasma sheet convection. Since thermal ions and magnetic fluxes are transported in different ways, a large-scale asymmetry may arise in the plasma sheet. For example, *Fairfield et al.* [1986] indicated that there is a dawn-dusk asymmetry in the magnetic field intensity in the plasma sheet. They showed that the Bz (northward) component of the magnetic field is larger on the dawn side than on the dusk side on average in the near-Earth plasma sheet and they attributed this field asymmetry to the diamagnetic effect of duskward drifting ions. This result is consistent with the convection profile of ions derived in the present study;

ions are transported preferentially duskward and the resultant concentration of ions on the dusk side may cause the diamagnetic effect.

The difference in the convection pattern between ions and magnetic flux means a difference in the convection pattern between ions and electrons. Past studies on the temperature ratio between ions and electrons in the plasma sheet [e.g., *Baumjohann et al.*, 1989] showed that the electron temperature is by a factor of 5-7 smaller than the ion temperature on average. This means that the electron pressure gradient drift is very small and is negligible as compared to the E×B drift. Thus the resultant flow pattern for electrons should be almost the same as that for the magnetic flux, and therefore significantly different from that for ions. This difference between ions and electrons will cause a global charge separation in the near-Earth plasma sheet, which could be a source of the large-scale current system. Such a current system caused by charge separation was thought to occur in the inner region of the magnetosphere and contribute to the ring current. In the inner magnetosphere on the night side, the strong earthward field gradient there will induce a westward current through the charge-dependent gradient-B drift of ions and electrons. The present study suggests that the westward ring current extends outward and may extend even into the near-Earth plasma sheet.

Although I have not mentioned the generation process of thermal plasma in Chapter 2, the most plausible mechanism for heating the thermal component is thought to be magnetic reconnection in the magnetotail. Basically magnetic reconnection converts the magnetic energy stored in the lobe into kinetic energy of plasma, and can thereby energize plasma effectively to energies of ~several keV, which are typical for thermal ions in the near-Earth plasma sheet. Because the reconnection induces plasma convection on both sides of the reconnection point, it can explain both the generation and the subsequent earthward convection of thermal plasma in the near-Earth plasma sheet. The present study can only show that the reconnection occurs beyond the near-Earth plasma sheet, and cannot specify its downtail distance. *Nishida et al.* [1996] derived two plausible reconnection sites from their statistical study of plasma flows in the magnetotail. One of them is located in the mid-tail region ($-40\ R_E < x < -30\ R_E$), and another in the distant tail ($X \sim -140\ R_E$), with the latter being interpreted to be the distant neutral line discussed in the past. So far, the origin of thermal plasma in the near-Earth plasma sheet is likely to be the distant neutral line, because many observations indicated that thermal plasma in the plasma sheet seem to be supplied rather continually from the source. These features are consistent with a

fairly stable characteristic of the distant neutral line. In addition, it was reported that the ion distribution function of the near-Earth plasma sheet is reasonably explained by the thermalization of ion beams coming from the distant tail along the plasma sheet boundary layer [*Fujioka*, 2001], also supporting the plasma supply from the distant neutral line.

As stated above, the thermal plasma is supplied to the plasma sheet rather stably through the tail reconnection and associated plasma convection. On the contrary, the production and transport of suprathermal plasma is found to be a transient phenomenon. This energetic population is negligibly small in geomagnetically quiet times, but the energetic component drastically increases during substorms. As shown in Chapter 3, this energetic population is produced near the midnight meridian at downtail distances of $X > -15\ R_E$, and subsequently drifts in the azimuthal direction away from midnight and is transported to the other local time sectors in the magnetosphere. Because theoretical studies showed that the tail reconnection itself cannot accelerate particles to energies higher than a few tens of keV, other acceleration processes are needed to produce energetic particles with energies higher than several tens of keV. As a possible mechanism, *Birn et al.* [1997b] suggested acceleration by the strong duskward electric field that is induced temporarily at the time of the near-Earth reconnection. This inductive electric field is induced by the interaction between the dipole-like magnetic field near the Earth and the fast earthward flow of thermal plasma caused by the near-Earth reconnection. Thermal ions and electrons trapped in the region of strong electric field experience nonadiabatic acceleration processes and then gain substantial energies. After a while, the inductive electric field is reduced as the near-Earth reconnection decays, and the associated energetic particle acceleration stops. The present study shows that the accelerated particles having large pitch angles will reach the dawn or dusk side magnetopause in several minutes and be lost from the magnetosphere. The rest of energetic particles having small pitch angles is expected to be lost by interaction with neutral atoms near the Earth. Thus energetic particles generated during substorms will disappear from the magnetosphere in a few hours.

The transport of these energetic particles occurs through their gradient- and curvature-B drifts. Gradient- and curvature-B drifts are both proportional to the particle energy and inversely proportional to the particle charge. Because the accelerated particles have high energies, the gradient- and curvature-B drifts are much faster than the E×B drift component associated with the convection electric field. Since the former two drift components are charge-dependent, ions and electrons drift

azimuthally in the opposite directions in a symmetric way, when they are transported toward the dayside region. In addition to the difference in the spatial properties of transport, the time scale is very different from that of usual plasma convection. The earthward convection in the near-Earth plasma sheet transports plasma from the night side to the day side on the time scale of several hours, while the azimuthally drifting energetic particles generated on the night side go around the Earth in only a few tens of minutes. Thus it takes only a few tens of minutes for energetic particles accelerated on the night side to be distributed to all local time sectors in the magnetosphere.

Taking two different types of transport processes for the thermal and energetic plasmas, an important piece of information is derived for the magnitude of inductive electric field responsible for the acceleration of substorm-associated energetic particles. Because gradient- and curvature-B drift velocities for energetic particles are very large, a strong duskward electric field is needed to inject plasma radially into the inner magnetosphere. Past studies on fast plasma flows in the plasma sheet [e.g., *Angelopoulos et al.*, 1996] indicated that the near-Earth reconnection responsible for these fast flows can induce electric fields (~1 mV/m) which are one order of magnitude larger than the usual convection electric field (~0.1-0.3 mV/m). Even with this magnitude of electric field, the resultant earthward $E \times B$ drift will be at most comparable to the gradient- and curvature-B drifts and the energetic particles cannot be easily injected into the local midnight region of the inner magnetosphere. Hence in order to transport energetic plasma into the inner magnetosphere effectively to cause sudden flux enhancements as observed actually at geosynchronous distances, even a duskward electric field of about a few tens of mV/m has to exist in the near-Earth plasma sheet. Accordingly, a strong inductive electric field as suggested by *Birn et al.* [1997b] is needed not only for the energetic particle acceleration but also for their subsequent injection into the inner magnetosphere. The magnitude of the inductive electric field reproduced in their MHD simulation is about 10 mV/m at $X = -10\ R_E$ and thus is consistent with the magnitude of electric field discussed above.

There is also a characteristic of the plasma transport common to both thermal and energetic plasmas. Thermal ions in the plasma sheet turn away from the sunward convection and, as a whole, tend to be transported duskward by the pressure gradient drift, while thermal electrons are subject only to $E \times B$ drift because of their relatively low temperature, and basically transported sunward symmetrically on the dawn and dusk sides of the Earth. Also in the case of the energetic particle enhancement associated with substorms discussed in Chapter 3, electrons seem to be transported

more in the sunward direction and accelerated in inner regions than ions at the midnight sector. Thus ions are energized efficiently and then start to drift azimuthally duskward, while electrons are still transported toward the inner magnetosphere with little acceleration, showing the transport direction similar to the thermal plasma convection. Since the E×B drift works equally for ions and electrons with all energies, the difference in the transport direction between ions and electrons is caused by the gradient-/curvature-B drifts, which are proportional to the particle energy. Thus the above difference between ions and electrons indicates that, generally in the magnetosphere, ions tend to be preferentially accelerated and gain higher energies as compared to electrons. In other words, we can say that the energization processes playing an important role in the generation of the thermal and energetic plasmas tend to work more efficiently for ions than electrons. This can be reasonably understood by assuming an acceleration process through particle's nonadiabatic motion, because ions can violate their gyromotion more easily than electrons due to their lager mass, and thereby can gain energy from the electric field by moving in the direction of the electric field.

References

Angelopoulos, V., F. V. Coroniti, C. F. Kennel, M. G. Kivelson, R. J. Walker, C. T. Russel, R. L. McPherron, E. Sanches, C.-I. Meng, W. Baumjohann, G. D. Reeves, R. D. Belian, N. Sato, E. Friis-Christensen, P. R. Sutcuiffe, K. Yumoto, and T. Harris, Multipoint analysis of a bursty bulk flow event on April 11, 1985, *J. Geophys. Res., 101*, 4967, 1996.

Baumjohann, W., G. G. Paschmann, and H. Luhr, Average plasma properties in the central plasma sheet, *J. Geophys. Res., 94*, 6597, 1989.

Birn, J., M. F. Thomsen, J. E. Borovsky, G. D. Reeves, D. J. McComas, R. D. Belian, and M. Hesse, Substorm ion injections: Geosynchronous observations and test particle orbits in theree-dimensional dynamic MHD fields, *J. Geophys. Res., 102*, 2325, 1997b.

Fairfield, D. H., The magnetic field of the equatorial magnetotail from 10 to 40 Re, *J. Geophys. Res., 91*, 4238, 1986.

Fujioka, S., 地球磁気圏プラズマ中で観測される沿磁力線ビーム, Master's thesis, Nagoya University, 2001.

Nishida, A., T. Mukai, T. Yamamoto, Y. Saito, and S. Kokubun, Magnetotail convection in geomagnetically active times. 1. Distance to the neutral lines, *J. Geomagn. Geoelectr., 48*, 489, 1996.

Chapter 5

Summary and concluding remarks

In this dissertation, using the data obtained by the GEOTAIL spacecraft, I have studied energization and transport processes of magnetospheric particles. In the magnetosphere, the plasma sheet is one of the most active sites where the particle distribution consists of not only the thermal component (~several keV) but also the suprathermal component (~several tens – hundreds of keV) as a result of various acceleration and transport processes. The thermal component is a major component of plasma in the plasma sheet and is responsible primarily for interactions with ambient electric and magnetic fields. On the other hand, the suprathermal component is a minor component negligible in geomagnetically quiet times. However the energetic component is substantially generated at large in the near-Earth plasma sheet and results in significant perturbation in macroscopic properties of magnetosphere such as the geomagnetic field intensity during substorms. Accordingly, I have paid my attention to two typical physical phenomena in which either the thermal component or the suprathermal (energetic) component plays a crucial role. One is plasma convection in the near-Earth plasma sheet. Another is a flux enhancement of energetic particles associated with substorm activity. Thereby I examined general properties of each component to understand the acceleration and transport processes of magnetospheric plasmas comprehensively.

First I made a statistical study of ion flows, pressure, and the magnetic field directly observed in the plasma sheet and derived their large-scale structures. These plasma and field structures in the near-Earth plasma sheet are rather common as a result of global interaction between the geomagnetic field and the earthward convection induced by the magnetic reconnection in the magnetotail. The results are summarized as follows:

1. Ion flows in the near-Earth plasma sheet are generally directed earthward. The

flow velocities are ~100 km/s at X = -25 R_E, and the flows are decelerated to ~ a few tens km/s as it approaches the near-Earth region (R~10 R_E). On the other hand, there also exists a significant dawn-dusk flow component, showing clear dawn-dusk asymmetry. . The flows have large duskward components at midnight and on the dusk side, while have relatively small dawnward components on the dawn side.

2. The equatorial distribution of ion pressure shows that the ion pressure increases toward the Earth both for the midnight and off-midnight dawn and dusk regions. The X-dependence of ion pressure is more remarkable in the midnight region.

3. The duskward component of the pressure gradient drift derived from the observed ion pressure profile is significantly large and even comparable to the duskward or dawnward components of ion flows. This fact indicates that the pressure gradient drift contributes much to observed ion flows in the plasma sheet. On the contrary, earthward and tailward components of the pressure gradient drift are very small and negligible as compared to the earthward component of ion flows.

4. The distribution of the convection electric field shows that, all over the plasma sheet, the electric field has a dawn-to-dusk component corresponding to the earthward convection. In addition to the duskward components, the electric field has a significant earthward (tailward) component on the dawn (dusk) side, indicating that the convection flow tends to bifurcate, with one branch deviating duskward and the other deviating dawnward, avoiding the Earth at the center. Because a significant Ex component exists not only near the Earth but also at considerable distances down the tail (R > 15 R_E), this fact indicates that the convection toward the Earth begins to bifurcate at positions much farther away from the Earth than expected from the past studies.

5. Two-dimensional distribution of the E×B drift vectors obtained from the calculated E vectors shows that the beginning of the bifurcation of the sunward convective flow is already evident at X = -28 R_E. The E×B drift vectors have rough mirror symmetry about the midnight meridian in contrast to the asymmetric ion flow pattern.

From these observational results, it is concluded that the convection electric field, which is applied to the plasma sheet by the tail reconnection, is rather symmetric about the midnight meridian. However, even under such a symmetric electric field configuration, the resultant bulk motion of ions (essentially representing the motion of thermal ions) is not symmetric, particularly a duskward flow component is significant at midnight and on the dusk side. This result indicates the important fact that, in the

near-Earth plasma sheet, the assumption of frozen-in of magnetic fluxes is not valid and thermal ions and magnetic fluxes are transported in different ways. This discrepancy of convection can be also considered as the discrepancy of convection profile between ions and electrons, because the electron pressure is small as compared to ions and thereby electrons tend to E×B drift along almost the same way as the magnetic fluxes do. This indicates a possibility that the plasma convection in the near-Earth plasma sheet causes global charge separation between ions and electrons, and thereby induces a large-scale current system in the magnetosphere.

Another important conclusion is that the electric field has a significant Ex component which bifurcates the earthward plasma transport towards dawn and dusk. This fact indicates that earthward-flowing thermal plasma (and also energetic components) are deflected dawnward or duskward and cannot easily approach the near-Earth region under the usual convection electric field. Therefore an additional duskward electric field is needed to transport plasmas into the inner magnetosphere, for example, during substorms.

Next, I studied the acceleration and transport processes of energetic particles by investigating flux enhancements of energetic particles during substorms on the basis of GEOTAIL HEP-LD observation. A sudden flux increase of energetic particles is observed frequently in the near-Earth plasma sheet during substorm activity. I found that some of the flux enhancements exhibit clear signatures either of energy-dispersed or of dispersionless features. These characteristics give us important clues to estimate how far away the observation points are from the source of energetic particles. In particular, the dispersionless signature shows that the observation point is in the vicinity of the source region. Using these clues, I examined spatial and temporal properties of enhanced energetic particles during substorms. A detailed temporal correlation with substorms is also investigated. The results of my studies are summarized as follows:

1. Dispersionless events are found around the local midnight sector, while dispersed events are frequently observed at other local time sectors away from midnight. This result is consistent with the interpretation that energetic particles constituting such flux enhancements are generated around local midnight in the near-Earth plasma sheet, and subsequently drift away from midnight and then are dispersed in energy.

2. Dispersionless ion events are distributed slightly duskward of the midnight region, while dispersionless electron events are centered slightly dawnward. The sense

of the shift of event occurrence is consistent with the direction of gradient- and curvature-B drift for ions and electrons. The same tendency is also seen for dispersed ion and electron events with much clearer dawn-dusk separation for ions and electrons. This result also supports the above interpretation.

3. Both for dispersionless and dispersed events, electron events are relatively rare as compared to ion events. In particular, dispersionless electron events are substantially less frequent than the ions. This fact implies that, in the near-Earth plasma sheet, the acceleration mechanism responsible for the generation of energetic particles during substorms is less effective for electrons in the near-Earth plasma sheet.

4. A correlation study with substorm activity showed that both of the dispersionless and dispersed events are closely correlated with substorm activities. In particular, dispersionless events occur almost simultaneously with the corresponding substorm expansion onsets. This fact indicates that energetic particles are generated at the substorm expansion onset.

5. Most of the dispersed events exhibit a short (~several minutes) energy dispersion and the time scale of energy dispersion increases as we go away from local midnight toward the dawn and dusk flanks. The time scale agrees quantitatively with the values estimated from the drift path calculation assuming the source of energetic particles at local midnight.

6. Some dispersed events have long (~ tens of minutes) dispersion and cannot be explained by a simple azimuthal drift from local midnight to the observed local time sectors. Because these events are found in all local time sectors, i.e., even on the flanks opposite to the direction of grad- and curvature-B drift for ions and electrons, these events with a long dispersion indicate that energetic particles have a closed drift path around the Earth, even to the radial distances much further than the inner magnetosphere. A detailed investigation showed that dispersed events with a long dispersion on the night side show clear parallel pitch angle anisotropy, while those found on the dayside exhibit isotropic or even perpendicular pitch angle anisotropy.

7. Drift path calculation for particles with different pitch angles showed that only particles with small pitch angles in the night side plasma sheet can go around the Earth and then return to the midnight region. In addition, particles with large pitch angles which start from the midnight region in the inner magnetosphere can take a closed drift path around the Earth and have access to the outer magnetosphere on the dayside. Thus dispersed events observed on the dayside are mixtures of small pitch

angle particles starting in the plasma sheet and large pitch angle particles starting in the inner magnetosphere on the night side. These simulation results are consistent with the observed pitch angle distributions of dispersed events having a long dispersion.

From these results, It is concluded that energetic particles with energies higher than several tens of keV are generated almost simultaneously with substorm expansion onset around the midnight sector in the near-Earth plasma sheet, and subsequently drift away from midnight and are transported to other local time sectors. As a result, energetic particles are supplied to the entire local time sectors in the outer magnetosphere. It is also concluded that the acceleration of energetic particles does not seem to be caused by near-Earth reconnection, because the substorm-associated generation of energetic particles occurs within a distance of 15 R_E down the tail, which is much earthward of the near-Earth reconnection site. The randomly varying characteristics of pitch angle distribution observed in dispersionless events indicate that particles are accelerated in a non-adiabatic manner in the near-Earth plasma sheet.

Finally, I would like to comment on the future prospect of the research I presented in this dissertation. In the present study, all observational results are based on observations in the outer magnetosphere achieved by the GEOTAIL spacecraft. Since a single spacecraft can observe physical parameters only at a fixed point in space at a given instance, we have to collect events obtained at various positions and analyze them statistically to infer their spatial structure. If other spacecraft observing the same phenomenon simultaneously are available, we can examine the spatial extent and also spatial evolution of the event directly. Multiple-point observations are needed especially for the study of flux enhancement of energetic particles presented in Chapter 3. From the statistical analyses in the present study, I was not able to obtain the azimuthal extent of the dispersionless flux enhancement, which reflects the dawn-dusk width of the acceleration site. If multiple satellites are placed at certain longitudinal intervals in the night side magnetosphere, we can determine the azimuthal extent of the acceleration site by checking the dispersionless characteristic at each satellite. It is also important to examine the radial extent of the flux enhancement region. By examining the detailed temporal correlation between observations in the near-Earth plasma sheet and at a geosynchronous distance, we can follow the earthward evolution of enhanced energetic particle region, that is, the injection of energetic particles during substorms. Such information on the spatial extent of flux enhancement regions is

important not only for the investigation of the corresponding acceleration processes but also for examining spatial correlation with the aurora brightening in the ionosphere.